MRI Master Class 2009/2010:

Numerical Bifurcation Analysis of Dynamical Systems

WEEK 15, Apr 13 & 15:

Bob W. Kooi
Faculty of Earth and Life Sciences,
Department of Theoretical Biology, Vrije University,
De Boelelaan 1085,
1081 HV Amsterdam,
The Netherlands
Tel.: +31 20 5987129, Fax: +31 20 5987123,
Email:kooi@bio.vu.nl
URL: http://www.bio.vu.nl/thb/

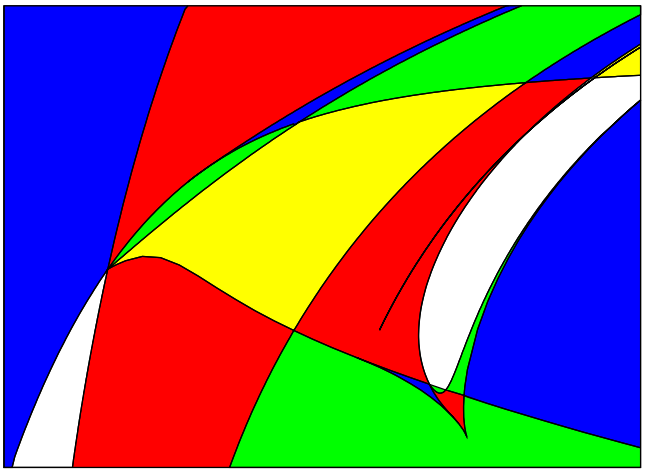

Contents

Chapter 1

Ecosystem models

Numerical bifurcation analysis of ecosystems in a spatially homogeneous environment
B.W. Kooi
Acta Biotheoretica 51: 189–222, 2003

The dynamics of single populations upto ecosystems, are often described by one or a set of non-linear ordinary differential equations. In this paper we review the use of bifurcation theory to analyse these non-linear dynamical systems. Bifurcation analysis gives regimes in the parameter space with quantitatively different asymptotic dynamic behaviour of the system. In small-scale systems the underlying models for the populations and their interaction are simple Lotka-Volterra models or more elaborated models with more biological detail. The latter ones are more difficult to analyse, especially when the number of populations is large. Therefore for large-scale systems the Lotka-Volterra equations are still popular despite the limited realism. Various approaches are discussed in which the different time-scale of ecological and evolutionary biology processes are considered together.

1.1 Introduction

In population based models the state of the population is described by one or a finite number of state variables, such as the number of individuals, the total biomass and so on. The temporal changes of these variables are mathematically given as one or a set of difference equations (discrete-time) or a set of differential equations (continuous-time). These equations and a rationale together form a model. A phenomenological model is inspired by data. Other models, often called mechanistic, are based on first principles such as conservation laws.

In a food chain each population in consumed by at most one other population. The composition is called a food web when besides this predator-prey interaction other trophic interactions such as omnivory, multiple predators and multiple resources occur. Generally these interactions describe feeding relations among a subset of the species in the community of species living together in a spatially discrete habitat, for example a pond, island and so on. Ecosystems consist of one or more communities which interact with their physical and chemical environment taking into account for instance light supply, energy dissipation, nutrient cycling, immigration, and emigration. Ecosystem ecology is mainly concerned with the functioning (rates and fluxes) and structure (abundances and species composition) of the overall (biotic and abiotic) system.

Nonlinear dynamical system theory was first applied to single population dynamics. May (1976) found that for a population with non-overlapping generations (for instance discrete breeding seasons), described by the logistic discrete time equation (logistic map), a cascade of period doubling ultimately leads to chaotic dynamics when the per capita growth rate is increased. In this section we focus on the application to continuous time systems. The continuous time version of the logistic equation exhibits only simple dynamics [56].

When descriptive formulations are used for each population the formulation of the interactions with the environment often remain vague. We will use a mass-balance formulation where the environment has to be specified. This formulation facilitates an integration between population dynamics and the flow of energy, mass and nutrients in ecosystems. We will consider two types of environment, the batch reactor and the chemostat system. The batch reactor is a closed system with neither material influxes nor outfluxes. A lake of constant volume where water carrying nutrients flows in at a given rate, and water carrying organisms and nutrients flow out at the same rate [100, 118] is an example of a chemostat environment.

When the operation conditions are constant the system of ordinary differential equations is called an autonomous system. For these systems it is useful to look for equilibrium states in which the state variables do not change in time. These states, solutions of a nonlinear set of equations, can be stable or unstable. Stable means that after arbitrary small perturbations the system returns asymptotically to this state whereas if unstable it does not. For a specific parameter setting, the stability properties of all equilibria gives knowledge about the dynamics only for initial conditions in the neighbourhood of the equilibria. When an equilibrium is stable it is a point attractor, but there are other types of attractors as well, namely limit cycles, periodic solutions, and chaotic attractors, with sensitive dependency on initial conditions for a given set of parametric values. The set of states from which the solution converges to the attractor is called the basin of attraction. Knowledge of the basins belonging to all attractors yields full information about the dynamic behaviour. Separatrices form the boundary of these basins. Generally they are geometrically smooth but in [63] it is shown by simulation that for models of interaction populations, the basins of attraction may have intermingled fractal geometry. That is, small perturbations in initial conditions can change the final attractor of the dynamics.

Bifurcation analysis focuses on the dependency of the long-term dynamics behaviour on model parameters [54, 86]. In a bifurcation point the asymptotic dynamical behaviour of the system changes quantitatively, for example a stable equilibrium becomes unstable when a parameter is varied. In this way the parameter space is divided into regions with different long-term behaviour. Computer packages are available to calculate the boundaries of regions.

The classical Lotka-Volterra (LV) model [96] is still popular with modelling large-scale food webs with many state variables and parameters. The main reason for choosing the LV model formulism is that the procedure to calculate the equilibria and their stability and the return time, which is a quantitative measure of the resilience stability in stable equilibria, is straightforward.

For modelling small-scale food webs the linear functional response is often replaced by more realistic population interaction formulations. Many alternative formulations have been proposed. The Holling type II functional response, whereby the consumption rate becomes saturated as the food level increases, is popular. However, with this type of functional response, multiple stationary long-term dynamic behaviours are possible and this complicates the analysis of these models. These models with more biological detail have been analysed frequently using numerical bifurcation analysis. Bazykin (1998) studied various small-scale

food web systems. He gives a rather complete overview of the different types of local and global bifurcations.

Throughout this section we will use (unless stated otherwise) the stability concept derived from mathematics and physics, that is a return to the reference state after a perturbation. We refer to [52] for an inventory and analysis of discussions of ecological stability. They consider 163 definitions of 70 different stability concepts and conclude that: "the general term 'stability' is so ambiguous as to be useless".

The individual level of organization is often used as a staring point for modelling manily because reproduction occurs at this level. We have to bridge this gap generally done via a number of intermediate levels, individuals, populations, communities, ecosystems. Individuals can have a complicated life cycle with many life stages, such as: egg, larvae, juvenile and adult, and different modes of reproduction; division and sexual reproduction. Each individual is unique and therefore there is variability at the population level. The "large number assumption" is used to describe the state of a population with a few population state variables and the vital parameters depend anyhow on the parameters of the individual model. Mathematically the population model can be expressed in partial differential equations for a physiologically structured (for instance by age or size) population, delay differential equations for a stage-structured population and a ordinary differential equation for an unstructured population where all individuals are treated identically. In this review only unstructured population models in a spatially homogeneous environment are discussed.

1.2 Small-scale models

1.2.1 One-population models in a closed system

We start with a very simple model for a population feeding on a abiotic nutrient under batch reactor conditions

$$\frac{dN}{dt} = -I\frac{N}{k}R \tag{1.1a}$$

$$\frac{dR}{dt} = \mu\frac{N}{k}R \tag{1.1b}$$

where $N(t)$ is the state of the nutrient mass and $R(t)$ the population biomass. The parameter I is the per capita ingestion rate. The dimension of I is nutrient mass per biomass per unit of time and k nutrient. We assume $\mu = yI$, where y is the efficiency of the nutrient/biomass conversion. In order to obtain mass conservation we introduce products P excreted by the population and defined by the ODE

$$\frac{dP}{dt} = (I-\mu)\frac{N}{k}R \tag{1.1c}$$

Mass conservation gives $d(N+R+P)/dt = 0$. This requires that all state-variables use the same currency, for instance carbon.

Since Equation (1.1c) is decoupled from Equations (1.1a) and (1.1b), we can solve these latter two coupled ODEs first, and thereafter calculate $P(t)$ by substitution of the solutions $N(t)$ and $R(t)$ into Equation (1.1c).

We can reduce the remaining system of two equations (1.1a) and (1.1b) even further. Consider $yN(t) + R(t)$ then $d(yN+R)/dt = 0$. We remark that the state variables $N(t)$

and $R(t)$ do not need to have the same currency here, it is corrected by the dimension of the efficiency. Because the efficiency y is constant the weighted sum of the nutrient mass and population biomass is time-independent. Substitution of $N(t) = k - R(t)/y$ into (1.1b) yields the single governing equation for the population biomass

$$\frac{dR}{dt} = r(1 - \frac{R}{K})\, R \tag{1.2}$$

where $r = \mu$ and $K = ky$. This is the well-known logistic growth equation where r is the intrinsic growth rate and K the carrying capacity. Observe that this equation is generally considered to be a descriptive model in which case the exponential growth model, which is the linear term on the right hand side, is augmented with a second order term, the quadratic term, of the Taylor series. Often this term is linked with intraspecific competition for a, not explicitly modelled, nutrient. In another mechanistic interpretation the second term models cannibalism.

The derivation of (1.2) yields an interpretation of the carrying capacity in terms of (initially) available nutrient $N(0) = k - R(0)/y$ that supports population existence.

Equilibria There is an explicit expression for the solution $R(t)$ for the logistic growth equation (1.2) but in order to elucidate the bifurcation analysis technique we do not use it here. When interested in the long-term dynamics, we look for stationary solutions where time goes to infinity. Stationary solutions can be equilibria (that is the state variables do not change in time), periodic solutions (that is the state variables change periodically in time) or chaos. The equilibrium equation, where the right-hand side of equation (1.2) is equal to zero, has two solutions, namely $R^* = 0$ and $R^* = K$. Consequently $R(0) = 0$ implies $R(t) = 0$ for all $t > 0$ and similar when $R(0) = K$ then $R(t) = K$ for all $t > 0$. The next question is whether these equilibria are stable or not.

Notice that although we have one equation there are multiple equilibria. This is typical for nonlinear models where the equilibrium equations are nonlinear as well. In this example the equilibrium values can be calculated easily, but for large ODE systems this can be a tremendous task and they have to be approximated numerically.

Stability Fortunately there is a systematic way to determine whether an equilibrium is stable or not. For that purpose, the system is approximated in the vicinity of the equilibrium point. This approximation yields a linear system, which mathematically is more manageable than a non-linear system. For example, consider the zero equilibrium $R = 0$. When R is small, the second term is small with respect to the first one, $R/K \ll 1$. Therefore $dR/dt \approx rR$ and hence $R(t) \approx R(0)\exp(rt)$. Since the growth rate r is positive, arbitrary small perturbations $R(0) \neq 0$ grow in time exponentially and consequently the zero equilibrium is unstable. In a similar way one can show that the equilibrium $R^* = K$ is stable. That is, after arbitrary small perturbations from $R(0) = K$ the system returns to the equilibrium value, which is the carrying capacity K.

Parameter dependency We continue with the influence of parameter values on the long-term dynamics behaviour. We are interested in those critical values at which the asymptotic behaviour changes qualitatively when the critical values is passed. In the logistic growth example we can take the intrinsic growth rate as a free or bifurcation parameter. Obviously

$r = 0$ is a critical point. If $r > 0$ the trivial equilibrium $R^* = 0$ is unstable and at the same time $R^* = K$ is stable. If $r < 0$ (indeed not very realistic from a biological point of view) the trivial equilibrium is stable and the equilibrium $R^* = K$ is unstable. Starting below the carrying capacity, $R(0) < K$, gives convergence to zero, but if starting above the carrying capacity, $R(0) > K$, the population explodes to an unlimited size; the value K is a separatrix.

So, we are looking for parameter values where the stability properties of an equilibrium (or other stationary solution) changes. At this point the system is called structurally unstable. For a one dimensional system with one state variable R, as in the logistic growth case, this is easy; linearise the right-hand side of the ODE at the equilibrium and set the linear term, the "growth rate", zero. For higher dimensions a similar, but more elaborate, procedure works.

1.2.2 One-population models in an open system

Now suppose that the population lives in an open environment, a chemostat. Then (1.1) changes into

$$\frac{dN}{dt} = (N_r - N)D - I\frac{N}{k}R \tag{1.3a}$$

$$\frac{dR}{dt} = (\mu\frac{N}{k} - D)\,R \tag{1.3b}$$

There are three additional terms which model the interaction with the environment. One for the influx of nutrient, DN_r, two for the outfluxes of the nutrient DN and population DR. The dilution rate D (fraction of the volume replaced per unit of time) and the nutrient density N_r of the inflow medium are the chemostat control parameters that can be experimentally manipulated.

We try to follow the same procedure as for the closed system. Mass conservation is obtained after introduction of a product which leaves the reactor with rate D

$$\frac{dP}{dt} = (I - \mu)\frac{N}{k}R - DP\,. \tag{1.3c}$$

Mass conservation gives for this open system $d(N + R + P)/dt = -D(N + R + P - N_r)$; not an algebraic equation but an ODE. This equation is the amount of material supplied minus that removed from the reactor, both per volume of the reactor and per unit of time.

We define $H(t) = N(t) + R(t)/y - N_r$ and, since N_r and y are constant, evaluation of the time derivative of H gives directly $dH/dt = -DH$ and therefore $H(t) = H(0)\exp(-Dt)$. Substitution of the solution into (1.3b) gives

$$\frac{dR}{dt} = \big(\mu\frac{N_r + H(0)\exp(-Dt) - R/y}{k} - D\big)\,R \tag{1.4}$$

However, this single equation is non-autonomous. Mass conservation gives only a simple algebraic equation at the equilibrium. The original two-dimensional system (1.3) is asymptotically dynamically equivalent to the one-dimensional system where $H = 0$

$$\frac{dR}{dt} = \big(\mu\frac{N_r - R/y}{k} - D\big)\,R \tag{1.5}$$

This is the logistic growth equation where $r = \mu N_r/k - D$ and $K = y(N_r - kD/\mu)$ and we discussed its equilibria and their stability in the previous section.

There are two equilibria: the trivial equilibrium $N^* = N_r$ and $R^* = 0$, and the interior equilibrium $N^* = kD/\mu$ and $R^* = y(N_r - kD/\mu)$. The original model is two-dimensional and stability analysis at these equilibria is now more complicated. For a two dimensional system there are two variables, N and R and therefore an equilibrium can be perturbed by varying two variables simultaneously, yielding a much richer repertoire.

Linearization leads now to the following linear set of ODEs. which can be analysed mathematically. There are two resulting exponential growth rates which can be associated with the so-called eigenvalues of the Jacobian matrix evaluated in the equilibrium. When all eigenvalues are negative it is stable. Unfortunately, this is not a complete picture. There are situations where oscillatory behaviour occurs and the eigenvalues are complex numbers instead of real numbers. Complex numbers have a real part and an imaginary part. When the imaginary part is zero it is in fact a real number. When all eigenvalues have negative real parts the equilibrium is stable, that is, the sign of the eigenvalue with largest real part decides on stability.

The trivial equilibrium $N^* = N_r$ and $R^* = 0$ is stable when $\mu N_r/k - D < 0$ and the interior equilibrium $N^* = kD/\mu$ and $R^* = y(N_r - kD/\mu)$ is stable when $\mu N_r/k - D > 0$. Observe that R^* is non-negative only when the trivial equilibrium is unstable.

In summary: if $\mu N_r/k < D$ then there is one non-negative solution, the trivial solution which is stable. If $\mu N_r/k > D$ then besides the trivial solution, which is unstable, there is one interior solution which is stable. Hence $\mu N_r/k = D$ is a bifurcation curve, called a transcritical bifurcation curve, in the parameter space N_r, D, where all other parameters are fixed. For a given N_r, the population can invade the nutrient system when the trivial solution is unstable, that is when D is not too large. Invasion is possible when the initial rate of increase of the population is positive, that is, its per capita growth rate is larger than its depletion rate. In a biologically context the bifurcation curve marks regions in the parameter space where a population can invade an existing system which was stable before invasion but becomes unstable when the population appears.

When one equilibrium is stable, the other is unstable and vica versa. In general, with multiple equilibria this need not to be true. Therefore we must investigate the stability of all possible equilibria. For biologically relevant problems, we have to investigate only those with non-negative state variables.

1.2.3 Predator-prey models

The resources are now consumed by a consumer of which the biomass is denoted by C. Like for the nutrient–resource interaction, we assume a Holling type II functional response for the consumer–resource interaction. Furthermore, there are per capita loss rates of the living populations. The nutrient–resource–consumer model in the chemostat reads

$$\frac{dN}{dt} = (N_r - N)D - I_{NR}\frac{N}{k_{NR} + N}\,R \tag{1.6a}$$

$$\frac{dR}{dt} = (\mu_{NR}\frac{N}{k_{NR} + N} - D - m_R)\,R - I_{RC}\frac{R}{k_{RC} + R}\,C \tag{1.6b}$$

$$\frac{dC}{dt} = (\mu_{RC}\frac{R}{k_{RC} + R} - D - m_C)\,C \tag{1.6c}$$

Observe that for $C = 0$ the system reduces to the nutrient–resource system discussed in the previous section (except that for the nutrient–resource interaction the LV is replaced by

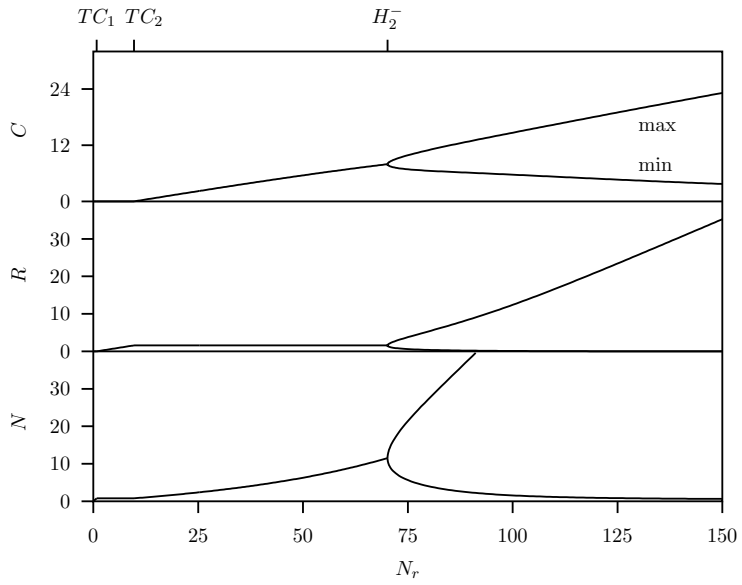

Figure 1.1: A one-parameter bifurcation diagram for a population (1.6) in the chemostat. The stationary biomass of the nutrient N, resource R and consumer C is depicted as a function of the nutrient level N_r. For high nutrient levels the system oscillates with extrema indicated.

Holling type II functional response). Thus all results obtained for that system are relevant. Again we search for parameter values where the consumer can invade the stable nutrient–resource system which becomes unstable in the nutrient–resource–consumer system which is one dimension higher.

Explicit expressions for all equilibria can be derived straightforwardly. Evaluation of the stability, that is the eigenvalues of the Jacobian matrix evaluated at these points, is much more complicated. Therefore we use a computer program to approximate the bifurcation curves where an eigenvalue or its real part equals zero.

A new version of the Hopf bifurcation the supercritical version is found. For certain parameter combinations the real part of two complex conjugate eigenvalues is zero. At this point the equilibrium, which is first stable, then becomes unstable and eventually a stable limit cycle emanates. This is illustrated in Figure 1.1.

We use the species parameter set for bacterium-ciliate models, after [24] given in Table 1.1. We fix $D = 0.02$ and vary x_r. For low values the resource cannot invade the reactor with only the nutrient present. On the right-hand side of the transcritical bifurcation TC_1 it can. Increasing x_r further, also the consumer can invade the nutrient–resource system on the right-hand side of TC_2. Unexpectedly, when the system is enriched by increasing x_r, the interior equilibrium becomes unstable and the system starts to cycle at the Hopf bifurcation point denoted by H_2^-. This phenomenon is know as the "paradox of enrichment" [110].

Reduction is possible with Holling type II functional response when the assimilation efficiency is constant, and $m_R = 0$ and $m_C = 0$. Definition of the function $H(t) = N(t) + R(t)/y_{NR} + C(t)/(y_{NR}y_{RC}) - N_r$ gives $dH/dt = -DH$ and $H \to 0$ for $t \to \infty$.

In the two dimensional RM model the prey population is self-reproducing and its growth

Table 1.1: Parameter set for bacterium-ciliate model, after [24]. The control parameters that can be experimentally manipulated are D and N_r.

Parameter	Unit	Values				
		$i = N$		$j = C$		$j = P$
		$j = R$	$j = M$	$i = R$	$i = M$	$i = C$
$\mu_{i,j}$	h^{-1}	0.5	0.42	0.2	0.3	0.15
$I_{i,j}$	h^{-1}	1.25	1.25	0.333	0.333	0.25
$k_{i,j}$	$\mathrm{mg\,dm}^{-3}$	8.0	5.5	9.0	9.1	10.0
m_j	h^{-1}	0.025	0.025	0.01		0.0075

in absence of the predator is modelled using the logistic growth

$$\frac{dR}{dt} = r(1 - \frac{R}{K})R - I_{RC}\frac{R}{k_{RC} + R}\,C \tag{1.7a}$$

$$\frac{dC}{dt} = (\mu_{RC}\frac{R}{k_{RC} + R} - D - m_C)\,C \tag{1.7b}$$

To illustrate the relationship between the mass-balance formulation and the RM model we eliminate N with $H = 0$. The resulting term depends on C as well as on R. Consequently, the asymptotic growth rate of the resource depends also on the consumer C whereas with the logistic growth rate it depends solely on R. We conclude that the growth of the resource population is retarded because part of the ingested nutrients are meant for the consumer. The conservation law holds for the whole community and therefore if the resource population itself is consumed this effect is even larger.

If $m_R > 0$ and $m_C > 0$, both the products excreted by the resource population and the consumer population both consist of two terms. One term is associated with the assimilation process which is proportional to the functional response times the biomass and the other is related to the maintenance process and is proportional to the biomass. Observe that the mass-balance model cannot be reduced when $m_R > 0$ and or $m_C > 0$.

Two dimensional autonomous systems and hence also the RM model (1.7), cannot show chaotic behaviour but three dimensional systems can, [105]. The three dimensional mass-balance model (1.6) is analysed in [72] where we found that chaos can occur for biologically meaningful parameter values. Obviously the additional degree of freedom obtained from the modelling of the nutrients explicitly is important.

1.2.4 Small-scale food chain models

If the consumer is in its place consumed by a predator population the food chain consists of three species and one nutrient. The RM model formulation in which the nutrient is again modelled implicitly is studied in the literature to a fair degree. In [61] and later in [60] it was shown through simulation that chaotic behaviour can occur in the so-called three species

(resource, herbivore, carnivore) RM model.

$$\frac{dR}{dt} = r(1 - \frac{R}{K})R - I_{RC}\frac{R}{k_{RC} + R}\,C \tag{1.8a}$$

$$\frac{dC}{dt} = (\mu_{RC}\frac{R}{k_{RC} + R} - D - m_C)C - I_{CP}\frac{C}{k_{CP} + C}\,P \tag{1.8b}$$

$$\frac{dP}{dt} = (\mu_{CP}\frac{C}{k_{CP} + C} - D - m_P)\,P \tag{1.8c}$$

This system has been analysed in great detail by means of bifurcation analyses t [17, 49, 90, 92, 98, 99]. The long-term dynamics appear to be very rich. In addition to the familiar local bifurcations, transcritical, tangent (or saddle-node) and Hopf-bifurcation, global bifurcations were found. Sometimes these global bifurcations, such as the saddle-focus Shil'nikov bifurcation [90], form a 'skeleton' for the period doubling of which a cascade leads to chaotic dynamics. In other cases, such as the homoclinic bifurcation for a limit cycle marks interior and boundary crises, see [17, 50, 51, 105]. A discussion of the various types of global bifurcations that are mentioned in the literature on food web dynamics is beyond the scope of this review section.

In [93, 122] the interaction between the consumer and the resource population is modelled by a modified Leslie-Gower scheme described in [6]. The loss in a predator population is proportional to the reciprocal of per capita availability of its most favourite food. The generalist consumer is assumed to reproduce sexually. In this model Equation (1.8c) is replaced by

$$\frac{dP}{dt} = \mu_{CP}P^2 - I_P\frac{P^2}{k_{CP} + C} \tag{1.9}$$

Aziz-Alaoui (2002) stated that: "in the absence of the consumer the predator goes extinct if $\mu_{CP}k_{CP} < I_P$ and grows unbounded if the opposite, which is biologically not acceptable". Indeed this trichotomy is similar to that of exponential growth in the case the growth rate is proportional to P instead of proportional to P squared. Nevertheless, if this condition holds similar long-term dynamic behaviour is found, including the crisis route to chaos and the saddle-focus Shil'nikov bifurcation.

If the consumer C is consumed by a predator P then a straightforward extension of system (1.6) gives

$$\frac{dN}{dt} = (N_r - N)D - I_{NR}\frac{N}{k_{NR} + N}\,R \tag{1.10a}$$

$$\frac{dR}{dt} = (\mu_{NR}\frac{N}{k_{NR} + N} - D - m_R)\,R - I_{RC}\frac{R}{k_{RC} + R}\,C \tag{1.10b}$$

$$\frac{dC}{dt} = (\mu_{RC}\frac{R}{k_{RC} + R} - D - m_C)\,C - I_{CP}\frac{C}{k_{CP} + C}\,P \tag{1.10c}$$

$$\frac{dP}{dt} = (\mu_{CP}\frac{C}{k_{CP} + C} - D - m_P)\,P \tag{1.10d}$$

Figure 1.2 gives the stationary biomasses for the tri-trophic food chain as a function of N_r. Again, the results for N_r below the point TC_3, where the predator cannot invade the bi-trophic stable nutrient–resource–consumer system, are the same as those of Figure 1.1 for the bi-trophic food chain. On the right-hand side of the transcritical bifurcation TC_3 the predator can invade. On the left-hand side of the Hopf bifurcation H_2^- this is via a stable equilibrium

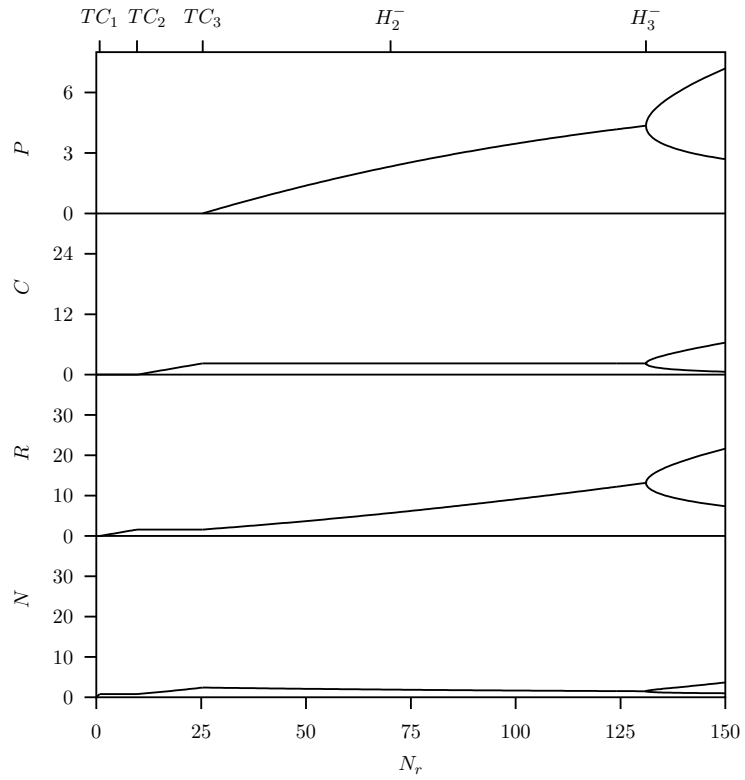

Figure 1.2: A one-parameter bifurcation diagram for a population (1.10) in the chemostat. The stationary biomass of the nutrient N, resource R, consumer C and predator P is depicted as a function of the nutrient level N_r. For high nutrient levels the system oscillates with extrema indicated.

of the bi-trophic food chain. However, on the right-hand side of H_2^- the equilibrium of the bi-trophic food chain itself is unstable and there is a stable limit cycle. The invasion criterion is now that the mean rate of increase of the predator size over the limit cycle has to be positive, instead of the rate of increase of the population size at the unstable equilibrium itself. Points in the parameter space where the mean growth rate is zero also mark a transcritical bifurcation, now a transcritical bifurcation of a limit cycle.

The tri-trophic system starts to cycle via a Hopf bifurcation, here denoted H_3^-. This bifurcation for the tri-trophic food chain occurs at a higher N_r value than the Hopf bifurcation H_2^- of the bi-trophic food chain. This means that in the parameter range between these points the predator stabilizes the bi-trophic food chain; it now invades via a stable boundary limit cycle and converges to a stable interior equilibrium.

Biomass distribution under nutrient enrichment Early ecologists like Elton (1927) were able to show that pyramids, by which is meant a decrease in biomass between successively higher trophic levels, are a consistent feature of real ecosystems [69]. The calculated biomass distribution for the bi-trophic (Figure 1.1) and tri-trophic (Figure 1.2) food chain do not follow this rule. The stable equilibrium biomass distributions are in agreement with the "cascade hypothesis" [123]. Increases in the nutrient input to the bottom of the system should increase the abundance of the top level and those that are even numbers of levels below the top and not affecting the abundances of those that are odd number of levels below the top. We refer to [1] for a discussion of the biomass distribution over the trophic levels when the equilibrium is unstable. The tri-trophic results of Figure 1.2 are often related to the "world is green" proposition [57]. The idea is that green plant biomass (the resources) accumulate in the world because predators keep consumers in check [11].

Routes to chaos The results in Figure 1.2 are depicted only for ranges of parameters where the dynamic behaviour is simple, such as an equilibrium or a limit cycle. In a number of papers this mass-balance model of tri-trophic food chain was analysed using numerical bifurcation analysis [16,18,73,74]. A rich repertoire of long-term dynamic behaviour was found for relative high dilution rates and high nutrient supply concentrations. As an example, in Figure 1.3.a a chaotic attractor in the state-space is shown for the tri-trophic food chain with the per capita loss terms zero.

Chaotic behaviour itself may be interesting, but routes to chaos are also important. The most observed route is via a cascade of period doubling. The system starts to oscillate at a Hopf bifurcation. The emanating stable limit cycle becomes unstable via a so called flip bifurcation. At that point, in addition to the unstable limit cycle, a stable (supercritical version) or unstable (subcritical version) limit cycle with a double period is born. Varying the parameter further, this process repeatedly leads to stable limit cycles with high periods and finally it ends up in chaos. Chaos can also end at boundary crises. Hastings (1996) also discussed this long lasting transient behaviour. This is illustrated in Figure 1.3 where for an intermediate parameter value a global homoclinic bifurcations to a saddle limit cycle occurs, as pointed out in [17]. On one side of the global bifurcation point there is coexistence of an interior chaotic attractor and a boundary limit cycle, but on the other side only the boundary limit cycle exist. Here starting in the interior the solution possibly follows the "ghost" of a chaotic attractor for a long time firstly and finally approaches an attractor where the top-predator is absent. Continuation of this global bifurcation in the parameter space for the

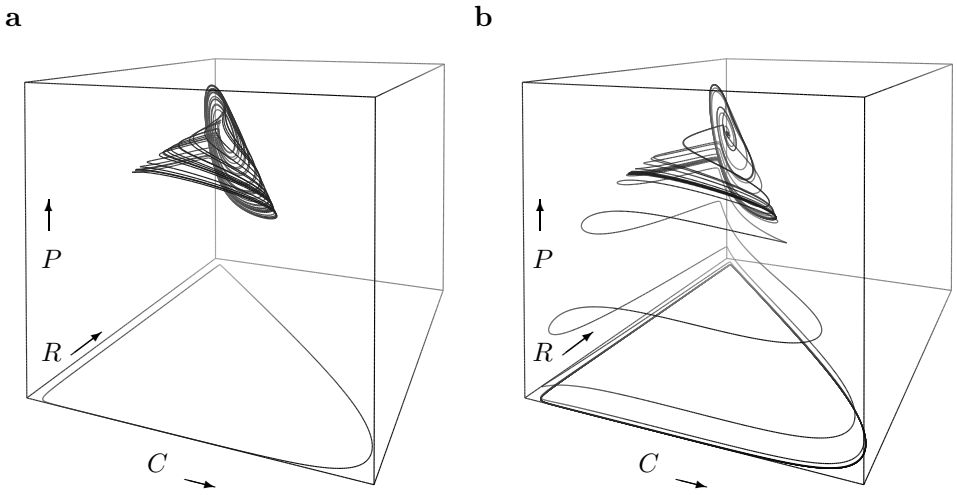

Figure 1.3: Phase plane plot for system (1.10) where $m_R = m_C = m_P = 0$ and control parameter values $N_r = 200.0$ and **a**: $D = 0.08732$ and **b**: $D = 0.0873$. For $D = 0.08732$ there are multiple attractors; a chaotic attractor and the attracting limit cycle which is characterised by the absence of the top-predator. The initial condition is chosen so that there is convergence to the chaotic attractor. For $D = 0.0873$ and similar initial conditions the solution follows the "ghost" of a chaotic attractor for a long time before approaching an attractor where the top-predator is absent.

tri-trophic food chain in the chemostat gives the boundaries of the regimes where chaotic behaviour occurs.

Multiple attractors occur for a considerable variety of control parameter values. Figure 1.3.a shows two attractors in the state-space. In the chaotic interior attractor all trophic levels coexist and in the other attractor a limit cycle exist in which the top-predator is absent. In general, starting near the saddle equilibrium gives chaotic dynamics whilst if P is initially small the system converges to the stable limit cycle where the top-predator is absent. The boundary between the two regions of attraction (the separatrix) is the stable manifold of a saddle cycle [16].

In [74] a top-predator that feeds on the predator is introduced. The bifurcation pattern of this four-species food chain indicate also that regions of persistence for food chains with increasing length are nested. That is, higher nutrient input is required for a top-predator to be able to invade while at the same time the trough-put rate may not be too high. The interval where invasion is possible is bounded by the transcritical bifurcations $TC_i, i = 1, 2, ...$ The nutrient levels at which these bifurcations occur, increase with the length of the food chain, compare Figure 1.1 and 1.2. These equilibria are stable within a nutrient level range between TC_i and H_i^-. This suggests that, theoretically, long food chains can persist.

1.2.5 Small-scale food web models

In food webs different trophic levels are distinguished and a population can consume multiple populations at a lower level. Therefore, at the same time two new trophic interactions can occur besides predator-prey interaction, namely competition for resources where multiple predators consume one resource and one predator consuming multiple resources. In [71,76] we used numerical bifurcation analyses to study the dynamics of a nutrient–resource–competitor–

predator system. Competitive exclusion prevents coexistence of the resource and competitor populations feeding both on the nutrient in the chemostat. The equations for this simple food web are

$$\frac{dN}{dt} = (N_r - N)D - I_{NR}\frac{N/k_{NR}}{1+N/k_{NR}}\,R - I_{NM}\frac{N/k_{NM}}{1+N/k_{NM}}\,M\ , \tag{1.11a}$$

$$\frac{dR}{dt} = R\big(\mu_{NR}\frac{N/k_{NR}}{1+N/k_{NR}} - D - m_R\big) - I_{RC}\frac{R/k_{RC}}{1+R/k_{RC}+M/k_{MC}}\,C\ , \tag{1.11b}$$

$$\frac{dM}{dt} = M\big(\mu_{NM}\frac{N/k_{NM}}{1+N/k_{NM}} - D - m_M\big) - I_{MC}\frac{M/k_{MC}}{1+R/k_{RC}+M/k_{MC}}\,C\ , \tag{1.11c}$$

$$\frac{dC}{dt} = C\big(\frac{\mu_{RC}R/k_{RC}+\mu_{MC}M/k_{MC}}{1+R/k_{RC}+M/k_{MC}} - D - m_C\big)\ . \tag{1.11d}$$

That is, for the consumer C, both the consumer populations R and the competitor population M are substitutable. This implies that a deficiency in one of the resources can be compensated by using the other, so both are non-essential. Most heterotrophs probably consume resources that are substitutable.

The results for system (1.11) are presented by one-parameter diagrams where N_r is the bifurcation parameter. The diagram for the nutrient–competitor–predator N, M, C system looks similar to the one for the nutrient–resource–consumer N, R, C system given in Figure 1.1 except that the system start to oscillate earlier. The reader is referred to [76] for more detailed results.

For a given dilution rate $D = 0.02$ and without predation the competitor always wins. However, with predation, the results depicted in Figure 1.4 differ greatly.

Below the transcritical bifurcation point TC_{31} the results are those for the N, M, C system. At the point TC_{31} the resource is able to invade this system and the interior solution for the full food web is stable. Increasing N_r this remains true until the transcritical bifurcation point TC_{32} is reached at which the competitor becomes extinct. Hence, above this point the results for the N, R, C system shown in Figure 1.1 are valid. These results imply the following invasion scenarios. For $N_r = 25$ the N, R, C system can be invaded by the competitor and it replaces the resource population. For $N_r = 50$ the N, R, C system can be invaded by the competitor and the N, M, C system can be invaded by the resource. So, there is mutual invasibility. In both cases after invasion with $N_r = 50$, an interior equilibrium for the whole food web is the result. For $N_r = 75$ the N, M, C system can be invaded by the prey that replaces the competitor. The resulting N, R, C system can not be invaded by the competitor.

When one attractor or multiple interior attractors exist, invasion does not have to lead to convergence to one of these attractors, but replacement can still occur. In [77, 85] we studied a tri-trophic food web with omnivory, that is the predator consumes the resources as well as the consumer. We showed that crossing a global bifurcation point, invasion of the consumer into the nutrient–resource–predator system leads to convergence to different attractors on both sides of this global bifurcation which is a connection between a boundary equilibrium and an interior limit cycle.

Resources can also be complementary. Then the two (or more) resources are essential at the same time, they cannot be substituted by the other, [121]. Autotrophs require mineral nutrients like carbon, nitrogen, phosphorus and sulfur. These are examples of multiple resources trophic interactions where resources are essential (see Grover (1997)). For essential resources often Liebig's "Law of the Minimum" is assumed where the consumer is limited by

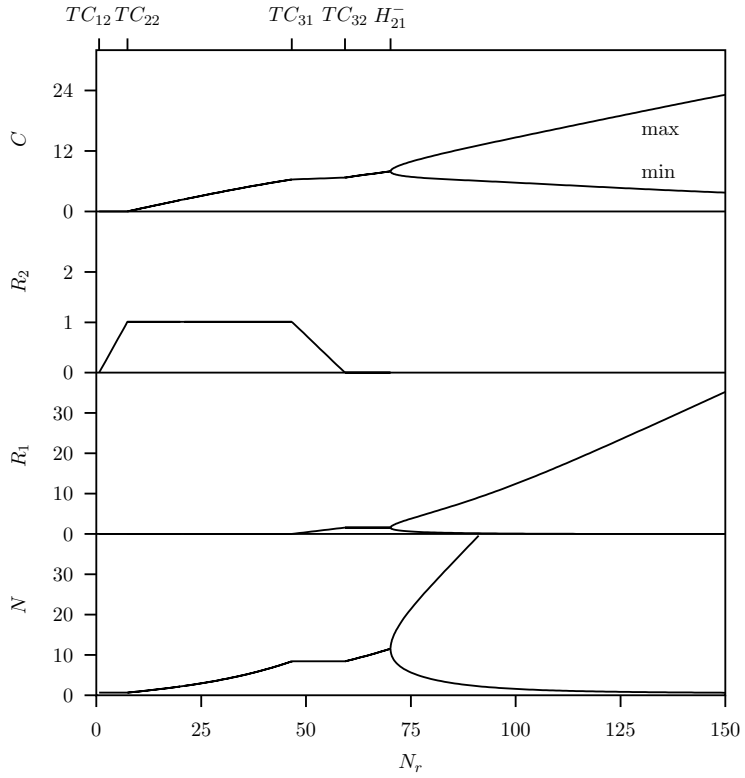

Figure 1.4: A one-parameter bifurcation diagram for food web (1.11) in the chemostat. The stationary biomass of the nutrient N, resource R, competitor M and consumer C is depicted as a function of the nutrient level N_r. For high nutrient levels the system oscillates with extrema indicated.

only one resource at a time and its growth rate depends on only the abundance of that most limiting resource. The rate of change of the consumer changes discontinuously when another resource becomes most limiting. The final values of the state variables before the switch are their initial values for the dynamics after the switch. Generally the resulting ODE system is well-posed because the Lipschitz condition is satisfied. With respect to parameter changes it is not that simple. The Jacobian matrix evaluated in an equilibrium may change discontinuously with respect to a varying parameter when another resource becomes most limiting. For example limit cycles with positive amplitude can emanate abruptly at a bifurcation point where on the one side of the bifurcation point where the switch occurs, the real parts of all eigenvalues are negative (stable equilibrium) and on the other side they are positive (unstable equilibrium). A formulation without switches and based on mechanistically well-founded principles called a synthesizing unit, is proposed in [78].

1.3 Discussion

Recently in [42, 115], predator prey cycles in an aquatic community consisting of a mineral resource (nitrogen), producer (green algae) and herbivore (rotifer) where found both experimentally and theoretically. The model is essentially the mass-balance model (1.6) where the consumer population is described by two state variables, the total rotifer biomass B and the biomass of the reproducing fraction C

$$\frac{dC}{dt} = \left(\mu_{RC}\frac{R}{k_{RC}+R} - D - m_C - \lambda\right) C \tag{1.12a}$$

$$\frac{dB}{dt} = \mu_{RC}\frac{R}{k_{RC}+R}\, R - (D + m_C)\, B \tag{1.12b}$$

The parameter λ is the decay rate of fecundity and m_C the mortality rate of the herbivore. This model shows, for the parameter range chosen in [42], coexistence at equilibrium, coexistence on limit cycles, or extinction of the predator or both populations. Qualitatively similar results were obtained with model (1.6) of which the results are depicted in Figure 1.1. It was concluded that the qualitative dynamical behaviour of this system consisting of equilibria, cycles and extinction is highly predictable by the simple model (1.6) where (1.6c) is replaced by (1.12).

Concrete evidence of chaotic dynamics in real populations has rarely been found. Causes are environmental stochasticity, biological variablity, poor data quality, but also the simplifying assumptions made to keep models manageable.

Studying the dynamics of the community can be performed by simulation at given initial values. Gaining insight into the dynamic behaviour of the community under various environmental conditions with this method will be computer-time consuming and large amounts of data will be generated. Finding the desired information from this bulk of data can be a formidable task.

An equilibrium of a dynamic system is just the solution of a set of algebraic equations, the equilibrium equations in which the changes of all state variables are set to zero. If the dimension of the system is high with multiple solutions, then it can still be problematic to find all the solutions. If multiple attractors (equilibria, limit cycles) exist, the state space is divided into different regions, the basins of attraction of which each attractor has one. Starting in a particular point in a basin, convergences to the specific attractor to which the basin belongs.

Finding the boundaries of these basins gives in a compact fashion a good overview of the long-term dynamics depend on initial conditions. In general the boundaries have a lower dimension than the total state space and therefore calculation of the basin boundaries saves computing time. Sometimes, performing simulations in time and starting in a sufficiently dense grid in the region of interest in the state space, is the only way to go; for instance if the basins of attraction are fractal.

If sensitivity of the long-term dynamics with respect to parameters is the subject of interest, we can repeat the calculations for different parameter settings and study the enormous amounts of data gathered in this way. In the case that the sensitivity with respect to the initial state variable is smooth, a reduction of efforts can be obtained by dividing the parameter space in regions with a specific long-term dynamic behaviour, such as stationary or oscillatory, or the composition of the community at the final state. It is advantageous to look for the boundaries of these regions, now in the parameter space. This presupposes that there is a criterion which can be checked to determine which region applies for specific parameter values. This is precisely what bifurcation analysis does. Coupled with continuation techniques it gives the opportunity to divide the parameter space in regimes with qualitatively different long-term dynamic behaviour. In the biological sense, it gives the circumstances under which a community can survive or, for example, how much fish can be landed without the danger of extinction.

In this review we have explained the bifurcation analysis approach by elaboration of some case-studies. The results are obtained as simple expressions derived by 'pencil and paper' or computer packages such as Maple and Mathematica to perform symbolic operations. In practice this is seldom the case and one has to use computer packages, we mention: AUTO [31], LOCBIF [65], CONTENT [91], DsTool [8] and XPPAUT [40].

A complete description of all possible uninvasible endpoints of a community assembly is problematic. In practice, using intermediate results, the parameters associated with the numerical algorithms (tolerances, continuation step size and discretization constants) have to be adjusted interactively by the user, so it seems impossible to generate complete bifurcation diagrams in a stand-alone process. It is a challenge to apply the bifurcation analysis approach, based on nonlinear dynamics system theory, to large-scale food webs and variable parameter models. That the bifurcations pattern, which include both local and global bifurcations, are robust with respect to model formulations is promising. This insight obtained from small-scale food webs can be used to find the relationship between web structure and dynamics in large-scale food webs.

Chapter 2

Predator-prey with Allee effects

Heteroclinic orbits indicate overexploitation in predator–prey systems
with a strong Allee effect.
G.A.K. van Voorn, L. Hemerik, M.P. Boer and B.W. Kooi
Mathematical Biosciences, 209:451-469.

In this section we deal with the dynamics of the predator–prey system where the prey population suffers from an Allee effect. A strong Allee effect is known to occur when near extinction the net prey growth rate is negative. A literatyre survey shows that this occurs in plant and animal populations. It leads to an extinction threshold, defined as a density below which population densities decrease. We discuss two models. In the Bazykin and Berezovskaya (1998) model the quadratic function in the general Lotka-Volterra model is replaced by a third order polynomial as the growth rate. Besides the toe zero growth rates of the logistic growth rate, the zero biomass and the carrying capacity, there is an intermediate biomass, the extinction threshold, with zero growth. We expand on their analysis of the model and explain the fact, why limit cycles seemingly are not supported by an Allee effect. The existence of a point-to-point heteroclinic cycle in these models is shown. In a two-parameter space the continuation of these cycles form the boundary of a region where the system collapse, that is where both populations go extinct. Different numerical methods for continuation of a globally connecting cycle are discussed.

2.1 Introduction

We study the rich dynamical behaviour of a predator-prey model described in [9] using numerical bifurcation analysis. In the Bazykin-Berezovskaya (BB)-model a strong Allee effect for the prey population is formulated by incorporation of an extra factor in the logistic growth equation such that the population growth rate is negative at zero biomass. The trophic interaction is modeled with a linear Lotka-Volterra functional response (see Eqn. (2.1) below), but qualitatively similar results are obtained for the in many cases more realistic Holling type II functional response (Holling, 1959) [62].

When the predator is able to invade the prey system that is subject to an Allee effect at its positive stable equilibrium, it becomes an unstable boundary equilibrium (saddle point) of the predator-prey system. Due to the predation and the existence of the two equilibria with only prey (both saddle points) a heteroclinic cycle between these two equilibria can

arise. Generally, invasion by the predator will lead to stable coexistence of both populations. However, there appears to be a Hopf bifurcation at which this positive equilibrium becomes unstable and the system starts to oscillate around that equilibrium when a parameter is varied. The stable limit cycle grows when the parameter is varied further. Then, at some point this periodic orbit touches the two saddle boundary equilibria, collides with these and disappears abruptly. As a consequence invasion of the predator leads to a total collapse of the system, where both the prey and predator population go extinct.

The region in the parameter space where an unstable positive equilibrium exists while the zero solution is globally attracting is bounded by a global bifurcation curve, that is, a heteroclinic cycle for the two saddle boundary equilibria. This curve is sketched in [9, page 86] and anticipated in [83]. Here, we calculate this curve by continuation, and we discuss the applicability of the numerical techniques proposed in [12, 13, 20, 21, 86] to continue homo- and heteroclinic connections. We also discuss the implications of an Allee effect for biological populations.

2.2 Formulation of the BB-model

The BB-model is described and analysed in [9]. The size of the prey population is denoted by $X_1(t) \geq 0$ and of the predator population by $X_2 \geq 0$. The prey population grows following the logistic equation (with growth rate $R \geq 0$ and carrying capacity K) extended for the strong Allee effect with threshold $L \geq 0$. The trophic interaction is modeled with a linear (or Lotka-Volterra) functional response with efficiency $E \geq 0$. Finally the predator population has a constant mortality rate $M \geq 0$. Then the governing equations read

$$\frac{dX_1}{dT} = RX_1(X_1 - L)(K - X_1) - AX_1X_2 \,, \tag{2.1a}$$

$$\frac{dX_2}{dT} = (EX_1 - M)X_2 \,. \tag{2.1b}$$

In [73] we pointed out that combining this equation with (2.1b) considered as the nutrient–prey–predator system violates the mass balance. Nevertheless, because system (2.1) is mathematically more tractable than the full mass-balance equation we analyse this system and we stress that the latter system can display more complex dynamics.

System (2.1) can be made dimensionless by setting $t = TRK^2/k^2$, $x_1 = kX_1/K$ and $x_2 = k^2X_2A/(RK^2)$ where $l = kL/K$, $e = E/(RK)$ and $m = M/(EK)$. This gives the dimensionless form of the predator–prey system

$$\frac{dx_1}{dt} = x_1(x_1 - l)(k - x_1) - x_1x_2 \,, \tag{2.2a}$$

$$\frac{dx_2}{dt} = e(x_1 - m)x_2 \,, \tag{2.2b}$$

where l and m are compound parameters which will serve as bifurcation parameters.

2.3 Bifurcation analysis of the BB-model

The local bifurcations are analysed in [9, page 85] and in the textbook [83, Chapter 8]. We start with a summary of the results. In addition to the stable trivial equilibrium point E_0

point $(0,0)$ (the eigenvalues are $-l$ and $-m$), there are two boundary equilibria with positive prey and zero predator biomass density, namely two equilibria E_2 point $(1,0)$ (the eigenvalues are $l-1$ and $1-m$), and E_1 point $(l,0)$ (the eigenvalues are $l-m$ and $l-l^2$). Furthermore there is a positive equilibrium E_3 point $(m,(m-l)(1-m))$ in the region $m > l$ and $0 < m < 1$ of the parameter space (l,m). At that equilibrium point we have $\operatorname{tr}(\mathbf{J}) = m(1-2ml)$ and $\det(\mathbf{J}) = m(1-m)(m-l)$ so that $\operatorname{disc}\mathbf{J} = \operatorname{tr}\mathbf{J}^2 - 4\det\mathbf{J}$ and the eigenvalues read $\lambda_{1,2} = (\operatorname{tr}\mathbf{J} \pm \sqrt{\operatorname{disc}\mathbf{J}})/2$. So, the equilibria are given by

$$E_0 := (0,0)\ , \tag{2.3a}$$
$$E_1 := (l,0)\ , \tag{2.3b}$$
$$E_2 := (1,0)\ , \tag{2.3c}$$
$$E_3 := (m,(m-l)(1-m))\ . \tag{2.3d}$$

In Figure 2.1 the three dimensional plot with one free parameter m and two state variables: x_1, x_2 is shown. Figure 2.2 gives the long-term dynamics of the biomasses of the prey and predator population where $l = 0.5$ and m is varied. There are two transcritical bifurcation curves denoted by TC, at $m = 0.5$ and $m = 1$ where the equilibrium value for the predator population equals zero, $x_2 = 0$. A Hopf bifurcation point where $Re(\lambda_{1,2}) = 0$ denoted by

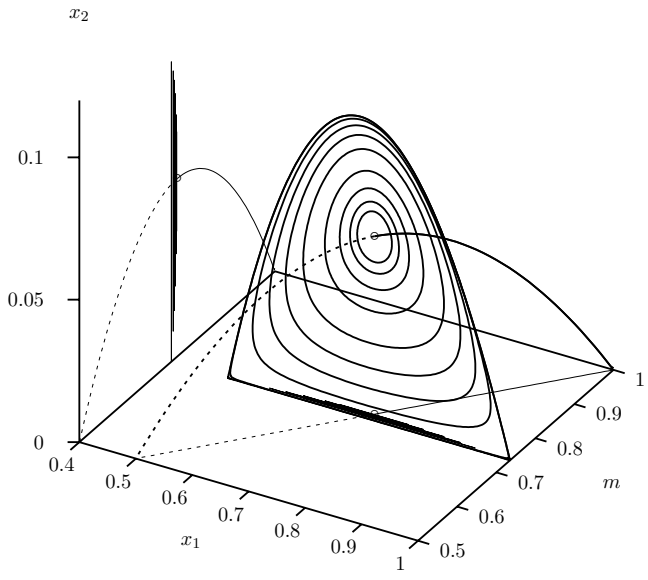

Figure 2.1: A three dimensional bifurcation diagram with one free parameter and two state variables: x_1, m, x_2 and $l = 0.5$ fixed. The equilibrium curve and its vertical projection is also shown; solid line: stable and dashed line: unstable.

H_3 occurs at $m = 0.75$, the subindex 3 is because this is a bifurcation point for equilibrium

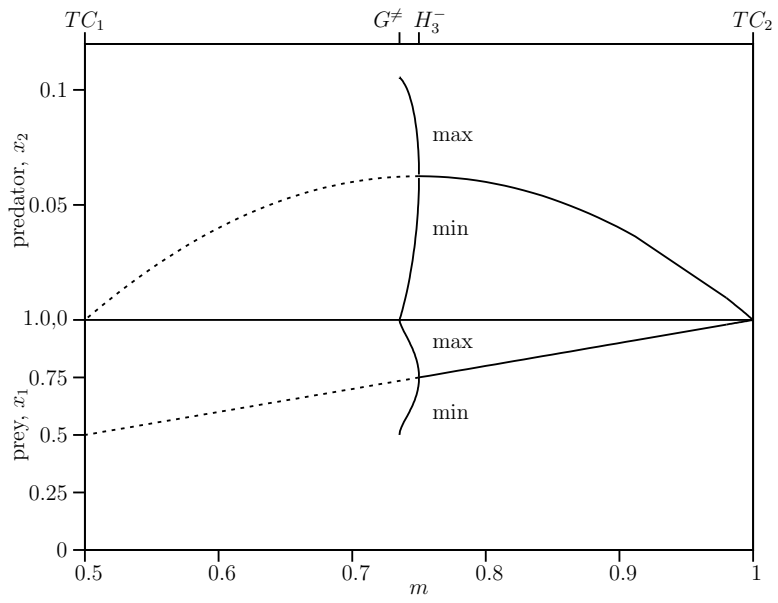

Figure 2.2: One-parameter bifurcation diagram with free parameter m for predator-prey model with Allee effect for prey population system (2.2) where $e = 1$, $k = 1$ and $l = 0.5$. Points TC_1 and TC_2 are transcritical bifurcation points. Point H_3 is the Hopf bifurcation point and $G^{\neq}$ indicates the heteroclinic orbit. Between these two points the solution is a stable limit cycle of which the extrema are plotted. At the heteroclinic orbit the prey biomass ranges from 0.5 to 1 while the predator biomass becomes very small during one cycle of which the period is infinitely large. Region A: bistability $E0$ or $E2$; Region B/C: positive stable equilibrium $E3$, Region D: positive stable limit cycle $E3$, E: zero equilibrium $E0$ is global attracting when predator is invading.

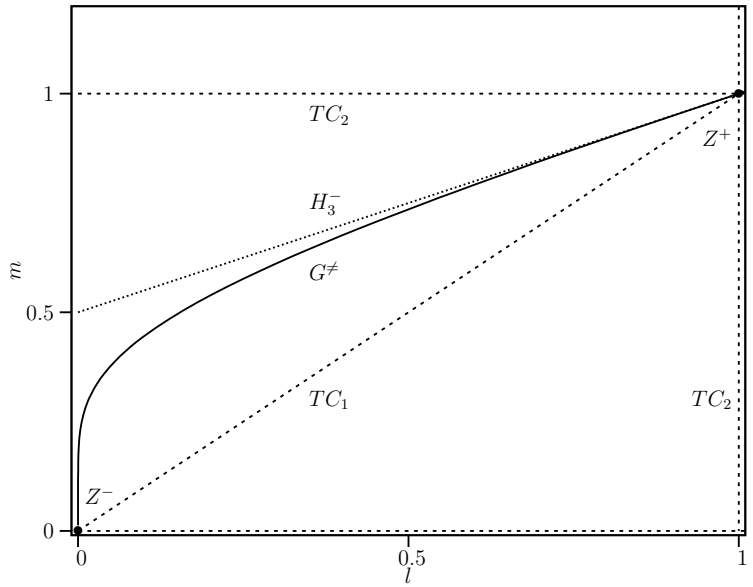

Figure 2.3: Two-parameter bifurcation diagram for predator-prey system (2.2). The bifurcation parameters are l (the threshold value of the Allee effect) and m (the mortality rate of the predator). Curves TC are transcritical bifurcation curves. At the curves TC and TC the predator biomass equals zero, that is these curves mark regions where both population can coexists. At N the predator biomasses is negative and therefore this curve is not interesting from a biological point of view. Curve H_3 is the supercritical Hopf bifurcation curve and $G^{\neq}$ the heteroclinic orbit. The points Z^+ point $(1, 1)$ and Z^- point $(0, 0)$ are different types of codim 2 points.

E_3. Below this Hopf bifurcation point the positive equilibrium is unstable and a stable limit cycle around this point exists (we recall that the system is two dimensional and Poincaré–Bendixson theorem [83, page 137] applies). Lowering m gives an increasing period of this limit cycle. The period goes to infinity at a global bifurcation point, denoted by $G^{\neq}$. At that point the minimum value during the cycle goes to zero and the peak value to the carrying capacity equal to $k = 1$.

The two-parameter bifurcation diagram is given in Fig. 2.3. The curve $m = 0$ is a curve, denoted by N, where each point is an equilibrium with two zero eigenvalues. Substitution of $m = 0$ in Eqn. (2.2) shown that with $x_1 = 0$ all values for x_2 give an equilibrium, so there is a continuum of solutions. There are several transcritical bifurcation curves TC. Two transcritical bifurcation curves are associated with the equilibrium E_2 originating $l = 1$ and $m = 1$. The vertical curve $l = 1$ and the horizontal curve $m = 1$ are both transcritical curve TC_2. The curve TC_1 on the diagonal $m = l$ is associated with the equilibrium E_1. Above the horizontal curve TC_2 and below the diagonal curve TC_1, denoted by region A the predator is absent and the prey population is at carrying capacity equilibrium E_2 or zero equilibrium E_0, depending on the initial state. Between the last two curves in region denoted by B/C there is a positive equilibrium E_3. In this region there is a Hopf bifurcation curve H_3 described by the relationship $m = 0.5l + 0.5$. Between this curve and the global bifurcation curve $G^{\neq}$ denoted by region D, the positive equilibrium is unstable and a positive stable limit cycle exists. Below the curve $G^{\neq}$, denoted by region E the trivial solution E_0 is the global attractor. Below the

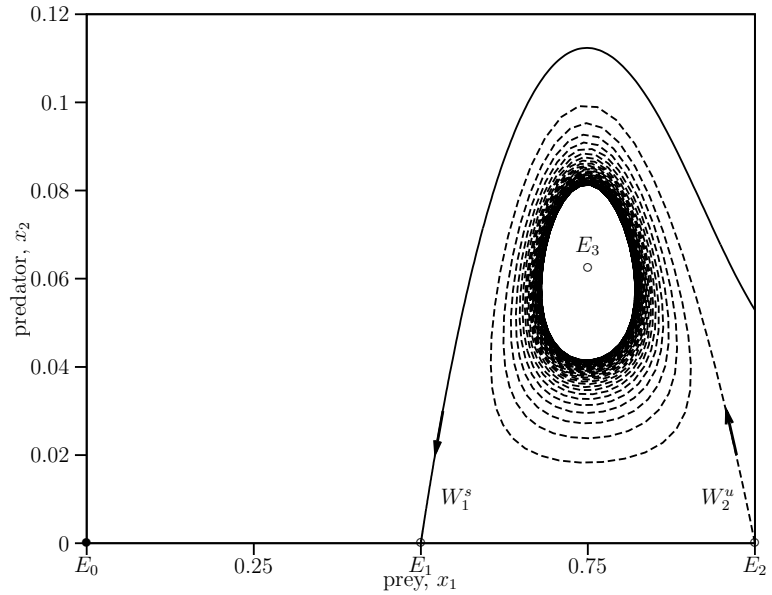

Figure 2.4: Stable and unstable manifold where $m = 0.74837$ and $l = 0.5$. For the saddle E_2 point $(1, 0)$ the unstable manifold W_2^u (dashed line) and for the saddle E_1 point $(0.5, 0)$ the stable manifold W_1^s (solid line) are shown. Since the m-value is between the Hopf bifurcation H_3 and the heteroclinic orbit $G^{\neq}$ values, there is a stable limit cycle. All orbits above the stable manifold W_1^s converge to the stable zero equilibrium E_0 point $(0, 0)$. All orbits below the stable manifold W_1^s converge to the stable limit cycle.

diagonal in region F, E_0 is also the global attractor.

In order to get more insight into the dynamics around the global bifurcation point $G^{\neq}$ we study the dynamics in the phase plane for fixed $l = 0.5$ while we vary m in the next three Figs. 2.4, 2.5 and 2.6.

Figure 2.4 shows the stable and unstable manifold where $m = 0.74837$ and $l = 0.5$. For the saddle E_2 point $(1, 0)$ the unstable manifold W_2^u and for the saddle E_1 point $(0.5, 0)$ the stable manifold W_1^s are shown. All orbits above this curve converge to the the zero equilibrium E_0 point $(0, 0)$. That is the stable manifold W_1^s acts as a separatrix for the stable limit cycle and the stable equilibrium E_0. The unstable manifold converges toward this stable limit cycle. These manifolds were calculated using DSTOOL [8].

In Fig. 2.5 the heteroclinic cycle is shown. It visits the two saddles E_1 point $(0.5, 0)$ and E_2 point $(1, 0)$. The cycle is broken into two pieces being heteroclinic connections between these two saddle points denoted by $G^{\neq}$. Outside the heteroclinic cycle the solution goes asymptotically to the stable zero state E_0. Inside the heteroclinic cycle there is convergence towards the heteroclinic cycle.

Figure 2.6 shows the stable and unstable manifold where $m = 0.735$ and $l = 0.5$. For the saddle E_2 point $(1, 0)$ the unstable manifold W_2^u and for the saddle E_1 point $(0.5, 0)$ the stable manifold W_1^s are shown. Now W_2^u is connected to E_0 point $(0, 0)$ while W_1^s is connected to the positive equilibrium E_3 which is a spiral source since the m-value is below the Hopf bifurcation value. All orbits above the W_2^u curve converge to the zero equilibrium E_0 point $(0, 0)$. Inside the curve bounded by the stable manifold of the saddle E_1 point $(0.5, 0)$ the

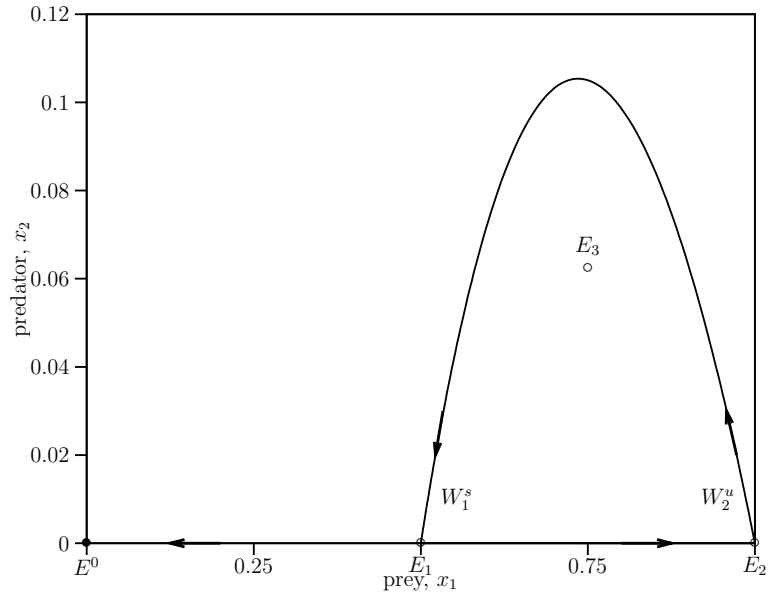

Figure 2.5: The heteroclinic connection plotted in the x_1, x_2 phase space for $l = 0.5$. The unstable manifold W_2^u and the stable manifold W_1^s intersect. For starting values inside the heteroclinic cycle the orbit converges outward to the heteroclinic cycle. With starting values outside the heteroclinic cycle the system converges to the stable zero equilibrium E_0 point $(0, 0)$.

orbit will oscillates and finally converges slowly to E_0 point $(0, 0)$ also. Observe that such an orbit can not leave this region by crossing the stable manifold which is invariant and due to uniqueness of the solution. The orbit can leave the region only via the narrow tunnel between the lowest part of the first turn of the stable manifold belonging to E_1 and the unstable manifold of E_2. This means that the stable limit cycle breaks open when the heteroclinic cycle occurs in the neighbourhood of the saddle E_2 where the stable manifold of E_1 and the unstable manifold of E_2 mismatch. Furthermore, even starting close to the spiral source the system makes a final oscillatory behaviour around the positive equilibrium before it eventually converges to E_0. Starting close to E_1 on the right-hand site of the stable manifold the system makes one single turn around the spiral source before extinction.

2.4 Heteroclinic cycle formulation and numerical methods

In this section we define the heteroclinic cycle (or loop) which occurs at the global bifurcation $G^{\neq}$. It is formed by two connections. One at the boundary of the positive quadrant of the state space (x_1, x_2), from E_1 to E_2, is the trivial branch where the predator is absent $x_2 = 0$ and the dynamics of the prey population is given by (2.2a). Hence this branch is not discussed further. The nontrivial branch is the intersection of the unstable manifold $W^u(\mathbf{x})$

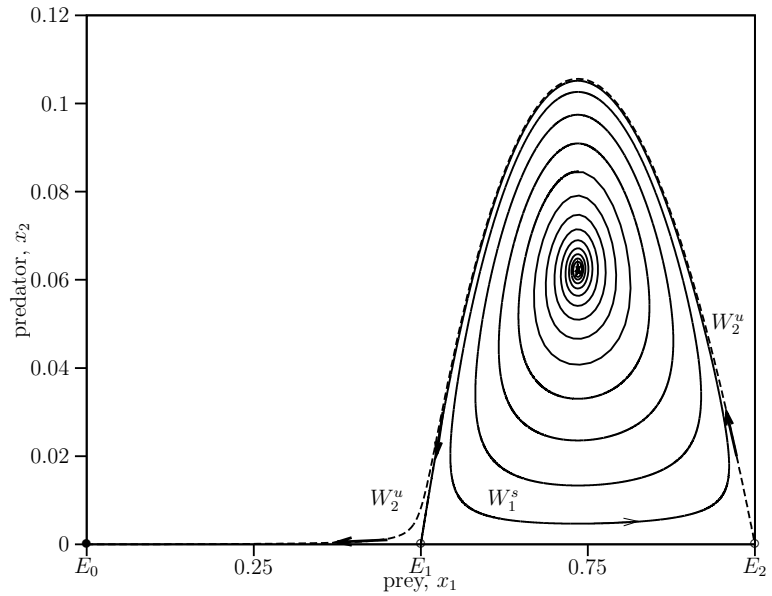

Figure 2.6: Stable and unstable manifold where $m = 0.735$ and $l = 0.5$, thus below $m^{\neq}$. For the saddle E_2 point $(1, 0)$ the unstable manifold W_2^u (dashed line) and for the saddle E_1 point $(0.5, 0)$ the stable manifold W^s (solid line) are shown. Since the m-value is below the heteroclinic orbit $G^{\neq}$ and hence below the Hopf bifurcation, there is an unstable positive equilibrium (spiral source). All orbits above the unstable manifold of E_2 point $(1, 0)$ curve converge directly towards the stable zero equilibrium E_0 point $(0, 0)$. Inside the curve bounded by the stable manifold of the saddle E_1 point $(0.5, 0)$, the orbit will oscillates and finally converges slowly to the stable zero equilibrium E_0 point $(0, 0)$ as well.

of the saddle E_2 and the stable manifold $W^s(\mathbf{y})$ of the saddle E_1. That is

$$\frac{d\mathbf{z}}{dt} = \mathbf{f}(\mathbf{z}) \,, \tag{2.4a}$$

$$\varphi^t(\mathbf{z}) \to \mathbf{x} \quad , \quad t \to -\infty \,, \tag{2.4b}$$

$$\varphi^t(\mathbf{z}) \to \mathbf{y} \quad , \quad t \to \infty \,, \tag{2.4c}$$

where $\mathbf{f} : \mathbb{R}^2_+ \to \mathbb{R}^2_+$ (the system is autonomous, hence there is no explicit dependency on time t) and equilibrium point $\mathbf{x}$ belongs to E_2, $\mathbf{y}$ belongs to E_1. The flow $\varphi^t : \mathbb{R}^2_+ \to \mathbb{R}^2_+$ corresponding to (2.4), that is, $\varphi^t(\mathbf{z}_0) = \mathbf{z}(t, \mathbf{z}_0)$ where the function $\mathbf{z}(t)$ considered as a function of t, is the solution starting at $\mathbf{z}_0$ of the boundary value problem (BVP) (2.4). The stable and unstable manifolds $W^u(\mathbf{x})$ and $W^s(\mathbf{y})$ are defined by

$$W^s(\mathbf{x}) = \{\mathbf{z} \in \mathbb{R}^2 | \varphi^t(\mathbf{z}) \to \mathbf{x} \text{ as } t \to -\infty\} \,, \tag{2.5a}$$

$$W^u(\mathbf{y}) = \{\mathbf{z} \in \mathbb{R}^2 | \varphi^t(\mathbf{z}) \to \mathbf{y} \text{ as } t \to \infty\} \,. \tag{2.5b}$$

In the previous section we showed that for a fixed l-value decreasing m yields a point where the period of the limit cycle goes to infinity while is passes both saddle points E_2 and E_1 closely. The global bifurcation is fixed by the parameter value where the cycle breaks via the heteroclinic cycle defined by (2.4).

The numerical schemes described in the next section were used to calculate and continue the heteroclinic cycle $G^{\neq}$ in the two-parameter diagram Fig. 2.3. This heteroclinic cycle curve connects two codim 2 points Z^+ point $(1, 1)$ and Z^- point $(0, 0)$. In end-point Z^- point $(1, 1)$ the heteroclinic cycle vanishes into the equilibrium point $(1, 0)$. The point Z^+ is on the intersection of transcritical bifurcations, TC_2 and TC_2, and the Hopf bifurcation curve H_3. At the critical codim 2 point Z^+ point $(1, 1)$, the Jacobian matrix evaluated at the equilibrium $(1, 0)$ is nilpotent of index 2, that is, there are two zero eigenvalues. Also at the other end-point Z^- point $(0, 0)$ the heteroclinic cycle is degenerated. At this point there is a continuum of solutions $x_1 = 0$ and $x_2 \in \mathbb{R}$, so the predator biomass is not determined. The eigenvalue of the single stable equilibrium $(0, 0)$, and is a double 0 with eigenvector $(1, 0)$ and generalized eigenvector $(0, 1)$. The global bifurcation curve $G^{\neq}$ intersects the transcritical bifurcation TC_1 curve and the curve N of which each point is an equilibrium with a continuum of solutions $x_1 = 0$ and $x_2 \in \mathbb{R}$.

2.4.1 Formulation of the truncated boundary conditions

Calculating the global bifurcation curve boils down to solving the BVP (2.4) and its continuation. The BVP is truncated into a finite time interval $(-T, T)$ where T is large enough, and certain boundary conditions BC's at the end points of that interval are imposed. An appropriate ODE solver can be used to calculate the orbit. In the following we will discuss two techniques.

First the BC's have to be adapted to this finite time interval. The local linear approximation of the unstable invariant manifold $W^u(\mathbf{x})$ is denoted as $T^u(\mathbf{x})$ and of the stable invariant manifold $W^s(\mathbf{y})$ is denoted as $T^s(\mathbf{y})$. This requires calculation of the Jacobian matrix evaluated at the saddle points, its eigenvalues and eigenvectors. For system (2.2) this can be done analytically but this is not exploited here.

The saddle equilibria and the eigenvalues and eigenvectors of the Jacobian matrix evaluated in that point are calculated by solving

$$\mathbf{f}(\mathbf{z}) = 0 \,. \tag{2.6}$$

where $\mathbf{z}$ is the equilibrium and

$$\mathbf{J}\ \mathbf{p} = \lambda\ \mathbf{p}\ , \tag{2.7}$$
$$\langle \mathbf{p}, \mathbf{p} \rangle = 1\ , \tag{2.8}$$

where λ is the eigenvalue, $\mathbf{p}$ the associated eigenvector and $\langle \mathbf{r}, \mathbf{s} \rangle = \mathbf{r}^T \mathbf{s}$ is the standard scalar product in $\mathbb{R}^2$.

In some formulations the eigenvalues and eigenvectors of the adjoint Jacobian matrix evaluated in that point are used

$$\mathbf{J}^T\ \mathbf{q} = \lambda\ \mathbf{q}\ , \tag{2.9}$$

where λ is again the eigenvalue, the same as for the original Jacobian matrix, $\mathbf{q}$ the adjoint eigenvector corresponding the eigenvalue. The eigenvectors are normalized by

$$\langle \mathbf{q}, \mathbf{q} \rangle = 1\ , \tag{2.10}$$

When $\mathbf{p}$ and $\mathbf{q}$ correspond to different eigenvalues we have $\langle \mathbf{p}, \mathbf{q} \rangle = 0$, that is they are orthogonal.

Generally no explicit expressions are know for the equilibrium values, the eigenvalues and the eigenvectors and each set of equations for the two saddles E_1 and E_2 leads to the additional scalar equations for additional scalar variables which are solved at each continuation step. Although here analytical expressions are available, these quantities are numerically determined.

With explicit BC's we use the local linearizations of the stable and unstable manifolds at E_2 and E_1, respectively. The BC's read [41]

$$\mathbf{z}(-T) = \mathbf{x} + \varepsilon \mathbf{p}_u^-\ , \tag{2.11a}$$
$$\mathbf{z}(T) = \mathbf{y} + \xi \mathbf{p}_s^+\ , \tag{2.11b}$$

where ε and ξ are two fixed sufficiently small parameters and $\mathbf{p}_u^-$ is the eigenvector belonging to the negative eigenvalue at E_2, in Fig. 2.5 tangent to the unstable manifold W_2^u and $\mathbf{p}_s^+$ is the eigenvector belonging to the positive eigenvalue at E_1 in Fig. 2.5 tangent to the stable manifold W_1^s.

2.4.2 Numerical techniques to solve and continue bvp

In order to solve the BVP we can distinguish two popular numerical techniques, namely the (single and multiple) shooting method and the orthogonal collocation method. The methods can be used together with each boundary condition formulation: projection and/or explicit.

To start the calculation of the heteroclinic connection in both approaches, we have to start with an appropriate initial guess for the connection. We used the part of the stable limit cycle for fixed l and varying m to a m-value where the period of the limit cycle was large, and the orbit passes the two saddles closely (see Fig. 2.2).

Shooting methods

Shooting methods for solving BVP of ODE-systems are combinations of an initial value problem (IVP) solver and a non-linear set of equations solver. Starting point is the formulation of the initial conditions the explicit BC's at E_2 (2.11a), of which some are the boundary conditions at one end while the remaining variable have to be guessed (within a continuation procedure the values in a previous step can be used). However, the solution of this IVP does not fulfil exactly the boundary conditions at the other end, the final point mentioned above (2.11b). In this way this method yields a system of equations depending on the unknown initial variables. These equations can be solved by, for instance, Newtonian equation solvers.

The continuation of the connection was done by means of a predictor-corrector continuation method with step-size control [4, 86, 108].

In [77, Appendix] this method is described for the calculation of a heteroclinic connection between an equilibrium point and a limit cycle of four dimensional system consisting of a nutrient, prey, predator and omnivore. The predator as well as the prey is consumed by an omnivore. The heteroclinic cycle in the parameter space separates two regions with convergence to an positive stable equilibrium or convergence to a boundary limit cycle.

We describe the implementation of a multiple shooting method for the calculation of the heteroclinic cycle of system (2.2). In order to get reliable results for the whole parameter range close to $l = 1$ and $m = 1$ the equations a midpoint $\mathbf{u}$ is introduced in the plane given by

$$\mathbf{u} = \varphi^0(\mathbf{x} + \varepsilon \mathbf{p}_u^-) \,, \tag{2.12}$$

$$0 = \langle \mathbf{x} - \mathbf{y}, \mathbf{u} - 0.5(\mathbf{x} + \mathbf{y}) \rangle \,. \tag{2.13}$$

where $\varphi^{-T}(\mathbf{x} + \varepsilon \mathbf{p}_u^-) = \mathbf{x} + \varepsilon \mathbf{p}_u^-$.

The truncated heteroclinic cycle starts at the distance fixed by the scalar ε from E_2 with equilibrium point $\mathbf{x}$ on the local linear approximation $T^u(\mathbf{x})$, of the unstable manifold $W_2^u(\mathbf{x})$ fixed by the eigenvector corresponding to the positive eigenvalue of the Jacobian evaluated at $\mathbf{x}$. Staring in this point the system is solve numerically using a Runge-Kutta method for a fixed time period T: this point is denoted by $\mathbf{u}$. Thereafter integration starts from point $\mathbf{u}$ till a point on the stable manifold W_1^s is reached of E_1 with equilibrium point $\mathbf{y}$ by Eqn. (2.11b) is reached.

Orthogonal collocation methods

With collocation methods the solution is approximated by piecewise polynomials leading to a huge system of non-linear equations which has to be solved numerically using some Newtonian method. In AUTO [36] this technique is efficiently implemented together with a pseudo-arclength continuation technique. For local bifurcations the code detects higher order codimension bifurcations and calculates after detection the emanating branches of these bifurcations.

We used the computer package AUTO in two modes. First the part of AUTO called HomCont [31, Chapter 16], a collection of easy to use subroutines for the continuation of homo- and heteroclinic cycles. Secondly, we implemented the BC's in AUTO using facilities described in [31, Chapter 11] to solve the BVP's.

2.5 Discussion and conclusions

Characteristic for the strong Allee effect is the existence of three equilibria where the two extreme points are stable and one saddle equilibrium in the middle. The stable manifold of the saddle forms the separatrics in the phase plane for the two attractors. When the population is predated the positive equilibrium becomes also unstable, Then generally after invasion of the predator the system converges to a stable positive equilibrium. However, this equilibrium can become unstable at a Hopf bifurcation giving rise to stable limit cycles. Varying a parameter further can lead to a heteroclinic cycle. This is a global phenomenon since it can not be detected by local analysis of the equilibrium points involved. After this point the is a collapses of the complete system.

The two-parameter diagram Fig. 2.3 shows that there is only a positive equilibrium or limit cycle in an intermediate range of the mortality range of the predator.

We found a global bifurcation denoted by $G^{\neq}$ depicted in Fig. 2.3. This global bifurcation is a heteroclinic cycle that consists of two heteroclinic connections between two saddle equilibria in the zero predator biomass plane. This curve marks the region in the (l, m) parameter space where a collapse of the complete system occurs after invasion of the predator into the prey population at stable positive equilibrium. The global bifurcation was sketched in [9, page 86], but here we give algorithms to calculate this curve by continuation. This curve separates the region in the parameter space with positive coexistence of the prey and predator populations from the region where the system collapses and each initial point leads to convergence to the zero biomass state.

The bifurcation curve $G^{\neq}$ was calculated with AUTO [36] by using ordinary differential equation two-point boundary-value problem (BVP) solver facilities of AUTO based on the orthogonal collocation method. For the BB-model we also used the multiple shooting method with one intermediate step. The calculated curves with both methods are the same. We also used the more user-friendly HomCont [31, Chapter 16] program. Here in the region close to point Z^+ in Fig. 2.3 the user has to take case that the truncation time interval is allowed to increase when this point is approached.

The orthogonal collocation method with BVP formulation with explicit boundary conditions at both saddle points worked best. With the other BC formulations satisfactory results close to point Z^+ were obtained after introduction of an additional continuation step where the truncated time interval was enlarged.

The multiple shooting method using one midpoint $\mathbf{u}$, gave reliable results for the whole parameter range $0 \leq l \leq 1$ and $0 \leq m \leq 1$.

We conclude that the BVP solver implemented in AUTO gives flexibility in the choice of the formulation of the boundary conditions at the cost of coding of all boundary and integral conditions and no detection of the various higher order bifurcation points implemented in HomCont [31, Chapter 16].

In [25] using a size-structured, individual-based model show that catastrophic population collapses may be an intrinsic property of many communities, because of two general aspects of individual life history: size- and food-dependent individual growth and individual mortality decreasing with body size. Positive density dependence, characteristic for depensatory growth mechanisms and catastrophic behavior, results as a direct and robust consequence of the interplay between these individual life-history traits, which are commonly found in many species.

Chapter 3

Two stage population model

Multiparametric bifurcation analysis of a basic two stage population model
S.M. Baer, B.W. Kooi, Yu. A. Kuznetsov, H.R. Thieme
SIAM Applied Mathematics, 66(4):1339-1365.

In this section we investigate long-term dynamics of the most basic model for stage-structured populations, in which the per capita transition from the juvenile into the adult class is density dependent. The model is represented by an autonomous system of two non-linear differential equations with four parameters for a single population. We find that the interaction of intra-adult competition and intra-juvenile competition gives rise to multiple attractors, one of which can be oscillatory. A detailed numerical study reveals a rich bifurcation structure for this two dimensional system, originating from a degenerate Bogdanov-Takens (BT) bifurcation point when one parameter is kept constant. Depending on the value of this fixed parameter, the corresponding triple critical equilibrium has either an elliptic sector or it is a topological focus, which is demonstrated by the numerical normal form analysis. It is shown that the canonical unfolding of the codimension-three BT point reveals the underlying dynamics of the model. Certain new features of this unfolding in the elliptic case, which are important in applications but have been overlooked in available theoretical studies, are established. Various three-, two-, and one-parameter bifurcation diagrams of the model are presented and interpreted in biological terms.

3.1 Introduction

We deal with a model for one population with two stage introduced in [82] and further studied in [120, Chapter 11]. The life-history of the individuals comprises a juvenile and an adult stage. The population state is the number of juveniles and adults. Juveniles and adults die, while adults reproduce. The transition rate between the two stages, together with the per capita mortality and reproduction rates, form the parameters of the two first-order ordinary differential equations (ODE's) which specify the time derivative of the population state.

Our stage-structured population model is a two dimensional system with four parameters. When one parameter is fixed (b), a degenerate Bogdanov-Takens bifurcation (BT point for short) with a triple critical equilibrium is found. Different types of such degenerate BT points are studied in detail in [10, 37] where three categories of topological types are distinguished: the saddle, focus, and the elliptic case. We will derive a normal form with terms up to and

including fourth order for the codimension-three BT point by using a time re-parameterization combined with a smooth transformation that also includes fourth order terms. This analysis reveals that the elliptic or focus case applies for the two stage population model depending on the value of the fixed parameter (b). When this parameter is varied a transition from elliptic to focus codimension-three BT bifurcation is found.

The truncated normal form of the codimension-three BT point in the elliptic case is embedded into an appropriate three-parameter family, and we study its unfolding by performing a numerical bifurcation analysis for the neighborhood of the origin in that three dimensional parameter space. In the three-dimensional parameter space, two branches of codimension-two BT curves emanate from the codimension-three point. These curves form the intersection of saddle-node and Hopf bifurcation planes. Furthermore, codimension-two Bautin bifurcations as well as codimension-two homoclinic orbits to neutral saddles originate from the codimension-three BT point. In two parameter space, codimension-one homoclinic bifurcation curves can originate from BT points. Both saddle, saddle-node and neutral saddle homoclinic orbit bifurcations actually occur. The analysis reveals unexpected similarities between the elliptic and the focus cases, which have been overlooked in earlier theoretical studies.

The normal form analysis results are used to interpret those of the numerical bifurcation analysis study of the full planar two stage population model and consequently also those reported in [120, Chapter 11].

3.2 The two stage population model

The model is introduced in [82] and further motivated in [120, Chapter 11]. The population is split into juveniles (larvae, e.g.) and adults, the numbers of which are denoted by $L(t)$ and $A(t)$ respectively. The system has the form

$$\frac{dL}{dt} = \beta(L,A)A - \mu(L,A)L - f(L,A)L\,, \tag{3.1a}$$

$$\frac{dA}{dt} = f(L,A)L - \alpha(L,A)A\,, \tag{3.1b}$$

where β is the per capita reproduction rate of an average adult individual, μ is the per capita mortality rate of an average juvenile individual (α for the adults) and f the per capita transition rate from the juvenile into the adult stage. In general, these rates can depend on both the densities of juveniles and adults.

As in [82], a Ricker-type function is chosen for the stage transition rate,

$$f(L) = \frac{\mu}{m}e^{-L}\,. \tag{3.2}$$

The reproduction rate $\beta(A)$ is chosen as

$$\beta(A) = g\big(\frac{m}{\mu}A\big)\,. \tag{3.3}$$

After introducing the scaled number of adults y as

$$y = \frac{m}{\mu}A, \tag{3.4}$$

the stage-structured population model becomes

$$\frac{dL}{dt} = \frac{\mu}{m}\big[g(y)y - mL - Le^{-L}\big] \,, \tag{3.5a}$$

$$\frac{dy}{dt} = Le^{-L} - y \,. \tag{3.5b}$$

At equilibrium, Equation (3.5b) gives a fixed relationship between y^* and L^* which is independent of all parameters. Note, from Equation (3.5a), that these values are independent of the parameter μ. We assume that the birth rate $g(y)$ is also of Ricker-type:

$$g(y) = e^{(1/b)(a-y)} \,. \tag{3.6}$$

3.3 Organizing centers

This section is partially based on [120, Section 11.9]. The system (3.5) has been scaled in such a way that the equilibria do not depend on the parameter μ. The origin $(L = 0, y = 0)$ is always an equilibrium.

The parameter m can be expressed as a function of the L-component of the interior equilibria, L^*,

$$m = \big[g(L^*e^{-L^*}) - 1\big]e^{-L^*} =: M(L^*) \,. \tag{3.7}$$

Figure 3.1 shows the graph of the function M for $b = 2.2$ and various values of a. The dotted curve marks points where $M'(L^*) = 0$ when a is varied. This curve cuts the horizontal axis $m = 0 = M(L^*)$ at $L^* = 1$ where $a = a_\sharp = 0.3679$.

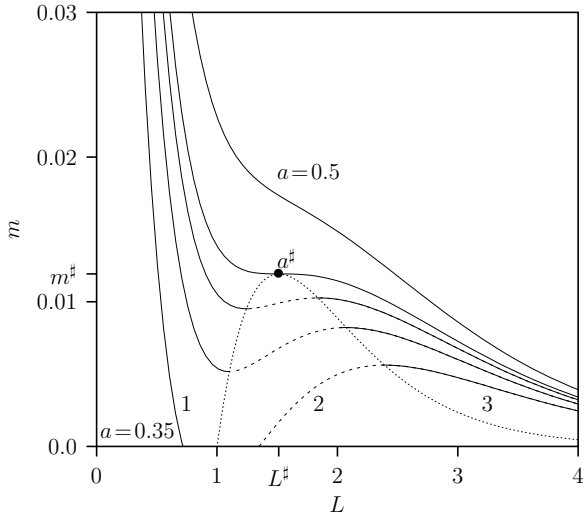

Figure 3.1: Graph of the function M for $b = 2.2$ and various values of a. From right to left: $a = 0.5$, $a = a^\sharp = 0.4492276697$, $a = 0.43$, $a = 0.4$, $a = 0.35$. The bullet gives the simultaneous point of inflection and critical point for $a = a^\sharp$. The dotted line connects the critical points where a is varied. The numbers label the branches where equilibrium E_i occurs at branch $i = 1, 2, 3$.

It can also be shown ([120, page 172]) that the trace of the Jacobian matrix evaluated at an interior equilibrium is a linear function of μ. The trace switches its sign from negative to positive at

$$\mu = \phi(L^*) := \frac{g(y^*) - 1}{L^* - g(y^*)}, \qquad y^* = L^* e^{-L^*}. \tag{3.8}$$

At $a = a^\sharp$ see Figure 3.1 the determinant and the trace of the Jacobian matrix evaluated at the equilibrium $(L^\sharp, y^\sharp)$ are zero. Therefore, for fixed $b > 0$ and $\mu = \mu^\sharp, m = m^\sharp$, and $a = a^\sharp$, we have a BT point. Moreover, the equilibrium is triple at this point, thus a degenerate BT point occurs.

For $b = 2.2$, we have

$$L^\sharp = 1.513180178, \;\; y^\sharp = 0.33321523 \tag{3.9}$$

and

$$\mu^\sharp = 0.01179614, \;\; m^\sharp = 0.01192386945, \;\; a^\sharp = 0.4492276697. \tag{3.10}$$

3.4 Normal form analysis

In this section we perform a normal form analysis of the degenerate BT point and study its canonical unfolding.

3.4.1 Critical normal form

First, we write system (3.1) for fixed $b > 0$ at the critical parameter values (3.10) in a coordinate system where the equilibrium with the coordinates (3.9) is shifted to the origin of the phase plane by the transformation

$$\mathbf{x} = \begin{pmatrix} x_1 \\ x_2 \end{pmatrix} = \begin{pmatrix} L - L^\sharp \\ y - y^\sharp \end{pmatrix}, \tag{3.11}$$

The transformed planar system becomes

$$\dot{\mathbf{x}} = \mathbf{J}\mathbf{x} + \mathbf{F}(\mathbf{x}) \,, \tag{3.12}$$

where $\mathbf{J}$ is the Jacobian matrix evaluated at the equilibrium and $\mathbf{F}(\mathbf{x}) = O(\|\mathbf{x}\|^2)$.

Next we use a similarity transformation to put the linear part in the Jordan canonical form. First we calculate two vectors $\mathbf{u}, \mathbf{v} \in \mathbb{R}^2$, such that

$$\mathbf{J}^2\mathbf{v} = 0 \,, \quad \mathbf{J}\mathbf{v} = \mathbf{u} \,, \quad \|\mathbf{u}\| = 1 \,, \tag{3.13}$$

where the vector norm is defined by $\|\mathbf{u}\|^2 = \langle \mathbf{u}, \mathbf{u} \rangle$ and $\langle \mathbf{u}, \mathbf{v} \rangle$ stands for the standard inner product in $\mathbb{R}^2$: $u_1 v_1 + u_2 v_2$. These two vectors (the eigenvector $\mathbf{u}$ and the generalized eigenvector $\mathbf{v}$), are linearly independent and form a basis in the plane. Notice that $\mathbf{v}$ is the eigenvector belonging to the zero eigenvalue of the the matrix $\mathbf{J}^2$ ($\mathbf{J}$ is nilpotent of index 2, that is $\mathbf{J}^2\mathbf{v} = \mathbf{0}$ but $\mathbf{J}\mathbf{v} \neq \mathbf{0}$). One can calculate $\mathbf{v}$ as an eigenvector associated with the zero eigenvalue of the squared Jacobian matrix evaluated at the equilibrium point.

The similarity transformation is now defined by

$$\mathbf{x} = \mathbf{U}\mathbf{y} \,, \tag{3.14}$$

where $\mathbf{U}$ denotes the matrix the columns of which are formed by a normalized eigenvector and a generalized eigenvector. The matrix $\mathbf{U}$ is invertible, since the vectors $\mathbf{u}$ and $\mathbf{v}$ are linearly independent, and we can write

$$\mathbf{y} = \mathbf{U}^{-1}\mathbf{x} \,. \tag{3.15}$$

Then

$$\mathbf{U}^{-1}\mathbf{J}\mathbf{U} = \mathbf{J}_0 = \begin{pmatrix} 0 & 1 \\ 0 & 0 \end{pmatrix} \,, \tag{3.16}$$

and

$$\dot{\mathbf{y}} = \mathbf{J}_0\mathbf{y} + \mathbf{U}^{-1}\mathbf{F}(\mathbf{U}\mathbf{y}) \,. \tag{3.17}$$

Taylor series expansion of the right-hand side of (3.17) at the equilibrium $\mathbf{y} = \mathbf{0}$ gives

$$\begin{aligned}
\frac{dy_1}{dt} &= y_2 + \frac{1}{2}a_{20}y_1^2 + a_{11}y_1y_2 + \frac{1}{2}a_{02}y_2^2 \\
&\quad + \frac{1}{6}a_{30}y_1^3 + \frac{1}{2}a_{21}y_1^2y_2 + \frac{1}{2}a_{12}y_1y_2^2 + \frac{1}{6}a_{03}y_2^3 \\
&\quad + \frac{1}{24}a_{40}y_1^4 + \frac{1}{6}a_{31}y_1^3y_2 + \frac{1}{4}a_{22}y_1^2y_2^2 + \frac{1}{6}a_{13}y_1y_2^3 + \frac{1}{24}a_{04}y_2^4 + O(\|\mathbf{y}\|^5), \qquad (3.18a) \\
\frac{dy_2}{dt} &= \frac{1}{2}b_{20}y_1^2 + b_{11}y_1y_2 + \frac{1}{2}b_{02}y_2^2 \\
&\quad + \frac{1}{6}b_{30}y_1^3 + \frac{1}{2}b_{21}y_1^2y_2 + \frac{1}{2}b_{12}y_1y_2^2 + \frac{1}{6}b_{03}y_2^3 \\
&\quad + \frac{1}{24}b_{40}y_1^4 + \frac{1}{6}b_{31}y_1^3y_2 + \frac{1}{4}b_{22}y_1^2y_2^2 + \frac{1}{6}b_{13}y_1y_2^3 + \frac{1}{24}b_{04}y_2^4 + O(\|\mathbf{y}\|^5). \qquad (3.18b)
\end{aligned}$$

The final transformation to the normal form

$$\begin{aligned}
\frac{d\xi}{d\tau} &= \eta \qquad (3.19a) \\
\frac{d\eta}{d\tau} &= A\xi^2 + B\xi\eta + C\xi^3 + D\xi^2\eta + E\xi^4 + F\xi^3\eta + O(\|(\xi,\eta)\|^5) \,, \qquad (3.19b)
\end{aligned}$$

is achieved by a time re-parameterization combined with a smooth change of coordinates. In this way it is possible to remove both 4th-order terms from (3.19) (using $BC \neq 0$ as will be verified numerically in our case).

The time re-parameterization introduces a new time τ as follows

$$dt = (1 + \theta_1 y_1 + \theta_2 y_1^2)d\tau, \tag{3.20}$$

where θ_1 and θ_2 are to be defined later. Alternatively one can use $(1 + \theta_1 y_1 + \theta_2 y_2)$ which leads to the same results. The smooth transformation reads

$$\begin{aligned}\xi = y_1 &+ \frac{1}{2}g_{20}y_1^2 + g_{11}y_1y_2 + \frac{1}{6}g_{30}y_1^3 + \frac{1}{2}g_{21}y_1^2y_2 + \frac{1}{2}g_{12}y_1y_2^2 \\ &+ \frac{1}{24}g_{40}y_1^4 + \frac{1}{6}g_{31}y_1^3y_2 + \frac{1}{4}g_{22}y_1^2y_2^2 + \frac{1}{6}g_{13}y_1y_2^3, \end{aligned} \tag{3.21a}$$

$$\begin{aligned}\eta = y_2 &+ \frac{1}{2}h_{20}y_1^2 + h_{11}y_1y_2 + \frac{1}{6}h_{30}y_1^3 + \frac{1}{2}h_{21}y_1^2y_2 + \frac{1}{2}h_{12}y_1y_2^2 \\ &+ \frac{1}{24}h_{40}y_1^4 + \frac{1}{6}h_{31}y_1^3y_2 + \frac{1}{4}h_{22}y_1^2y_2^2 + \frac{1}{6}h_{13}y_1y_2^3, \end{aligned} \tag{3.21b}$$

where g_{ij} and h_{ij} are unknown coefficients. Differentiating (3.21a) and (3.21b) with respect to τ yields

$$\frac{d\xi}{d\tau} = (1 + \theta_1 y_1 + \theta_2 y_1^2)\left(\frac{\partial \xi}{\partial y_1}\frac{dy_1}{dt} + \frac{\partial \xi}{\partial y_2}\frac{dy_2}{dt}\right), \tag{3.22a}$$

$$\frac{d\eta}{d\tau} = (1 + \theta_1 y_1 + \theta_2 y_1^2)\left(\frac{\partial \eta}{\partial y_1}\frac{dy_1}{dt} + \frac{\partial \eta}{\partial y_2}\frac{dy_2}{dt}\right). \tag{3.22b}$$

Substituting (3.18a) and (3.18b) into (3.22a) and (3.22b), and then equating coefficients (3.19a) and (3.19b), gives the equations to find the coefficients $g_{ij}, h_{ij}, \theta_1, \theta_2$ in (3.21) and (3.20), as well as A, B, C, D in (3.19), where θ_1 and θ_2 are used to enforce $E = F = 0$. This gives

$$A = \frac{1}{2}b_{20}, \tag{3.23a}$$

$$B = a_{20} + b_{11}, \tag{3.23b}$$

$$C = \frac{1}{6}b_{30} - \frac{1}{2}a_{20}b_{11}, \tag{3.23c}$$

$$\begin{aligned}D =& \frac{1}{2}\,b_{21} + \frac{1}{4}\,b_{02}(b_{11} - a_{20}) + \frac{1}{2}\,b_{11}a_{11} + \frac{1}{2}\,a_{30} + \frac{3(a_{20} + b_{11})}{20(3\,a_{20}b_{11} - b_{30})} \times \\ &\left(b_{40} - 6\,a_{20}b_{21} - 3\,b_{11}b_{02}a_{20} + 3\,b_{02}{a_{20}}^2 - 4\,b_{11}a_{30} + 6\,b_{30}a_{11} + b_{30}b_{02} - 6\,b_{11}a_{20}a_{11}\right). \end{aligned} \tag{3.23d}$$

Note that the 3rd-order coefficient D in (3.19) depends (via b_{40}) on the 4th-order terms of (3.18).

The Taylor coefficient A in (3.19) equals zero, since $b_{20} = 0$ because the critical equilibrium is triple. This implies that one of the non-degeneracy conditions for a classical codimension-two BT point is violated [86, p.272]. This leads to a bifurcation point with codimension three (or higher) and could, together with the requirement $\det \mathbf{J} = 0$ and $\operatorname{tr} \mathbf{J} = 0$, be used as defining functions to determine the critical parameter values corresponding to this bifurcation point.

If $CD \neq 0$, then the truncated critical normal form

$$\frac{d\xi}{dt} = \eta \tag{3.24a}$$

$$\frac{d\eta}{dt} = B\xi\eta + C\xi^3 + D\xi^2\eta \tag{3.24b}$$

can be simplified further by a linear coordinate and time scaling:

$$\frac{d\xi}{dt} = \eta \tag{3.25a}$$

$$\frac{d\eta}{dt} = \beta\xi\eta + \epsilon_1\xi^3 + \epsilon_2\xi^2\eta\ , \tag{3.25b}$$

where $\epsilon_1 = \pm 1, \epsilon_2 = \pm 1$, and

$$\beta = \frac{B}{\sqrt{|C|}}.$$

In [10, 37], three topologically different cases are distinguished:

- Saddle case $\epsilon_1 = 1$, any ϵ_2 and β;
- Focus case $\epsilon_1 = -1$ and $0 < \beta < 2\sqrt{2}$;
- Elliptic case $\epsilon_1 = -1$ and $2\sqrt{2} < \beta$.

When $b = 2.2$, the calculated values of the coefficients of the truncated critical normal form (3.24) are $B = 1.0538275511$, $C = -0.110108078$, and $D = -1.23163654$. This gives $\epsilon_1 = -1$ (because $C < 0$), $\epsilon_2 = -1$ (because $D < 0$), and

$$\beta = \frac{B}{\sqrt{-C}} = 3.175849820.$$

We conclude that with $b = 2.2$ the *elliptic case* applies, for $\beta = 3.175849820 > 2\sqrt{2}$. Direct numerical integration of (3.1) at the critical parameter values (3.10) confirms this conclusion (see Figure 3.2).

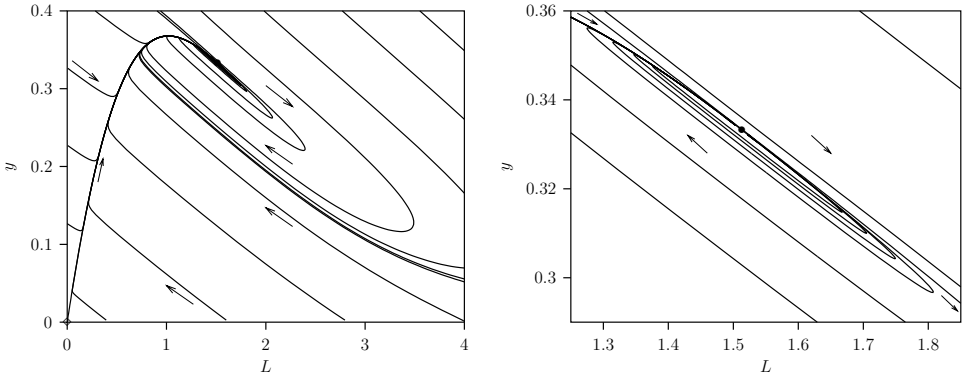

Figure 3.2: Phase portrait of (3.1) at the critical parameter values with b=2.2 (left) and an enlargement of a neighborhood of the critical equilibrium (right), where the elliptic sector is clearly visible.

Calculations showed that in an extended range of parameter values $b > 0$ the parameters C and D defined in (3.24b) are negative, implying $\epsilon_1 = -1$ and $\epsilon_2 = -1$. In Figure 3.3 we give the dependence of β on the parameter b. At $b^\natural = 1.7300228$, where $\beta = 2\sqrt{2}$, there is a transition from the elliptic case to the *focus* case. The phase portrait at the critical parameter values with $b = 1.5$ (when the focus case applies) is depicted in Figure 3.4. Compared with Figure 3.2 where $b = 2.2$, we see that the elliptic sector disappeared.

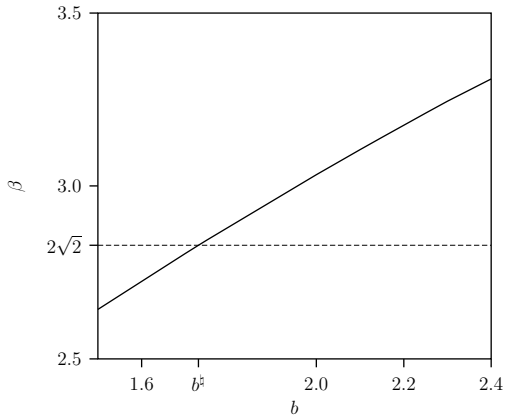

Figure 3.3: The coefficient β defined in (3.25b) as a function of the parameter b. There is a transition from the elliptic case to the focus case at the codimension-four bifurcation point where $b = b^\sharp = 1.7300228$.

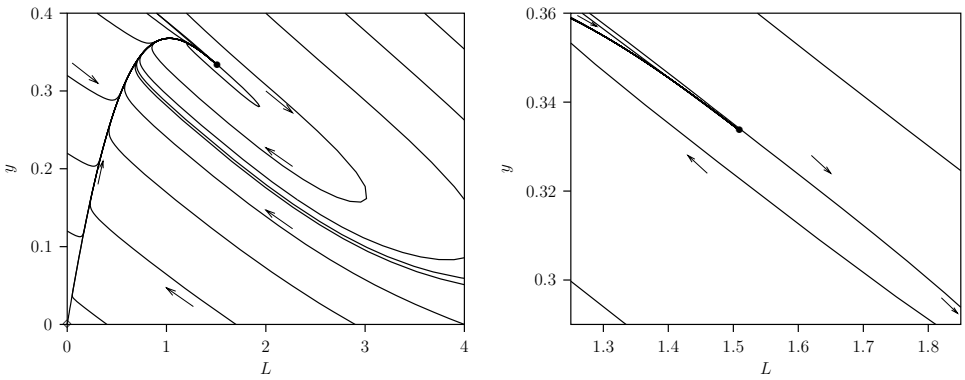

Figure 3.4: Phase portrait of (3.1) at the critical parameter values with b=1.5 (left) and an enlargement of a neighborhood of the critical equilibrium (right) where no elliptic sector is present.

The transition at $b = b^\natural$ is a bifurcation of codimension four (or higher), which could be considered as the ultimate organizing center in model (3.5). However, in the sequel we will deal with $b > b^\natural$ corresponding to the elliptic case because it is the most interesting one. The focus case is discussed extensively in applied literature (for example, in [9,86] with the analysis of the Rosenzweig-MacArthur predator-prey model having density dependent mortality rate for the predators).

3.4.2 Bifurcation diagram of the canonical unfolding

The local bifurcation diagram for the focus and elliptic case has been studied theoretically in [37], where the truncated critical normal form (3.25) is embedded in the following three-parameter family

$$\frac{d\xi}{dt} = \eta \,, \tag{3.26a}$$

$$\frac{d\eta}{dt} = -\mu_1 - \mu_2\xi + \nu\eta + \beta\xi\eta - \xi^3 - \xi^2\eta \,, \tag{3.26b}$$

with μ_1, μ_2, and ν serving as the unfolding parameters. Below we reconstruct the bifurcation diagram of (3.26) in the elliptic case using the same numerical continuation methods as applied in the next section to compute global bifurcation diagrams of (3.1).

The equilibria of (3.26) satisfy $\eta = 0$ and $-\mu_1 - \mu_2\xi - \xi^3 = 0$. Therefore, depending on the parameter values μ_1 and μ_2, there is one or there are three real solutions. For example, when $\mu_1 = 0$, we have $\xi = 0$ and $\xi = \pm\sqrt{-\mu_2}$ besides $\eta = 0$.

In Figure 3.5, a partial three-parameter bifurcation diagram near the codimension-three bifurcation point $\mu_1 = \mu_2 = \nu = 0$ is shown for the normal form (3.26) where $\beta = 3.175849820$ (elliptic case). Two BT curves of different type emanate from the codimension-three point denoted by $BT^=$. Locally attracting limit cycles bifurcate from the first curve which is called a *supercritical Bogdanov-Takens bifurcation curve* and is denoted by BT^-, while repelling limit cycles bifurcate from the curve of second type which is a *subcritical Bogdanov-Takens bifurcation curve*, denoted by BT^+. Another codimension-two bifurcation curve, namely a cusp curve denoted by N_e in the figure, passes through the point $BT^=$. Finally, from $BT^=$, a codimension-two Bautin (generalized or degenerated Hopf, see [86]) bifurcation curve B emanates. Software packages LOCBIF [65,86] and CONTENT [48,91] were used for the numerical continuation of these curves related to equilibrium bifurcations.

Figure 3.6 presents two-parameter slices of the complete bifurcation diagram of (3.26) with $\beta = 3.175849820$ for $\mu_2 = -0.1$ and $\mu_2 = -1$. The top diagram with $\mu_2 = -0.1$ gives a clear picture of the unfolding near the codimension-three BT point. The same diagram (together with corresponding phase portraits) is sketched in Figure 3.7, which we advise to consult while reading the rest of this section. The codimension-two $BT^\pm$ points and four saddle-node homoclinic bifurcation points $D_i, i = 1, \ldots, 4$ (analyzed theoretically in [95]) are indicated in all diagrams. These points lie all on the tangent bifurcation curves for equilibria $T_e^\pm$. At the supercritical BT^- point, a supercritical Hopf bifurcation curve H^- originates, and similarly a subcritical Hopf bifurcation curve H^+ emanates from the subcritical BT^+. From each BT point, BT^- and BT^+, a global bifurcation curve emanates, indicated by G^+ or G^-, respectively. These are saddle homoclinic bifurcation curves. The homoclinic orbits corresponding to them are "small", i.e. they go around one equilibrium only. There exists another saddle homoclinic bifurcation curve, denoted by G^0 in the figure. In contrast with G^+

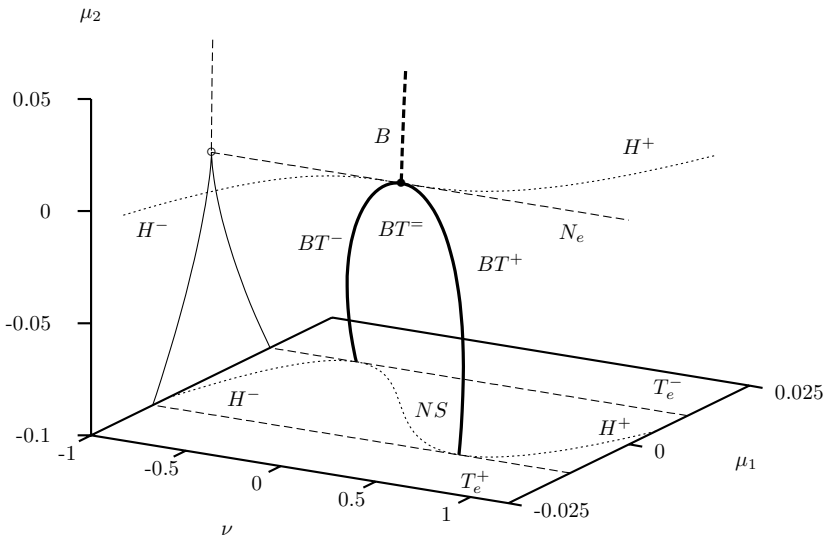

Figure 3.5: Three-parameter bifurcation diagram with μ_1, μ_2, and ν as bifurcation parameters for the normal form (3.26) where $\beta = 3.175849820$. Only equilibrium bifurcations are shown. The tangent bifurcation curves $T_e^{\pm}$ (dashed curves) and Hopf $H^{\pm}$ and neutral saddle NS curve (dotted curve) in the (μ_1, ν)-plane for $\mu_2 = -0.1$ are plotted.

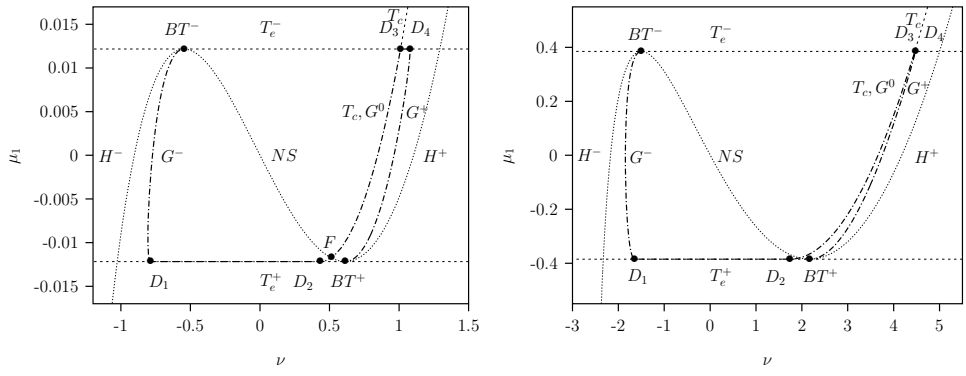

Figure 3.6: Two-parameter bifurcation diagrams of (3.26) with μ_1 and ν as bifurcation parameters and $\mu_2 = -0.1$ (left) and $\mu_2 = -1$ (right) for normal form (3.26) where $\beta = 3.175849820$. The labels are explained in the text.

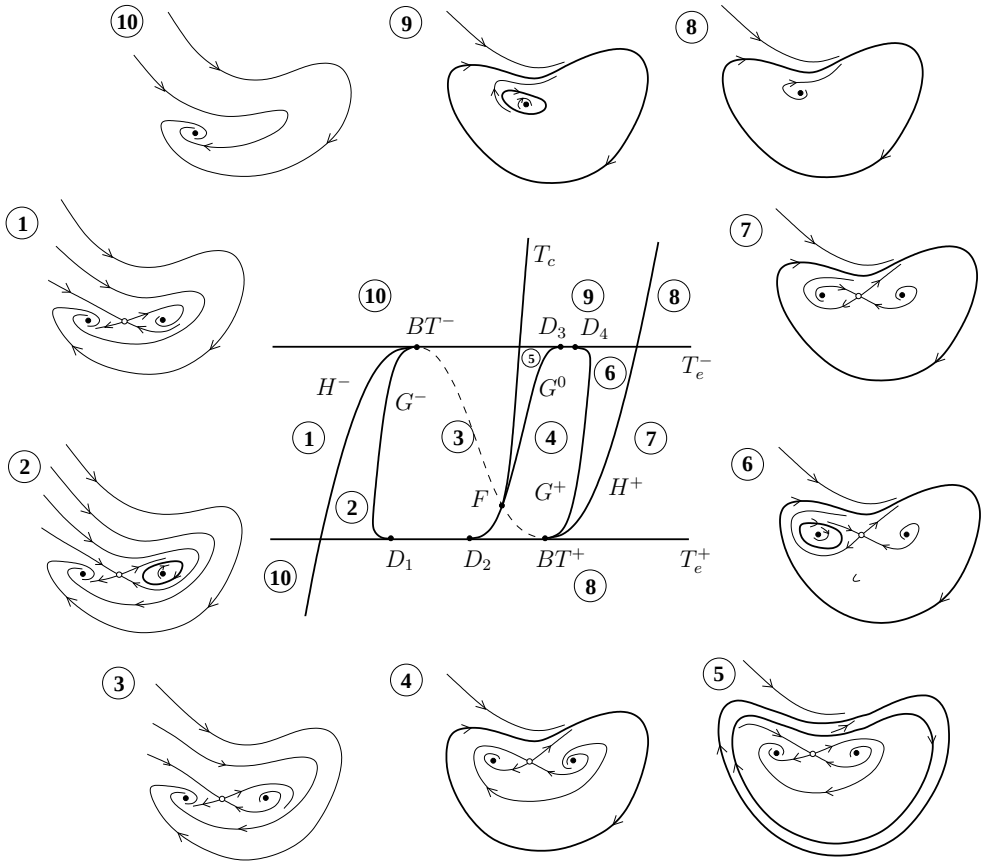

Figure 3.7: Schematic bifurcation diagram of (3.26) for small $\mu_2 < 0$ and $\beta > 2\sqrt{2}$.

and G^-, the homoclinic orbit corresponding to G^0 is "big", i.e. it surrounds two equilibria. The homoclinic curves were calculated using the package HomCont, a part of auto [31]. The implemented theory and numerical procedures are described in [20, 21].

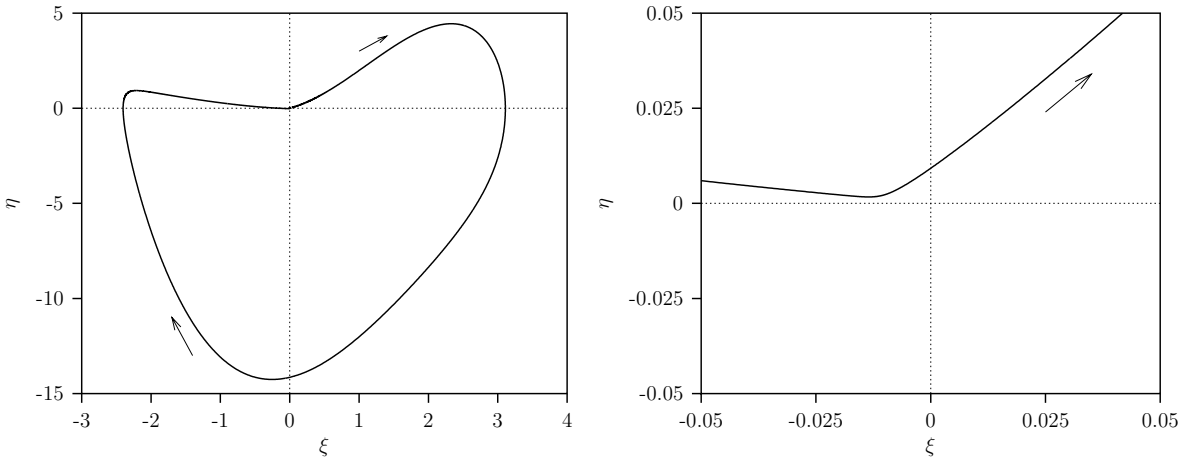

Figure 3.8: A nonhyperbolic limit cycle (see (4) in Fig 3.7) of (3.26) at the critical parameter value $\nu = 0.8458472970$ corresponding to T_c (left) and an enlargement of a neighborhood of the origin, where a saddle equilibrium is located (right). Other parameters are $\mu_1 = 0, \mu_2 = -0.1, b = 3.175849820$. We recall that the three equilibria are: $\eta = 0$ and $\xi = 0$ or $\xi = \pm\sqrt{0.1}$. The equilibrium in the origin is a saddle, the left one is stable and the right one unstable.

A tangent bifurcation curve for limit cycles T_c, where two limit cycles collide and disappear, crosses the curve T_e^- and ends at a point F in the intersection of the homoclinic curve G^0 and the neutral saddle curve NS connecting the Bogdanov-Takens points BT^- and BT^+. This point F corresponds to a codimension-two "big" homoclinic orbit to a neutral saddle, where the trace of the Jacobian matrix is zero [86]. The tangent bifurcation curve for limit cycles T_c and the homoclinic curve G^0 have an infinite-order contact at F [103]. It should be noted that T_c is indistinguishable from G^0 in Figure 3.6. Between the equilibrium bifurcation curves T_e^+ and T_e^-, the curve T_c is located just above G^0. This can be verified by accurate computations in auto or content with many mesh points (e.g., `NTST=1000`). Figure 3.8 demonstrates that the critical limit cycle corresponding to T_c is located at a small but clearly visible distance from the saddle equilibrium at the origin. This nonhyperbolic limit cycle bifurcates into an (outer) stable and (inner) unstable limit cycles, shown in Figure 3.9 for parameter values between the curves T_c and G^0. When we cross the homoclinic bifurcation curve G_0 above point F, the inner unstable limit cycle "collides" with the saddle and disappears via the saddle homoclinic orbit that is unstable from the outside, in accordance with the positive sign of the trace of the Jacobian matrix above the curve NS (see Figure 3.6). Crossing G^0 below F results in the appearance of a stable "big" cycle.

The saddle homoclinic curve G^-, originating at the point BT^-, terminates tangentially at a point D_1 on the bifurcation curve T_e^+. Between the two codimension-two points D_1 and D_2 the saddle-node equilibrium (existing along the tangent bifurcation curve T_e^+) has a smooth homoclinic orbit. On this line-segment D_1D_2, the global bifurcation and the local bifurcation occur simultaneously. The homoclinic orbit is asymptotic to a saddle-node rather

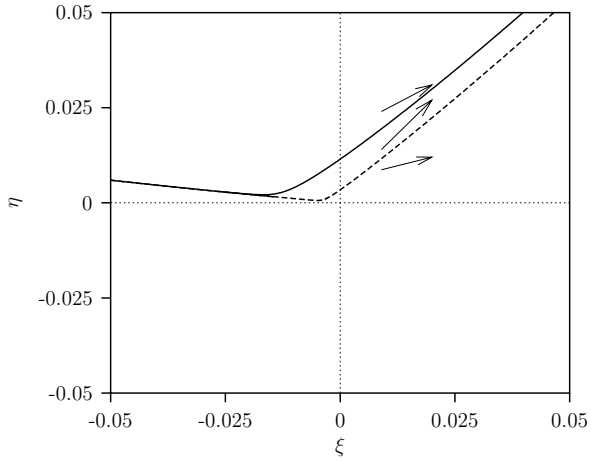

Figure 3.9: A stable limit cycle (outer, solid) and an unstable (inner, dashed) limit cycle of (3.26) at $\nu = 0.8458473000$. The other parameters are $\mu_1 = 0, \mu_2 = -0.1, b = 3.175849820$.

than to a saddle. In point D_2, the "big" saddle homoclinic curve G^0 departs tangentially from T_e^+. This curve G^0 ends also tangentially at a codimension-two point D_3 on T_e^-, which is similar to D_2. Another saddle homoclinic curve, G^-, originating at BT^+ on the bifurcation curve T_e^+, terminates tangentially at a point D_4 on T_e^-. In all points D_i, the corresponding homoclinic orbits are nonsmooth at the saddle-node. The right diagram with $\mu_2 = -1$ shows that already in the vicinity of the codimension-three point the two saddle-node homoclinic bifurcation points D_3 and D_4 are also close to each other and hardly distinguishable in Figure 3.6 (right).

3.4.3 Elliptic versus focus case

The bifurcation diagram of the normal form (3.26) presented in Figure 3.7 differs drastically from the theoretical bifurcation diagram for the elliptic case given in [37, p. 8]. The reason for this discrepancy is that the diagram in [37] concerns phase portraits in a *fixed* small neighborhood (in fact, an elliptic disk) of the origin. Therefore, additional bifurcation curves associated with boundary tangencies appear, while some parts of the global bifurcation curves described above become "invisible", since the corresponding bifurcations happen outside the neighborhood. This approach is absolutely legitimate in theoretical studies, but is of little use in applied analysis, where artificial boundaries have no meaning and global phase portraits in the whole phase plane must be considered. Only such portraits could provide a good understanding of the long-term dynamics of the model.

Figure 3.6 gives such global bifurcation diagrams of the normal form (3.26). It turns out that the two-parameter slices are topologically equivalent to those corresponding to the focus case (see [10, p. 36] or [37, p. 7], where an intersection of bifurcation surfaces with a small sphere centered at the origin in the three-dimensional parameter space is shown). However, the inner limit cycle demonstrates rapid amplitude changes ("canard-like" behavior) near the bifurcation curve T_c. It is this phenomenon that makes the continuation of limit cycles near T_c difficult. One could also observe that, in contrast with the focus case, the "big" homoclinic orbit to the neutral saddle (see point F) does not shrink to the origin of the phase plane, when

we approach the codimension-three elliptic BT point in the parameter space. Instead, this homoclinic orbit tends to the boundary of the elliptic sector that has a finite size in (3.26). The similarity between the focus and the elliptic cases implies that the transition between them at $b = b^\sharp$, although interesting from a theoretical point of view, is of minor importance in applications, since it does not affect dynamics away from the degenerate BT bifurcation points.

These similarities and differences between the focus and the elliptic cases were overlooked in all theoretical studies. Of course, global phase portraits arising from an elliptic BT case in a specific model could differ from the global bifurcation diagrams of the canonical unfolding (3.26) reported above. However, if other phase objects (equilibria, cycles, etc.) do not interact with the objects bifurcating around the codimension-three BT point, one would encounter the described bifurcation diagrams in his/her system, as it happens in our ecological model (3.1).

3.5 Bifurcation diagrams of the two-stage model

We show only one three, one two and some one-parameter bifurcation diagrams of (3.1) for a representative parameter value $b = 2.2$ (elliptic case). We also show explicitly various homoclinic orbits.

3.5.1 Three-parameter bifurcation diagram

In Figure 3.10, the three parameters μ, m, a are changed simultaneously. There is a codimension-three point, denoted by $BT^=$ at the critical parameter values $(\mu^\sharp, m^\sharp, a^\sharp)$ given by (3.10). The bifurcation pattern resembles that of the normal form (3.26) presented in Figure 3.5. There is now another codimension-two Bautin bifurcation curve B which is not connected to a codimension-three point $BT^=$. Varying the forth parameter b showed that such a connection never occurs in the region of the parameter space of interest in this paper.

Codim-one bifurcation curves for $a = 0.44$ is investigated in the next section using two-parameter bifurcation diagrams.

3.5.2 Two-parameter bifurcation diagram

The two-parameter bifurcation diagram for $a = 0.44$ in Figure 3.11 strongly resembles that given in Figure 3.6(right) where $\mu_2 = -1$. The Hopf bifurcation curves H^- (origination to the left in BT^-) and H^+ (origination to the right in BT^+), the neutral-saddle curve NS (between BT^- and BT^+), and the tangent bifurcation curves $T_e^\pm$ (straight lines parallel to the ν-axis) as well as the tangent bifurcation curve for limit cycles T_c are shown. Observe that although the parameter value $a = 0.44$ is rather close to $a^\sharp$, the two saddle-node homoclinic bifurcation points D_3 and D_4 are indistinguishable in the figure.

3.5.3 One-parameter bifurcation diagrams

In Figures 3.12 and 3.13 where $m = 0.01, a = 0.43$, the bifurcation parameter is μ. For all μ-values, there are three interior equilibria, denoted by E_1, E_2 and E_3, the positions of which are independent of μ. For the (scaled) numbers of juveniles and adults at these equilibria, $E_j = (L_j^*, y_j^*)$, we have $L_1^* < L_2^* < L_3^*$ and $y_1^* > y_2^* > y_3^*$, respectively. Hopf bifurcations of

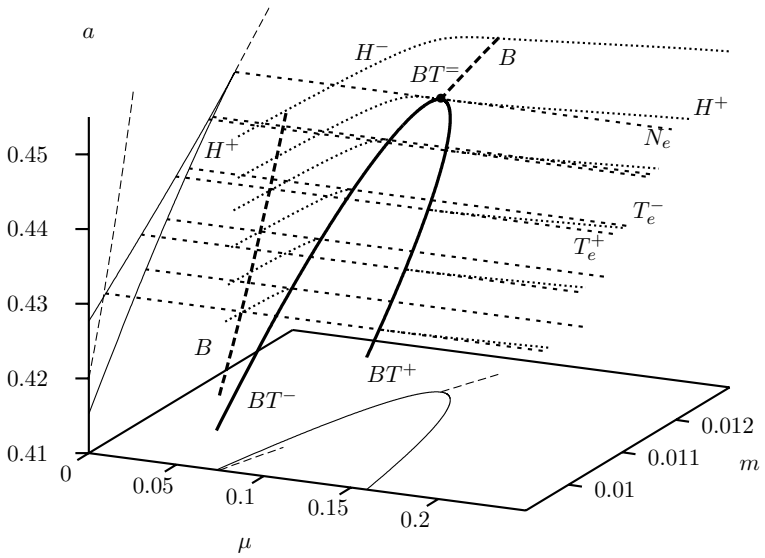

Figure 3.10: Three-parameter bifurcation diagram for equilibria in of (3.1) with μ, m and a as bifurcation parameters. The codimension-three Bogdanov-Takens point is denoted by $BT^=$. From this point two codimension-two BT curves, BT^- and BT^+, emanate. They are shown along with their projections. The codimension-two Bautin bifurcation curves B are long dashed. The Hopf bifurcation curves (dotted) and tangent bifurcation curves (short dashed) are shown for $a = 0.455$, $a = 0.4492277$, $a = 0.44$ and $a = 0.43$. The curve N_e passing through $BT^=$ is a cusp bifurcation curve for equilibria. The two curves $T_e^\pm$ for $a = 0.44$ are the intersections of the $a = 0.44$-plane with the tangent bifurcation surfaces. Similarly the H^+ and H^- curves from the intersections for the two-dimensional Hopf bifurcation surfaces. For a-values above the point $BT^=$ these sheets are separated by the codimension-two Bautin bifurcation curves B. These sheets are separated for a-values below the point $BT^=$ where the two codimension-two BT curves, BT^- and BT^+ form the end-curves of the separated sheets. For smaller μ-values there is always a codimension-two Bautin bifurcation curves B that separates super- and subcritical Hopf bifurcation surfaces.

E_1 and E_3 occur at H^+ and H^-, respectively, giving rise to limit cycles. Their maximum and minimum values are plotted in the figure, a stable one, denoted by C_3 and generated by the supercritical Hopf bifurcation from the equilibrium E_3 and an unstable one, denoted by C_1 and generated by the subcritical Hopf bifurcation from the equilibrium E_1. For large μ, there is a branch of "big" stable periodic orbits (also denoted by C_3) which surround all three equilibria. This branch also exists for μ values for which the unstable period orbits C_1 surrounding the equilibrium E_1 exist. There are homoclinic orbits at the points where these limit cycles touch the saddle equilibrium E_2.

Figure 3.14 shows approximations of these two homoclinic orbits, one "big" (solid) C_3 and one "small" (dashed) C_1 for $\mu = 1$ and $a = 0.43$. The period of the plotted limit cycles is very large, indicating a homoclinic orbit. There are two rather sharp bends in the "big"

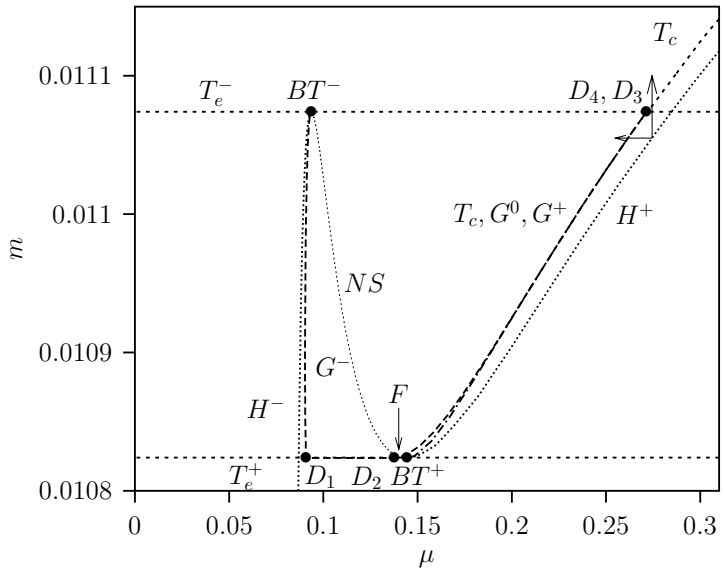

Figure 3.11: Two-dimensional bifurcation diagram with μ and m as bifurcation parameters where $a = 0.44$.

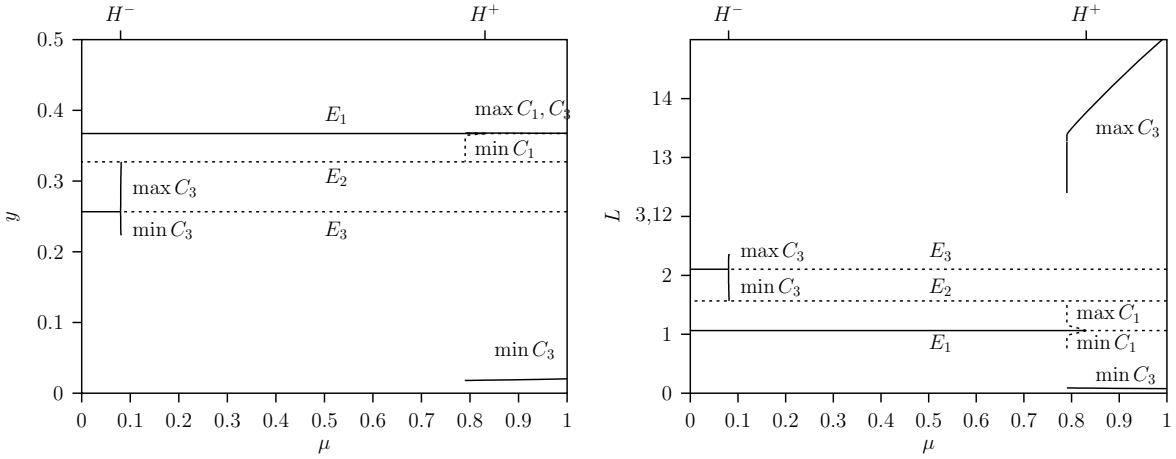

Figure 3.12: Bifurcation diagram where $m = 0.01$ and $a = 0.43$, and μ is the single bifurcation parameter. Stable equilibria are represented by solid lines and unstable equilibria by dashed lines which are horizontal because the y and L equilibrium values are independent of μ. A branch of stable limit cycles C_3 (solid curves) originate through the supercritical Hopf (H^-), and a branch of unstable limit cycles C_1 (dashed curves) through the subcritical Hopf bifurcation (H^+). A homoclinic orbit occurs where these limit cycles touch the saddle equilibrium E_2.

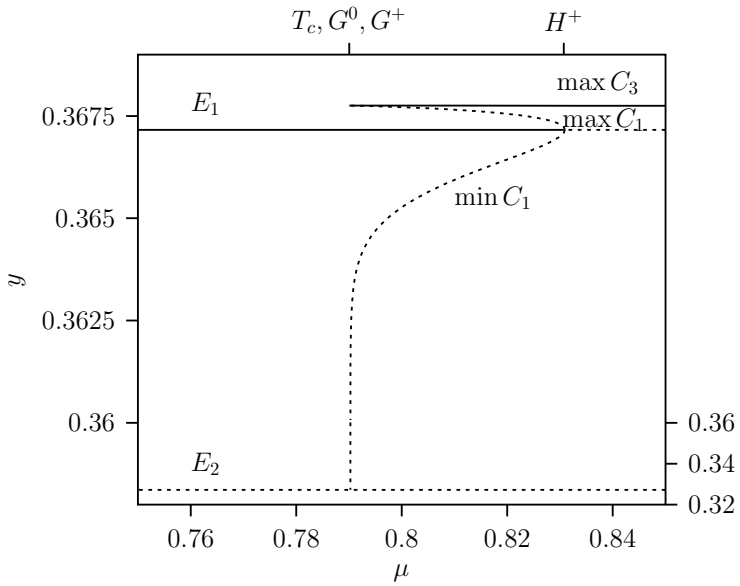

Figure 3.13: Detail of Figure 3.12. The solid curve is the maximum of the large amplitude cycle C_3. The dashed curve is the unstable limit cycle C_1 that emanates from the Hopf bifurcation point H^+. In order to get a better plot, the scaling of the y-axis below $y = 0.36$ is changed. The two homoclinic bifurcations G^0 and G^+, as well as the tangent bifurcation T_c of limit cycles, occur at almost the same value of μ.

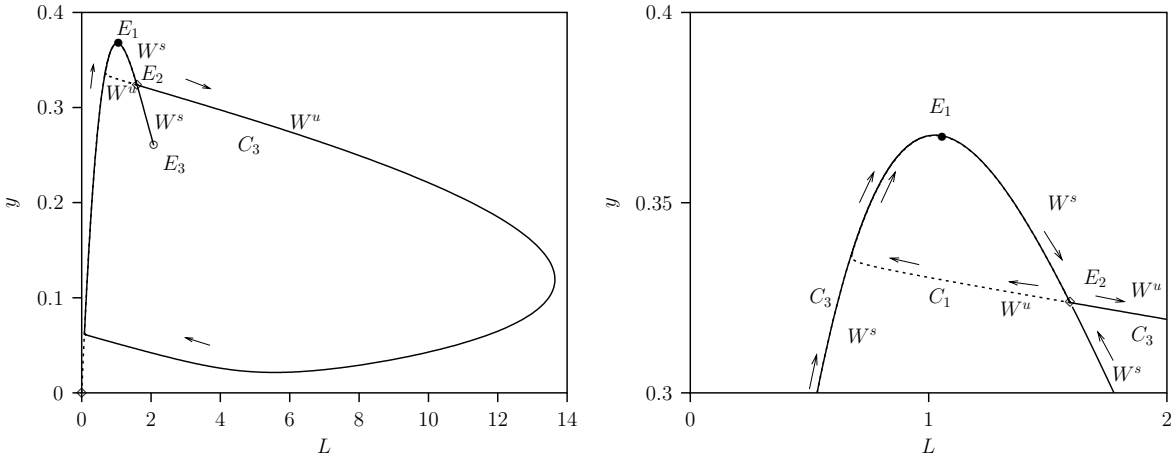

Figure 3.14: Two homoclinic orbits and time-evolution for $\mu = 1.0$ and $a = 0.43$, where $m = 0.01004953$ and $m = 0.01004952$ for large amplitude and small amplitude orbits, respectively. Right figure is an expanded view of the left figure. The stable W^s and unstable W^u manifolds of the saddle point indicated by a $\diamond$ are shown. The stable focus E_1 is indicated by a bullet and the source E_3 by a circle. Here the flow direction is indicated by arrows for the stable homoclinic orbit C_3 at the outside and for the unstable homoclinic orbit C_1 at the inside.

homoclinic orbit. The top one is close to the saddle point as expected. The lower bend is associated with the zero equilibrium ($L = 0, y = 0$) which is a saddle point for the parameter values used. Both orbits pass the stable focus E_1 closely.

3.6 Discussion

We have considered the most basic model for stage-structured populations in which per capita transition from the juvenile into the adult class is density dependent, namely a system of two ordinary differential equations. We established existence of a codimension-three BT bifurcation in our model and have verified its nondegeneracy by computing its normal form numerically. The normal form is computed using a preliminary linear transformation to simplify the linear terms, in this case to put the linear part in the Jordan canonical form. In [86, 87] this step is omitted by using a representation of any vector in the state space as a linear combination of the eigenvector and the adjoint eigenvector. That method is appropriate for higher-order dynamics systems where normalization on the center manifold is needed [89]. The nonlinear smooth transformation in this paper is combined with a time re-parameterization. This facilitates the removal of all 4th-order terms in the Taylor series expansion. Therefore the expression for the coefficient D of the $\xi^2\eta$ term given by (3.23d) differs from the classical expression [68] where only 3rd-order terms are taken into account. The expressions (3.23) agree with those reported in [43]. In this way, we have computed the relevant normal form coefficients and established that the critical equilibrium at the codimension-three BT point is triple and has an elliptic sector for $b > b^\natural = 1.7300228$. Apparently, this case has never been observed in ecological modelling. At $b = b^\natural$, a transition from the elliptic codimension-three BT to the focus codimension-three BT point occurs.

Using known theoretical results [10,37], we have concluded that two BT codimension-two curves emanate from the codimension-three BT point. Along these curves a Hopf bifurcation surface, as well as a tangent bifurcation and a homoclinic orbit surfaces meet. There is also a codimension-two Bautin bifurcation curve B in the Hopf bifurcation surface, where the supercritical Hopf bifurcation becomes subcritical or visa versa. This happens in a parameter region where only one interior equilibrium exists. In Bautin bifurcation points, a surface of tangent bifurcations of limit cycles originates.

Our numerical analysis of the global bifurcation diagram of the canonical unfolding of the normal form, Figure 3.6, has revealed other global bifurcation curves. On codimension-two bifurcation curves D_i, transitions of the homoclinic orbit to a saddle-node homoclinic orbit occur. There is also a bifurcation surface G^0 corresponding to a "big" homoclinic orbit to the saddle that surrounds two equilibria. In this surface, a line F of codimension-two homoclinic orbits to a neutral saddle exists. Figure 3.11 resemble that of the Bazykin's predator–prey model [9, Figure 3.5.3] and [86, Figure 8.10], despite the fact that the degenerate BT point is here of the elliptic type while in Bazykin's model it is of the focus type. The diagrams given in [37] for both types differ a lot on first sight. However, in [37] additional bifurcation curves associated with boundary tangencies are reported. In this paper, we do not have such artificial bifurcations, since we do not restrict our attention to a small neighborhood of the critical equilibrium. Instead, we consider global phase portraits, which allow us to obtain a better understanding of the long-term dynamic behavior of the model. It should be stressed that without a preliminary analysis of the canonical unfolding (3.26) it would have been practically impossible to understand the numerical continuation results for (3.5).

A large-time solution behavior of similar complexity has been found for certain planar predator-prey systems [9, 86, 114, 127, 128] and epidemic models [112]. Predator-prey and host-parasite system involve two species which influence each other in opposite ways with one suffering from a benefiting the other. The predator-prey models which show complex behavior take into account competition among prey and predator competition for prey. Our model involves two stages of one species which compete among themselves but influence each other positively because we assume pure intra-stage competition. (Adding interstage competition actually counteracts the complexity.) Mathematically, this is reflected in the fact that the nonlinear terms in our system only depend on one variable each, whereas predator prey and epidemic models always have nonlinear terms which involve both variables. In this paper, we find complex behavior in a class of planar systems that is different from predator prey models both biologically and mathematically.

The complex behavior only occurs in a small parameter region (see [120, Chapter 11] for a discussion of other parameter ranges). In this parameter region, the per capita mortality rate of juveniles is smaller than the one of adults ($\mu \leq 1 = \alpha$), and almost every juvenile makes it into the adult stage if there is no competition (the small values of m). This would hold for species where the juveniles are less prone to enemies than the adults and the juvenile stage is very short if there are plenty of resources available. We expect that the complex behavior can be observed in a larger parameter region if more sophisticated nonlinearities than the classical Ricker function are chosen to model the competition among juveniles and adults. A thorough understanding of the basic stage-structured model is important because its simplicity makes it a useful building block in models for several species. Recently it has been used (extended by an intermediate stage of sub-adult individuals) to explain emergent Allee effects in predators that feed on structured prey populations [26].

The results show that despite the low dimension of the system, the dependence of the resulting long-term dynamics on parameter values can be rather complex. The rich behavior of our model is caused by the interaction of intra-adult competition and intra-juvenile competition. None of the two alone can generate multiple positive attractors. It is essential that the intra-juvenile competition does not only affect juvenile mortality, but also juvenile maturation (the per capita transition rate). A density-dependent per capita juvenile mortality rate alone, even if combined with a density-dependent per capita birth rate, can neither generate Hopf bifurcation nor multiple interior equilibria. This feature seems to be related to the fact that in our ODE model the length of the juvenile period is exponentially distributed. If the length of the juvenile period is the same for all individuals (at least for those that are born at the same time), then a density-dependent per capita birth rate can lead to periodic solutions without any other nonlinear model ingredients [82, 102].

Chapter 4

Example: Ecotoxicology

Sublethal toxic effects in a simple aquatic food chain
B.W. Kooi, D. Bontje, G.A.K van Voorn and S.A.L.M. Kooijman. 2008.
Sublethal toxic effects in a simple aquatic food chain.
Ecological Modelling, 212: 304-318.

In this section we study the sublethal effect of toxicants on the functioning (biomass production, nutrient recycling) and structure (species composition and complexity) of a simple aquatic ecosystem in a well-mixed environment (chemostat reactor). The modelled ecosystem consists of a nutrient consumed by a prey (*e.g.* bacteria, algae) which, in turn, is consumed by a predator (*e.g.* ciliates, daphnia) population. The dynamic behaviour of this ecosystem is described by a set of ordinary differential equations (ODE)s: one for the nutrient and one for each population. The system is stressed by a toxicant dissolved in the in-flowing water. The transport of the toxicant is modelled using a mass balance formulation leading to an ODE. Bioaccumulation in the prey and predator populations is via uptake from the water, in case of the predator also via consumption of contaminated prey. Mathematically this process is described by a one-compartment model for the kinetics of the toxicant: uptake (from water and food) and elimination. The toxicant affects individuals which make up populations. In the model the physiological parameters depend on the internal concentration of the toxicant in individuals. Examples of physiological parameters are cost for growth and maintenance, and assimilation efficiency. In this paper we use bifurcation theory to analyse the long-term dynamics of the models. In this way the parameter space is divided into regions with qualitatively different asymptotic dynamic behaviour of the system. As logical choice for bifurcation parameters are the input rate of the nutrient and toxicant. The dynamic behaviour of the stressed ecosystem can be much more complicated than that of the unstressed system. For instance the nutrient–prey–toxicant system can show bi-stability and oscillatory dynamics. Due to the toxic effects a total collapse (both prey and predator population go extinct) of the nutrient–prey–predator–toxicant system can occur after invasion of a predator.

4.1 Introduction

In this section we analyse the lowest levels of an aquatic ecosystem. The model for the populations (*e.g.* bacteria or algae) that compose the ecosystem is a simplified version of the DEB model [78]. The toxic effects on the population level are described by the DEBtox

Table 4.1: State variables and control parameter set for nutrient–prey–predator chemostat model. The environmental parameters that can be experimentally manipulated are $D \in (0, 0.5)$ h^{-1}, $N_r \in (0, 150)$ mg dm^{-3} and $c_r \in (0, 9)$ μg dm^{-3}: m mass of toxicant, t time, v is dimension of the volume of the reactor and V biovolume or biomass of organism.

Var.	Description	Dimension
N	Nutrient mass density	$\mathrm{V\,v}^{-1}$
R	Prey biomass density	$\mathrm{V\,v}^{-1}$
c_W	Toxicant concentration in the water	$\mathrm{m\,v}^{-1}$
c_R	Prey internal toxicant concentration	$\mathrm{m\,V}^{-1}$
Par.	Description	Dimension
D	Dilution rate	t^{-1}
N_r	Nutrient mass density	$\mathrm{V\,v}^{-1}$
c_r	Toxicant concentration in influent	$\mathrm{m\,v}^{-1}$

Table 4.2: Parameter set for bacterium-ciliate model, after [24]: m mass of toxicant, t time, v is dimension of the volume of the reactor and V biovolume or biomass of organism.

Nutrient–Prey			
μ_{NR}	Max. growth rate	t^{-1}	0.5 h^{-1}
I_{NR}	Max. ingestion rate	t^{-1}	1.25 h^{-1}
k_{NR}	Saturation constant	$\mathrm{V\,v}^{-1}$	8.0 mg dm^{-3}
m_{R0}	Maintenance rate coefficient	t^{-1}	0.025 h^{-1}
c_{RM0}	NoEffect Concentration (NEC)	$\mathrm{m\,V}^{-1}$	0.1 μg mg^{-1}
c_{RM}	Tolerance concentration	$\mathrm{m\,V}^{-1}$	0.5 μg mg^{-1}
BCF_{WR}	BioConcentration Factor	$\mathrm{v\,V}^{-1}$	1.0 dm^3 mg^{-1}

approach for uni-cellular organisms with a simple life-history namely propagation by binary fission [80]. The effect module is not based on parameters estimated from descriptive models but on process-based models where physiological parameters depend on the internal toxicant concentration. The maintenance process is affected. Here we describe the consequences on the ecosystem functioning and structure where nutrients and toxicant are supplied and removed at a constant rate in a spatially homogeneous chemostat [118].

The model for the nutrient–prey system in the chemostat is formulated in Section 4.2. The model for the unstressed system predicts simple dynamic behaviour: a stable equilibrium when sufficient nutrient is supplied. In Section 4.3 we show that under toxic stress, the model predicts bi-stability under suitable environmental conditions.

Table 4.1 shows a list of the state variables and the control parameters. In Table 4.2 we give the parameter values used in this study. The physiological parameters are those for a bacterium-ciliate system and were also used for various food web studies, see [70] and reference therein.

4.2 Model for nutrient–prey system

4.2.1 Unstressed nutrient–prey system

Let $N(t)$ be the nutrient density and $R(t)$ the biomass density of the population. Then the governing equations for the simple ecosystem read (see [70])

$$\frac{dN}{dt} = (N_r - N)D - I_{NR}\frac{N}{k_{NR}+N}R\,, \tag{4.1a}$$

$$\frac{dR}{dt} = \big(\mu_{NR}\frac{N}{k_{NR}+N} - (D + m_{R0})\big)\,R\,. \tag{4.1b}$$

A verbal description of these equations is as follows. The dilution (flow-through) rate D (fraction of the volume replaced per unit of time) and the nutrient density N_r in the inflow are the chemostat control parameters. The following terms model the interaction of the population with the water: the influx of nutrient, DN_r, the outflow of the nutrient, DN, and of population, DR. The consumption of the nutrient by the population is modelled by a Holling type II functional response. The parameters are the maximum ingestion rate I_{NR}, the maximum growth rate μ_{NR} and the saturation constant k_{NR}. These three parameters are fixed for a specific prey-nutrient combination indicated by the double subscript of the variables. The ratio of the growth rate and ingestion rate is called the assimilation efficiency in ecology or yield in microbiology. The parameter m_{R0} is the maintenance rate and models a reduction of the growth rate due to overhead costs, related to keeping the organism alive. These costs are assumed to be proportional to the biomass density of the prey R.

4.2.2 Stressed nutrient-prey system

Let $c_W(t)$ be the ambient water concentration of the toxicant in the reactor and c_r the constant concentration of the toxicant in the inflow. The dynamics of the toxicant is described by the following mass-balance equation

$$\frac{d(c_W + c_R R)}{dt} = \big(c_r - (c_W + c_R R)\big)D\,, \tag{4.2}$$

where we use that the volume of the reactor is constant. The toxicant enters the reactor via the inlet with a concentration c_r, in a similar way as the nutrients (the term $N_r D$ in (4.1a)). The internal concentration of the toxicant in the organisms is denoted by c_R (concentration with respect to the biomass R). The rate at which the toxicant leaves the reactor consists of two terms, transport of the dissolved toxicant in the reactor, $c_W D$, and the toxicant absorbed by the population, $c_R R D$.

The one-compartment model for the internal toxicant concentration reads

$$\frac{dc_R}{dt} = k_{Ru}c_W - k_{Ra}c_R - \big((I_{NR} - \mu_{NR})\frac{N}{k_{NR}+N} + D + m_R(c_R) + \frac{1}{R}\frac{dR}{dt}\big)c_R\,, \tag{4.3}$$

where the last term is due to dilution by growth.

Equivalently, the dynamics of the exchange of the toxicant between the prey and its ambient water, is described by a mass-balance model for the total toxicant content in the

prey being the product of internal concentration c_R and the biomass density R as follows. Using the product rule we obtain

$$\frac{dc_R R}{dt} = (k_{Ru}c_W - k_{Ra}c_R)R - \big((I_{NR} - \mu_{NR})\frac{N}{k_{NR}+N} + D + m_R(c_R)\big)c_R R \,. \tag{4.4}$$

The first term on the right-hand side is the exchange between the water and the organisms and the second term is the flux of the toxicant into the organisms that leaves the reactor and the flux egested by the organisms as assimilation and maintenance products. The diffusion transport fluxes are proportional to the area of the surfaces summed over all organisms. We assume that the area of the surface (*e.g.* outer membrane) of the organisms is proportional to their volume. The same holds at the population level. For organisms that propagate by division this is justified. This means the surface area to volume ratio is included in the uptake and elimination rate constants. Furthermore the toxicant is absorbed into the assimilation and maintenance products and egested into the reactor as dissolved toxicant.

The exchange of the toxicant between the water and the organisms is assumed much faster than the other biological processes including dilution, assimilation, growth and maintenance. Due to the small size and large area to volume ratio for phyto- and zooplankton it is assumed that the uptake and elimination of toxicants predominate exchange between the organism and the water [47]. Similarly in [58] for a *Daphnia* population it is assumed that the characteristic time for internal distribution is short compared with the characteristic time for exchange with the water. We rewrite the system as a singular perturbation problem where $\kappa_a = \varepsilon k_{Ra}$ and $\kappa_u = \varepsilon k_{Ru}$ with $\tau = t/\varepsilon$ where time scale separation occurs when $\varepsilon \ll 1$

$$\frac{dc_R R}{d\tau} = (\kappa_u c_W - \kappa_a c_R)R - \varepsilon\big((I_{NR} - \mu_{NR})\frac{N}{k_{NR}+N} + D + m_R(c_R)\big)c_R R \,, \tag{4.5a}$$

$$\frac{dc_W}{d\tau} = -(\kappa_u c_W - \kappa_a c_R)R + \varepsilon\big((c_r - c_W)D + m_R(c_R)c_R R\big) \,. \tag{4.5b}$$

At the fast time scale we have the sub-model where $\varepsilon \to 0$

$$\frac{dc_R R}{d\tau} = (\kappa_u c_W - \kappa_a c_R)R \,, \tag{4.6a}$$

$$\frac{dc_W}{d\tau} = -(\kappa_u c_W - \kappa_a c_R)R \,, \tag{4.6b}$$

where we used (4.2) and (4.4). In equilibrium we obtain

$$0 = \kappa_u c_W^* - \kappa_a c_R^* \,. \tag{4.7}$$

Thus, in quasi-steady state we have

$$\frac{k_{Ru}}{k_{Ra}} = \frac{\kappa_u}{\kappa_a} = \frac{c_R^*}{c_W^*} = \mathrm{BCF}_{WR} \,, \tag{4.8}$$

where the BioConcentration Factor for the population (BCF_{WR}) is the ratio of the internal toxicant concentration (with respect to the biomass density of the population) and the external

toxicant concentration (with respect to the reactor volume). This relationship is now also used in non-equilibrium situations on the slow time scale.

It is advantageous to introduce the total toxicant concentration in the reactor c_T. The set of governing equations then becomes

$$\frac{dN}{dt} = (N_r - N)D - I_{NR}\frac{N}{k_{NR}+N}\,R\,, \tag{4.9a}$$

$$\frac{dR}{dt} = \big(\mu_{NR}(c_R)\frac{N}{k_{NR}+N} - (D + m_R(c_R))\big)\,R\,, \tag{4.9b}$$

$$\frac{dc_T}{dt} = (c_r - c_T)D\,, \qquad \text{where} \quad c_T = c_W + c_R R = c_W\,(1 + \text{BCF}_{WR}R)\,. \tag{4.9c}$$

The effect of the toxicant on the physiology of the populations is modelled as a dependency on physiological parameters, such as growth rate and maintenance rate, on the internal toxicant concentration. In [80] the following expressions are proposed

$$m_R(c_R) = m_{R0}\big(1 + \frac{(c_R - c_{RM0})_+}{c_{RM}}\big)\,, \tag{4.10a}$$

$$\mu_{NR}(c_R) = \mu_{NR0}\big(1 + \frac{(c_R - c_{RG0})_+}{c_{RG}}\big)^{-1}\,, \tag{4.10b}$$

where the subscript plus operator is defined as $x_+ = \max(0, x)$. The parameter m_{R0} is the maintenance rate coefficient of the unstressed system ($c_r = 0$). The toxicological parameters are the No Effect Concentration NEC (a threshold concentration for the onset of effects) denoted by c_{RM0}, and c_{RM} called the tolerance concentration for maintenance. In [80] these two parameters are based on external concentration (per volume of the reactor), not on internal concentration (per biomass density) as is done here. Similarly, when the growth process is the mode of action we have c_{RG0} and c_{RG}, but this is not elaborated in the paper.

To calculate $c_R(t)$, $t \geq 0$ depending on the two state variables $c_T(t)$ and $R(t)$ we use

$$c_W = \frac{c_T}{1 + \text{BCF}_{WR}\,R} \quad , \quad c_R = \frac{\text{BCF}_{WR}\,c_T}{1 + \text{BCF}_{WR}\,R}\,. \tag{4.11}$$

This expression (4.11) is substituted into (4.10a) which, in turn, is substituted into (4.9b).

4.3 Analysis of the nutrient–prey system

Equilibria of a system are determined by the requirement that the time derivatives of the state variable are zero. Let equilibrium values N^* and R^* denote a possible solution. The equation for the dynamics of the toxicant concentration (4.11) yields the equilibrium situation $c_T^* = c_R^*\,(1 + \text{BCF}_{WR}R^*)/\text{BCF}_{WR}$. Depending on the environmental conditions, there will be one, E_1, or multiple positive equilibria, E_1 and E_2 where $N^* < N_r, R^* > 0, c_W^* < c_r$. Besides these equilibria there is a trivial solution $E_0 = (N^* = N_r, R^* = 0, c_W^* = c_r)$.

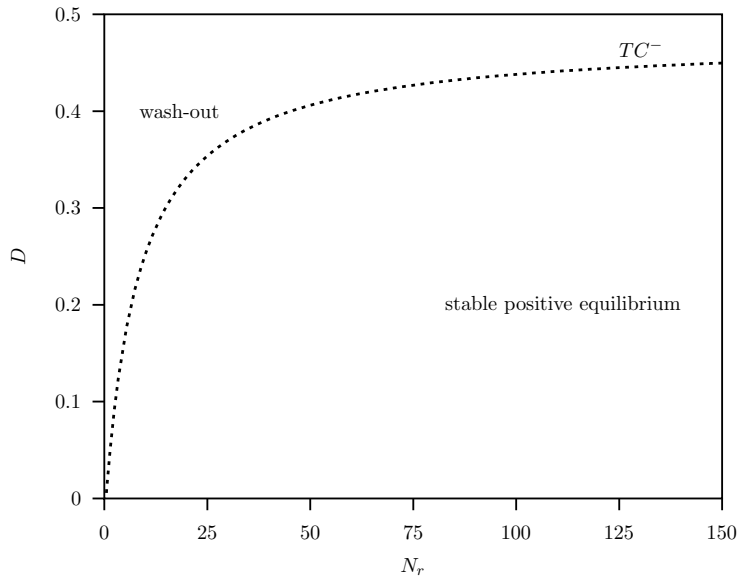

Figure 4.1: A two-parameter bifurcation diagram with nutrient inflow N_r and dilution rate D as free parameters for the population without toxicity stress ($c_r = 0$) in the chemostat system (4.1), with nutrient inflow N_r and dilution rate D as free parameters. Dashed lines are transcritical bifurcation curve TC^-. For dilution rates above this curve there is wash-out. Below the transcritical bifurcation curve the population can invade a nutrient system and establishes at a stable positive equilibrium.

Table 4.3: List of bifurcations, codim-one curves and codim-two points (for two-parameter bifurcation diagrams).

Bifurcation	Description
	Codim-one curves
$TC^{\pm}_{a,i}$	Transcritical bifurcation: − supercritical, + subcritical;
	$a = e$ or empty equilibrium : zero eigenvalue
	$a = c$ limit cycle: Floquet multiplier equal one
	$i = 1$: invasion by population prey, $i = 2$: invasion by predator
T	Tangent bifurcation for equilibrium: zero eigenvalue
	Codim-two points
N	Transition from sub- to supercritical transcritical bifurcation
	tangent bifurcation curve originates
	on boundary of region of bi-stability
BT	Intersection of Hopf and tangent bifurcation curves
	Origin of homoclinic connection (not shown)

4.3.1 Unstressed nutrient–prey system

For the unstressed system (4.1) the two-parameter bifurcation diagram is shown in Fig. 4.1 where the environmental parameters N_r and D are the bifurcation parameters. The most important bifurcations are characterised in Table 4.3.

Let the concentration nutrient in the inflow N_r be given, then it is realistic to assume that there is a maximum dilution rate that supports existence of the population. For instance, when the dilution rate is larger than the maximum growth rate of the population ($D > \mu_{NR}$) the population can never establish itself. For dilution rates below the D-value at the curve TC^- in Fig. 4.1 there is sufficient nutrient to support existence of the population. So, two regions can be distinguished in the bifurcation diagram. In one region the population is absent (equilibrium E_0 where $R^* = 0$), and in the other the population survives (equilibrium E_1 where $R^* > 0$). These two regions are separated by a so-called supercritical transcritical curve TC^-.

In summary, local stability analysis of the positive equilibrium yields the long-term dynamics when the initial values for the state variables, $N(0)$ and $R(0)$, are in the vicinity of the equilibrium. Calculation show that if the positive equilibrium exists it is stable. It is well-known that it is also globally stable [118], that is for all positive initial values, $N(0) > 0$ and $R(0) > 0$, there is convergence to the stable equilibrium. This property makes the chemostat a popular experimental apparatus for growth of uni-cellular organism populations.

4.3.2 Stressed nutrient–prey–toxicant system

In the stressed case where the toxicant concentrations have to be considered in system (4.9), (4.9c) with $c_r > 0$ can be solved analytically:

$$c_T(t) = (c_T(0) - c_r)\exp(-Dt) + c_r \ . \tag{4.12}$$

Substitution of this expression into the two-dimensional ecosystem with state variables $N(t)$, (4.9a), and $R(t)$, (4.9b), yields a non-autonomous system. For the asymptotic dynamics it suffices to study the autonomous system where $c_T = c_r$ is substituted in system (4.9a,4.9b), see [118].

The bifurcation diagram is shown in Fig. 4.2 for $c_r = 1$. In a toxic stressed system on the transcritical bifurcation curve there is a point N where a so-called tangent bifurcation curve T emanates. Below point N at the curve TC^- the situation is the same as with the unstressed system. Above point N there is a different kind of behaviour. The trivial equilibrium E_0 and equilibrium E_1 are both stable. There are two stable attractors and a third unstable equilibrium denoted by E_2 that functions as a separatrix (more precisely the point is a saddle and the stable manifold is the separatrix). The stable, E_1, and unstable, E_2, positive equilibria collide at the tangent bifurcation T. For parameter values above the T curve no positive equilibria exist, only the stable trivial equilibrium E_0 does and therefore in that region of the diagram the population goes extinct. This is illustrated in Fig. 4.3, a one-parameter bifurcation diagram for $N_r = 150$ and $c_r = 1$ with D the free parameter.

We conclude that the transcritical bifurcation curve in Fig. 4.2, changes character at point N from supercritical TC^- below N and subcritical TC^+ above N while in N the tangent bifurcation curve T emanates. Furthermore the reduction of the dimension of the system by taking $c_T = c_r$ holds for the analysis of the stability of the equilibria, but not when global

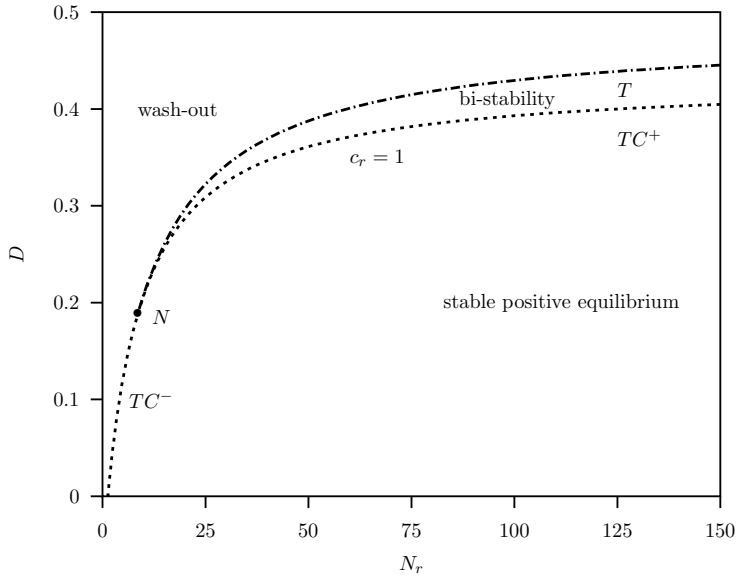

Figure 4.2: A two-parameter bifurcation diagram with nutrient inflow N_r and dilution rate D as free parameters for the population with toxicity stress in the chemostat system (4.9) where $c_r = 1$. Dashed lines are transcritical bifurcation curves $TC^{\pm}$ and dot-dashed curve the tangent bifurcations T. At point N the tangent curve T originates and the transcritical bifurcation changes for supercritical TC^- in subcritical TC^+. Wash-out occurs for dilution rates above the tangent curve T. Below the transcritical bifurcation curve the population can invade a virgin system and establishes at a stable positive equilibrium. Between the two curves T and TC^- there is bi-stability.

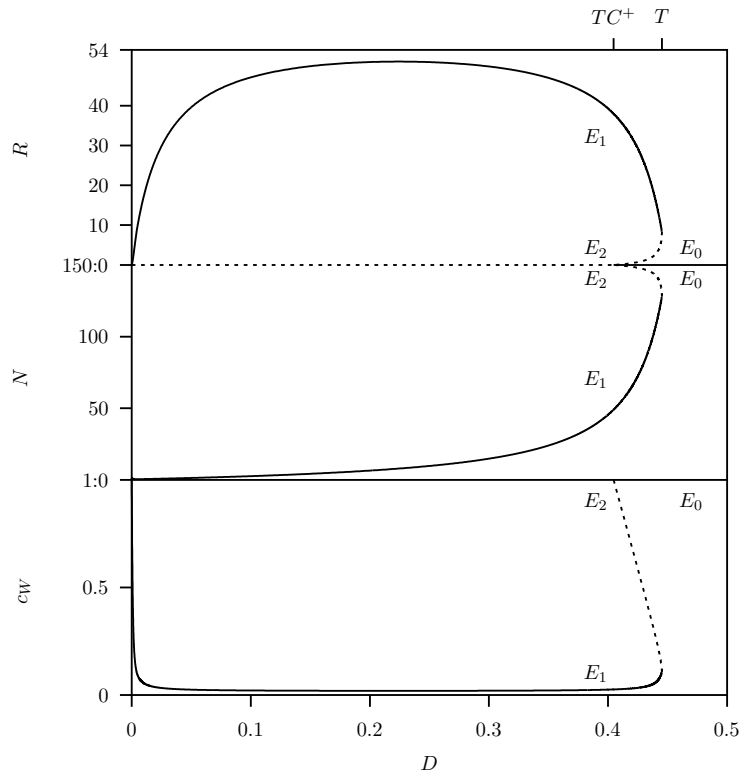

Figure 4.3: A one-parameter bifurcation diagram with dilution rate D as free parameter, for the population with toxicity stress in the chemostat system (4.9) where $N_r = 150$ and $c_r = 1$. Solid lines are stable equilibria E_0, E_1 and dashed curved lines ones E_2. Point T is a tangent bifurcation, TC^+ a subcritical transcritical bifurcation. Between the two points T and TC^+ there is bi-stability.

aspects are involved: for instance to determine to which equilibrium the system will converge when there are multiple equilibria.

4.4 Discussion

For an overview of different mathematical model formulations and their analysis of unstressed ecosystems, the reader may consult [70] and references therein. In this paper we focused on the sublethal effects of a toxicant on the ecosystem structure and functioning. Important effects are extinction of species, invasibility by a species from a neighbourhood, abundance of the different populations and long-term dynamics (stable equilibrium, oscillatory or chaotic behaviour).

For the simple ecosystems studied, we found that toxic effects have very large consequences for the long-term dynamical behaviour. When the maintenance process is the mode of action the per capita maintenance rate coefficient is not constant anymore, but increases with internal toxicant concentration. The concentration of the internal toxicant depends on the toxicant concentration in the water which is in turn linked with the dynamics of the biomass of the population since removal of the toxicant is partly via the biomass that leaves the reactor at the dilution rate. This is a feed-back mechanism. Due to this feed-back mechanism the repertoire of dynamical behaviour of the stressed system is much more diverse, for instance bi-stability, cyclic behaviour and global bifurcations occur.

Bi-stability of the nutrient–prey system can be the result of various mechanisms, we mention the Allee effect [3,124]. When a population possessing an Allee effect is consumed by a predator population this can lead to a collapse of the complete system when a predator invades the nutrient–prey system (see for instance [9, 64]). In [75] we showed that mathematically a heteroclinic bifurcation is associated with this biological phenomenon.

Given a toxic stress level c_r, it is possible to identify environmental conditions N_r and D, under which the toxic stress has no effect on the abundances. This threshold concentration value is determined by the requirement that to equals the NEC value of at least one mode of action of one population.

Chapter 5

Example: Forest-pest model

Forest-Pest Interaction Dynamics:
The Simplest Mathematical Models
M. YA. Antonovsky, R. A. Fleming, Yu. A. Kuznetsov and W.C. Clark, 1990.
Forest–Pest interaction dynamics: The simplest mathematical models *Theoretical Population Biology* 37:343-367.

In this section we deal with the dynamics of a Forest-Pest system. The model in described and analysed in [5]. The forest possesses two stages a young x and an old y stage. Therefore the forest population is modelled by two ODEs. It is assumed that the pest feeds on the young trees (undergrowth).

The bifurcation analysis shows that there is a global bifurcation involved with the destruction of a limit cycle. This stable limit cycle originates at a supercritical Hopf bifurcation of a stable positive equilibrium. Beyond this global bifurcation the system colapes completely, hence besides the pest and the yound trees also the old trees (due to lack of replacement by yound trees). This a a kind of over-exploitation similar to that found in [124] for a predator-prey system where the prey population growth shows an Allee effect.

5.1 Formulation of the model

The model equations in dimensionless form read

$$\frac{dx}{dt} = \rho y - (y-l)^2 x - sx - xz \;, \tag{5.1a}$$

$$\frac{dy}{dt} = x - hy \;, \tag{5.1b}$$

$$\frac{dz}{dt} = \epsilon z + Bxz \;, \tag{5.1c}$$

where ρ and h are compound parameters which will serve as bifurcation parameters. We will used the dimensioneless parameter values given in Table 5.1.

5.2 Bifurcation diagrams

A one-parameter diagram is shown in Fig. 5.1 where h is varied. Point $G^{\neq}$ indicates a heteroclines connection between the two positive saddle equilibria in the plane $z = 0$.

Table 5.1: Parameter values after [5, Table 1] and the used dimensionless values with the calculation of the bifurcation diagrams.

Parameter	Units	Values	dimensionless Values
a	$\text{ha}^2(103\text{ trees})^{-2}\text{yr}^{-1}$	0.00606	—
b	10^3 trees ha^{-1}	0.247	—
c	yr^{-1}	0.01	—
ρ	yr^{-1}	0.134	variable
f	yr^{-1}	0.017	—
h	yr^{-1}	0.04	variable
A	yr^{-1}	0.004	—
ϵ	yr^{-1}	1.5	2
B	yr^{-1}	0.8	1
s	yr^{-1}	—	1

Fig. 5.2 is the two-parameter bifurcation diagram with besides h now ρ is also a bifurcation parameter. Observe that Fig. 5.1 shows the three state variables as a function of h where $\rho = 10$. For low h values the abundance of the young trees is low and of the old trees rather high. Increasing h makes it possible for the pest to invade at TC_2. This positive equilibrium becomes unstable at a supercritical Hopf bifurcation H. Crossing this curve gives oscillatory dynamics of a stable limit cycles. The size of this cycle increases with increasing h. At the global bifurcation $G^{\neq}$ this cycle disappears by a collision with the two saddle equilibria where the pest is absent.Above this curve the zero equilibrium is globally stable.

Curve T is the tangent bifurcation curve. For parameter values on the left-hand side of this curve the system is absent. At this curve two positive equilibria collide. Both are unstable, see Fig. 5.1.

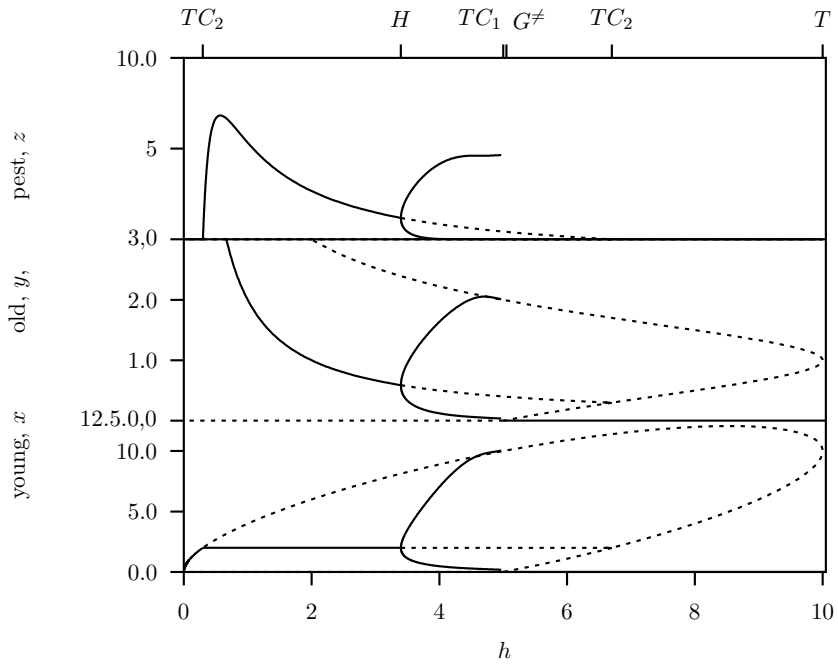

Figure 5.1: One-parameter bifurcation diagram with free parameter h for the Forest-Pest model system (5.1) where $\rho = 10$. Points TC_1 and TC_2 are transcritical bifurcation points. Point H is the Hopf bifurcation point and $G^{\neq}$ indicates the heteroclinic orbit.

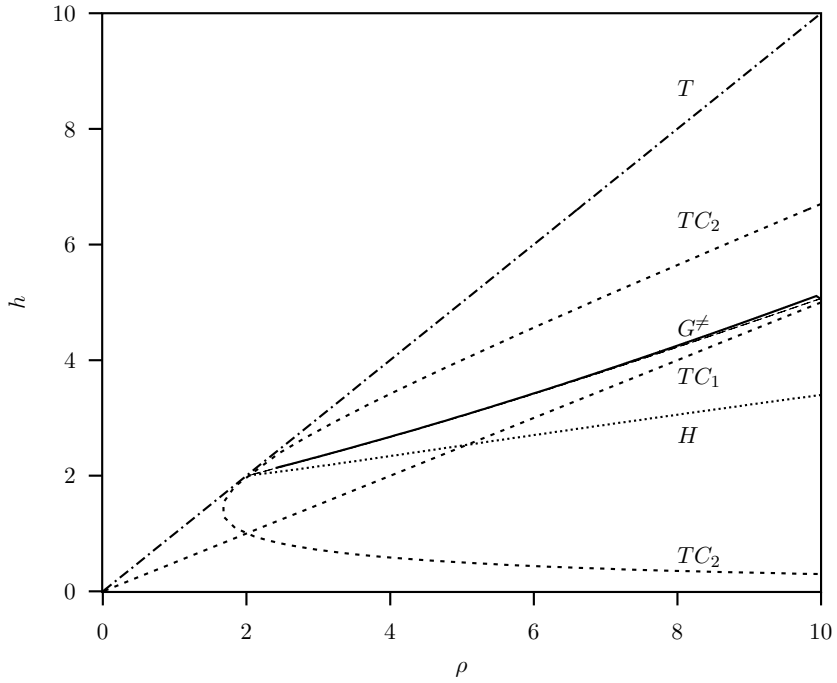

Figure 5.2: Two-parameter bifurcation diagram for the Forest-Pest model system (5.1) where $\rho = 10$. The bifurcation parameters are ρ and h. Curves TC_1 and TC_2 are transcritical bifurcation curves. Curve H is the Hopf bifurcation curve and $G^{\neq}$ indicates the heteroclinic bifurcation curve.

Chapter 6

Food chain: Point-to-cycle connections

Continuation of connecting orbits in 3D-odes: (I) Point-to-cycle connections
E.J. Doedel, B.W. Kooi, G.A.K. van Voorn and Yu.A. Kuznetsov
International Journal of Bifurcation and Chaos, 18(7):1889-1903.

We propose new methods for the numerical continuation of point-to-cycle connecting orbits in 3-dimensional autonomous ODE's using projection boundary conditions. In our approach, the projection boundary conditions near the cycle are formulated using an eigenfunction of the associated adjoint variational equation, avoiding costly and numerically unstable computations of the monodromy matrix. The equations for the eigenfunction are included in the defining boundary-value problem, allowing a straightforward implementation in AUTO, in which only the standard features of the software are employed. Homotopy methods to find connecting orbits are discussed in general and illustrated with one example. Complete AUTO demos, which can be easily adapted to any autonomous 3-dimensional ODE system, are freely available.

6.1 Introduction

Many interesting phenomena in ODE systems can only be understood by analyzing global bifurcations. Examples of such are the occurrence and disappearance of chaotic behaviour. For example, the classical Lorenz attractor appears in a sequence of bifurcations, where *homoclinic orbits* connecting a saddle equilibrium to itself and *heteroclinic orbits* connecting an equilibrium point with a saddle cycle, are involved [2]. In the ecological context, [18, 19] showed that regions of chaotic behaviour in parameter space in some food chain models are bounded by bifurcations of point-to-cycle and cycle-to-cycle connections.

Thus, in order to gain more knowledge about the global bifurcation structure of a model, information is required on the existence of *homoclinic* and *heteroclinic* connections between equilibria and/or periodic cycles. The first type is a connection that links an equilibrium or a cycle to itself (asymptotically bi-stable, so it necessarily has nontrivial stable and unstable invariant manifolds). The second type is a connection that links an equilibrium or a cycle to another equilibrium or cycle.

The continuation of connecting orbits in ODE systems has been notoriously difficult. In

[32]) and [13] direct numerical methods have been developed for the computation of orbits connecting equilibrium points and their associated parameter values, based on truncated boundary value problems with *projection boundary conditions*. Moreover, in [33] proposed efficient methods to find starting solutions by successive continuations (homotopies). These continuation methods have been implemented in HomCont, as incorporated in AUTO [20, 22, 36]. HomCont is only suitable for the continuation of homoclinic point-to-point and heteroclinic point-to-point connections.

More recently, significant progress has been made in the continuation of homoclinic and heteroclinic connections involving cycles. In [28, 29] a method has been developed based on earlier works by [14] and [107]. Their method is also based on projection boundary conditions, but uses an *ad hoc* multiple shooting technique and requires the numerical determination of the monodromy matrix associated with the periodic cycles involved in the connection.

In this paper, we propose new methods for the numerical continuation of point-to-cycle connections in 3-dimensional autonomous ODE's using projection boundary conditions. In our approach, the projection boundary conditions near each cycle are formulated using an eigenfunction of the associated adjoint variational equation, avoiding costly and numerically unstable computation of the monodromy matrix. Instead, the equations for the eigenfunction are included in the defining boundary-value problem, allowing a straightforward implementation in AUTO.

This section is organized as follows. In Section 7.2 we recall basic properties of the projection boundary condition method to continue point-to-cycle connections. In Section 6.3 this method is adapted to efficient numerical implementation in a special – but important – 3D case. Homotopy methods to find connecting orbits are discussed in Section 6.4. Section 6.5 demonstrates that the algorithms allow for a straightforward implementation in AUTO, using only the basic features of this software. The well-known standard three-level food chain model based on the Rosenzweig–MacArthur system [111] is used to illustrate the power of the new methods. In [34] also the Lorenz equations, an electronic circuit model are analysed.

6.2 Truncated BVP's with projection BC's

Before presenting a BVP for a point-to-cycle connection, we set up some notation.

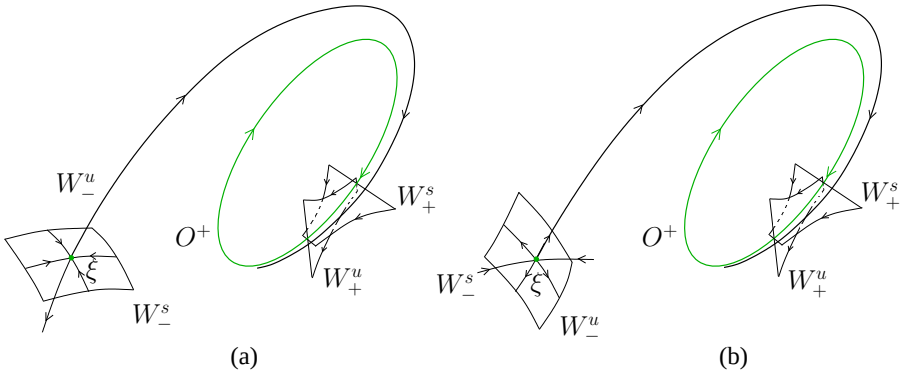

Figure 6.1: Point-to-cycle connecting orbits in $\mathbb{R}^3$: (a) $n_u^- = 1$; (b) $n_u^- = 2$.

Consider a general system of ODE's

$$\frac{du}{dt} = f(u, \alpha), \tag{6.1}$$

where $f : \mathbb{R}^n \times \mathbb{R}^p \to \mathbb{R}^n$ is a sufficiently smooth function of the state variables $u \in \mathbb{R}^n$ and the control parameters $\alpha \in \mathbb{R}^p$. Denote by φ^t the (local) flow generated by (6.1)[1].

Let O^- be either a saddle or a saddle-focus equilibrium, say ξ, and let O^+ be a hyperbolic saddle limit cycle of (6.1). A solution $u(t)$ of (6.1) defines a *connecting orbit* from O^- to O^+ if

$$\lim_{t\to\pm\infty} \mathrm{dist}(u(t), O^{\pm}) = 0 \tag{6.2}$$

(see Figure 6.1 for illustrations). Since $u(t+\tau)$ satisfies (6.1) and (6.2) for any phase shift τ, an additional scalar phase condition

$$\psi[u, \alpha] = 0 \tag{6.3}$$

is needed to ensure uniqueness of the connecting orbit. This condition will be specified later.

For numerical approximation, the asymptotic conditions (6.2) are replaced by *projection boundary conditions* at the end-points of a large *truncation interval* $[\tau_-, \tau_+]$: The points $u(\tau_-)$ and $u(\tau_+)$ are required to belong to the linear subspaces that are tangent to the unstable and stable invariant manifolds of O^- and O^+, respectively.

Let n_u^- be the dimension of the unstable invariant manifold W_-^u of ξ, *i.e.*, the number of eigenvalues λ_u^- of the Jacobian matrix $f_u = D_u f$ evaluated at the equilibrium which satisfy

$$\Re(\lambda^-) > 0. \tag{6.4}$$

Denote by $x^+(t)$ a periodic solution (with minimal period T^+) corresponding to O^+ and introduce the *monodromy matrix*

$$M^+ = D_x \varphi^{T^+}(x)\Big|_{x=x^+(0)}, \tag{6.5}$$

i.e., the linearization matrix of the T^+-shift along orbits of (6.1) at point $x_0^+ = x^+(0) \in O^+$. Its eigenvalues μ^+ are called the *Floquet multipliers*; exactly one of them equals 1, due to the assumption of hyperbolicity. Let $m_s^+ = n_s^+ + 1$ be the dimension of the stable invariant manifold W_+^s of the cycle O^+; here n_s^+ is the number of its multipliers satisfying

$$|\mu^+| < 1. \tag{6.6}$$

A necessary condition to have an isolated *family* of point-to-cycle connecting orbits of (6.1) is that (see [14])

$$p = n - m_s^+ - n_u^- + 2 \tag{6.7}$$

The projection boundary conditions in this case can be written as

$$L^-(u(\tau_-) - \xi) = 0\,, \tag{6.8a}$$
$$L^+(u(\tau_+) - x^+(0)) = 0\,, \tag{6.8b}$$

[1]Whenever possible, we will not indicate explicitly the dependence of various objects on system parameters.

where L^- is a $(n - n_u^-) \times n$ matrix whose rows form a basis in the orthogonal complement of the linear subspace that is tangent to W_-^u at ξ. Similarly, L^+ is a $(n - m_s^+) \times n$ matrix, such that its rows form a basis in the orthogonal complement to the linear subspace that is tangent to W_+^s of O^+ at $x^+(0)$.

It can be proved that, generically, the truncated BVP composed of (6.1), a truncation of (6.3), and (6.8) has a unique solution family $(\hat{u}, \hat{\alpha})$, provided that (6.1) has a connecting solution family satisfying (6.3) and (6.7).

The truncation to the finite interval $[\tau_-, \tau_+]$ implies an error. If u is a generic connecting solution to (6.1) at parameter value α, then the following estimate holds:

$$\|(u|_{[\tau_-,\tau_+]}, \alpha) - (\hat{u}, \hat{\alpha})\| \leq C\mathrm{e}^{-2\min(\mu_-|\tau_-|,\mu_+|\tau_+|)}, \tag{6.9}$$

where $\|\cdot\|$ is an appropriate norm in the space $C^1([\tau_-, \tau_+], \mathbb{R}^n) \times \mathbb{R}^p$, $u|_{[\tau_-,\tau_+]}$ is the restriction of u to the truncation interval, and $\mu_\pm$ are determined by the eigenvalues of the Jacobian matrix and the monodromy matrix. See [107] and [28, 29] for exact formulations, proofs, and references to earlier contributions.

6.3 New defining systems in $\mathbb{R}^3$

Here we explain how the projection boundary conditions (6.8) can be implemented efficiently in a special – but important – case $n = 3$. Thereafter we specify the defining system used to continue connecting orbits in 3D-ODE example systems with AUTO. A saddle cycle O^+ in such systems always has $m_s^+ = m_u^+ = 2$.

6.3.1 The equilibrium-related part

The equilibrium point ξ, an appropriate solution of $f(\xi, \alpha) = 0$, cannot be found by time-integration methods because it is a saddle. There are two different types of saddle equilibria that can be connected to saddle cycles in 3D-ODE's. These are distinguished by the dimension n_u^- of the unstable invariant manifold W_-^u of ξ: We have either $n_u^- = 1$ or $n_u^- = 2$ (see Figure 6.1). In the former case, the connection is structurally unstable (has codim 1) and, according to (6.7), we need two free system parameters for its continuation ($p = 2$). In the latter case, however, the connection is structurally stable and can be continued, generically, with one system parameter ($p = 1$). There is a small difference in the implementation of the projection boundary condition (6.8a) in these two cases.

If $n_u^- = 1$ (see Figure 6.2(a)), then the following *explicit projection boundary condition* replaces (6.8a):

$$u(\tau_-) = \xi + \varepsilon v, \tag{6.10}$$

where $\varepsilon > 0$ is a given small number, and $v \in \mathbb{R}^3$ is a unit vector that is tangent to W_-^u at ξ. Notice that this fixes the phase of the connecting solution u, so that (6.3) becomes (6.8a) in this case. The vector v in (6.10) is, of course, a normalized eigenvector associated with the unstable eigenvalue $\lambda_u > 0$ of the Jacobian matrix f_u evaluated at the equilibrium. Hence, we can use the following algebraic system to continue ξ, v and λ_u simultaneously:

$$\left\{ \begin{array}{rcl} f(\xi, \alpha) & = & 0\,, \\ f_\xi(\xi, \alpha)v - \lambda_u v & = & 0\,, \\ \langle v, v\rangle - 1 & = & 0\,, \end{array} \right. \tag{6.11}$$

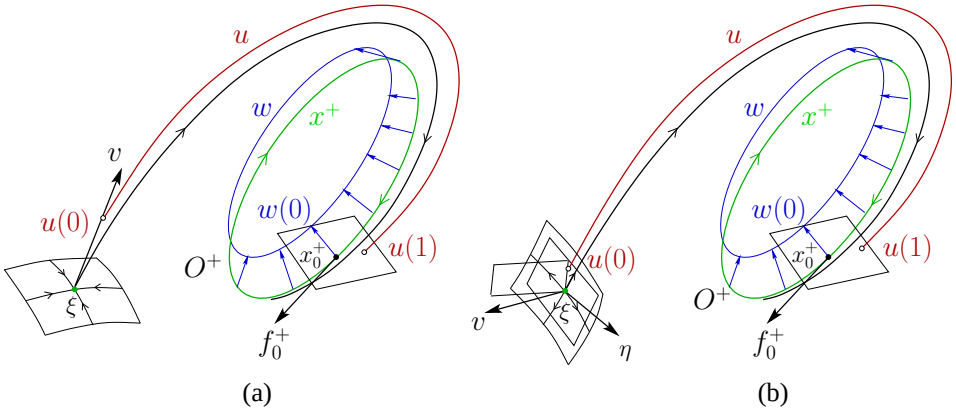

Figure 6.2: BVP's to approximate connecting orbits: (a) $n_u^- = 1$; (b) $n_u^- = 2$.

where $\langle x, u\rangle = x^{\mathrm{T}}u$ is the standard scalar product in $\mathbb{R}^n$.

If $n_u^- = 2$ (see Figure 6.2(b)), then W_-^u is orthogonal to an eigenvector v of the *transposed* Jacobian matrix f_u^{T} corresponding to its eigenvalue $\lambda_s < 0$, so that (6.8a) can be written as

$$\langle v, u(\tau_-) - \xi\rangle = 0. \tag{6.12}$$

To continue ξ, v, and λ_s, we use a system similar to (6.11), namely:

$$\left\{\begin{array}{rcl} f(\xi,\alpha) &=& 0\,, \\ f_\xi^{\mathrm{T}}(\xi,\alpha)v - \lambda_s v &=& 0\,, \\ \langle v, v\rangle - 1 &=& 0\,. \end{array}\right. \tag{6.13}$$

As a variant of the phase condition (6.3) in this case, we can use the linear condition

$$\langle \eta, u(\tau_-) - \xi\rangle = 0, \tag{6.14}$$

which places the starting point of the truncated connecting solution in a plane containing the equilibrium ξ and orthogonal to a fixed vector η (not collinear with v).

6.3.2 The cycle and eigenfunctions

The heteroclinic connection is linked on the other side to a saddle limit cycle O^+ (see Figure 6.2). Thus, we also need a BVP to compute it. We use the standard periodic BVP:

$$\left\{\begin{array}{ll} \dot{x}^+ - f(x^+,\alpha) & = 0\,, \\ x^+(0) - x^+(T^+) & = 0\,, \end{array}\right. \tag{6.15}$$

which is augmented by an appropriate phase condition that makes its solution unique. This phase condition is actually a boundary condition for the truncated connecting solution, and will be introduced below.

To set up the projection boundary condition for the truncated connecting solution u near O^+, we also need a vector, say $w(0)$, that is orthogonal at $x(0)$ to the stable manifold W_+^s of the saddle limit cycle O^+ (see Figure 6.2). It is well known that $w(0)$ can be obtained from

an *eigenfunction* $w(t)$ of the *adjoint variational problem* associated with (6.15), corresponding to its eigenvalue

$$\mu = \frac{1}{\mu_u^+}, \tag{6.16}$$

where μ_u^+ is a multiplier of the monodromy matrix M^+ satisfying

$$|\mu_u^+| > 1 \tag{6.17}$$

(see Appendix 6.8). The corresponding BVP is

$$\left\{ \begin{array}{rcl} \dot{w} + f_u^{\mathrm{T}}(x^+, \alpha) w & = & 0\,, \\ w(T^+) - \mu w(0) & = & 0\,, \\ \langle w(0), w(0) \rangle - 1 & = & 0\,, \end{array} \right. \tag{6.18}$$

where x^+ is the solution of (6.15). In our implementation the above BVP is replaced by an equivalent BVP

$$\left\{ \begin{array}{rcl} \dot{w} + f_u^{\mathrm{T}}(x^+, \alpha) w + \lambda w & = & 0\,, \\ w(T^+) - s w(0) & = & 0\,, \\ \langle w(0), w(0) \rangle - 1 & = & 0\,, \end{array} \right. \tag{6.19}$$

where $s = \text{sign}\ \mu = \pm 1$ and

$$\lambda = \ln |\mu| \tag{6.20}$$

(see Appendix 6.8). In (6.19), the boundary conditions become periodic or anti-periodic, depending on the sign of the multiplier μ, while the logarithm of its absolute value appears in the variational equation. This ensures high numerical robustness.

Given w satisfying (6.19), the projection boundary condition (6.8b) becomes

$$\langle w(0), u(\tau_+) - x^+(0) \rangle = 0. \tag{6.21}$$

6.3.3 The connection

Finally, we need a phase condition to select a unique periodic solution among those which satisfy (6.15), *i.e.*, to fix a *base point* $x_0^+ = x^+(0)$ on the cycle O^+ (see Figure 6.2). Usually, an integral condition is used to fix the phase of the periodic solution. For the point-to-cycle connection, however, we need a new condition, since the end point near the cycle should vary freely. To this end we require the end point of the connection to belong to a plane orthogonal to the vector $f_0^+ = f(x^+(0), \alpha)$. This gives the following BVP for the connecting solution:

$$\left\{ \begin{array}{rcl} \dot{u} - f(u, \alpha) & = & 0\,, \\ \langle f(x^+(0), \alpha), u(\tau_+) - x^+(0) \rangle & = & 0\,. \end{array} \right. \tag{6.22}$$

6.3.4 The complete BVP

The complete truncated BVP to be solved numerically consists of (6.11), with

$$u(0) = \xi + \varepsilon v, \tag{6.23}$$

or (6.13), with

$$\langle v, u(0) - \xi \rangle = 0 \,, \tag{6.24a}$$
$$\langle \eta, u(0) - \xi \rangle = 0, \tag{6.24b}$$

as well as

$$\dot{x}^+ - T^+ f(x^+, \alpha) = 0, \tag{6.25a}$$
$$x^+(0) - x^+(1) = 0, \tag{6.25b}$$
$$\langle w(0), u(1) - x^+(0) \rangle = 0, \tag{6.25c}$$
$$\dot{w} + T^+ f_u^{\mathrm{T}}(x^+, \alpha) w + \lambda w = 0, \tag{6.25d}$$
$$w(1) - s w(0) = 0, \tag{6.25e}$$
$$\langle w(0), w(0) \rangle - 1 = 0, \tag{6.25f}$$
$$\dot{u} - T f(u, \alpha) = 0, \tag{6.25g}$$
$$\langle f(x^+(0), \alpha), u(1) - x^+(0) \rangle = 0. \tag{6.25h}$$

Here the time variable is scaled to the unit interval $[0, 1]$, so that both the cycle period T^+ and the connecting time T become parameters.

If the connection time T is fixed at a large value, this BVP allows to continue simultaneously the equilibrium ξ, its eigenvalue λ_u or λ_s, the corresponding eigenvector v, the periodic solution x^+ corresponding to the limit cycle O^+, its period T^+, the logarithm of the absolute value of the unstable multiplier of this cycle, the corresponding scaled eigenfunction w, as well as (a truncation of) the connecting orbit u. These objects become functions of one system parameter (when $\dim W^u_- = 2$) or two system parameters (when $\dim W^u_- = 1$). These free system parameters are denoted as α_i.

If $\dim W^u_- = 2$ then, generically, limit points (folds) are encountered along the solution family. These can be detected, located accurately, and subsequently continued in two system parameters, say, (α_1, α_2), using the standard fold-following facilities of AUTO.

6.4 Starting strategies

The BVP's specified above can only be used if good starting data are available. This can be problematic, since global objects – a saddle cycle and a connecting orbit – are involved. However, a series of successive continuations in AUTO can be used to generate all necessary starting data, given little *a priori* knowledge about the existence and location of a heteroclinic point-to-cycle connection.

6.4.1 The equilibrium and the cycle

The equilibrium ξ, its unstable or stable eigenvalue, as well as the corresponding eigenvector or adjoint eigenvector can be calculated using MAPLE or MATLAB. Alternatively, this saddle

equilibrium can often be obtained via continuation of a stable equilibrium family through a limit point (fold) bifurcation.

To obtain the limit cycle O^+, one can continue numerically (with AUTO [36] or CONTENT [91], for example) a limit cycle born at a Hopf bifurcation to an appropriate value of α, from where we start the successive continuation.

6.4.2 Eigenfunctions

In the first of such continuations, the periodic solution corresponding the limit cycle at the particular parameter values is used to get an eigenfunction. To explain the idea, let us begin with the original adjoint eigenfunction w. Consider the periodic BVP (6.25a)–(6.25b) for the cycle, to which the standard integral phase condition is added,

$$\int_0^1 \langle \dot{x}^+_{old}(\tau), x^+(\tau)\rangle = 0\ , \tag{6.26}$$

as well as a BVP similar to (6.18), namely:

$$\left\{\begin{array}{rcl} \dot{w} + T^+ f_u^{\rm T}(x^+,\alpha)w &=& 0\ , \\ w(1) - \mu w(0) &=& 0\ , \\ \langle w(0), w(0)\rangle - h &=& 0\ . \end{array}\right. \tag{6.27}$$

In (6.26), x^+_{old} is a reference periodic solution, typically the one in the preceding continuation step. The parameter h in (6.27) is a *homotopy parameter*, that is set to zero initially. Then (6.27) has a trivial solution

$$w(t) \equiv 0, \quad h = 0, \tag{6.28}$$

for any real μ. This family of trivial solutions parametrized by μ can be continued in AUTO using a BVP consisting of (6.15) (with scaled time variable t), (6.26), and (6.27) with free parameters (μ, h) and fixed α. A Floquet multiplier of the adjoint system then corresponds to a branch point at μ_1 along this trivial solution family (see Appendix 6.8). AUTO can accurately locate such a point and switch to the nontrivial branch that emanates from it. Continuing this secondary family in (μ, h) until, say, the value $h = 1$ is reached, gives a nontrivial eigenfunction w corresponding to the multiplier μ_1. Note that in this continuation the value of μ remains constant, $\mu \equiv \mu_1$, up to numerical accuracy.

The same method is applicable to obtain a nontrivial scaled adjoint eigenfunction. For this, the BVP

$$\left\{\begin{array}{rcl} \dot{w} + T^+ f_u^{\rm T}(x^+,\alpha)w + \lambda w &=& 0\ , \\ w(1) - s w(0) &=& 0\ , \\ \langle w(0), w(0)\rangle - h &=& 0\ , \end{array}\right. \tag{6.29}$$

where $s = \mathrm{sign}(\mu)$, replaces (6.27). A branch point at λ_1 then corresponds to the adjoint multiplier se^{λ_1}. Branch switching then gives the desired eigendata.

6.4.3 The connection

Sometimes, an approximation of the connecting orbit can be obtained by time-integration of (6.1) with a starting point satisfying (6.10) or (6.12) and (6.14). These data (the periodic

solution corresponding to the limit cycle, its nontrivial eigenfunction, and the integrated connecting orbit) must then be merged, using the same scaled time variable and mesh points. This only works for non-stiff systems provided that the connecting orbit and its corresponding parameter values are known *a priori* with high accuracy, which is not the case for most models.

A practical remedy in most cases is to apply the method of *successive continuation* first introduced in [33] for point-to-point problems. This method does not guarantee that a connection will be found but works well if we start sufficiently close to a connection *in the parameter space*. Here we generalize this method to point-to-cycle connections.

We first consider the case $\dim W^u_- = 1$. To start, we introduce a BVP composed of (6.11), (6.23), and a modified version of (6.25), namely:

$$\dot{x}^+ - T^+ f(x^+, \alpha) = 0, \tag{6.30a}$$
$$x^+(0) - x^+(1) = 0, \tag{6.30b}$$
$$\Psi[x^+] = 0, \tag{6.30c}$$
$$\dot{w} + T^+ f_u^{\mathrm{T}}(x^+, \alpha) w + \lambda w = 0, \tag{6.30d}$$
$$w(1) - s w(0) = 0, \tag{6.30e}$$
$$\langle w(0), w(0) \rangle - 1 = 0, \tag{6.30f}$$
$$\dot{u} - T f(u, \alpha) = 0, \tag{6.30g}$$
$$\langle f(x^+(0), \alpha), u(1) - x^+(0) \rangle - h_1 = 0, \tag{6.30h}$$

where Ψ in (6.30c) defines any phase condition fixing the base point $x^+(0)$ on the cycle O^+; for example

$$\Psi[x^+] = x^+_j(0) - a_j, \tag{6.31}$$

where a_j is the jth-coordinate of the base point at some given parameter values, and h_1 is a *homotopy parameter*.

Take an initial solution to this BVP that collects the previously found equilibrium-related data, the cycle-related data (x^+, T^+) including $x^+(0)$, the eigenfunction-related data (w, λ), as well as the value of h_1 computed for the initial "connection"

$$u(\tau) = \xi + \varepsilon v \mathrm{e}^{\lambda_u T \tau}, \quad \tau \in [0, 1], \tag{6.32}$$

which is a solution of the scaled linear approximation of (6.1) in the tangent line to the unstable manifold W^u_- of ξ. By continuation in (T, h_1) for a fixed value of α, we try to make $h_1 = 0$, while $u(1)$ is near the cycle O^+, so that T becomes sufficiently large.

After this is accomplished, we introduce another BVP composed of (6.11), (6.23), and

$$\dot{x}^+ - T^+ f(x^+, \alpha) = 0, \tag{6.33a}$$
$$x^+(0) - x^+(1) = 0, \tag{6.33b}$$
$$\langle w(0), u(1) - x^+(0) \rangle - h_2 = 0, \tag{6.33c}$$
$$\dot{w} + T^+ f_u^{\mathrm{T}}(x^+, \alpha) w + \lambda w = 0, \tag{6.33d}$$
$$w(1) - s w(0) = 0, \tag{6.33e}$$
$$\langle w(0), w(0) \rangle - 1 = 0, \tag{6.33f}$$
$$\dot{u} - T f(u, \alpha) = 0, \tag{6.33g}$$
$$\langle f(x^+(0), \alpha), u(1) - x^+(0) \rangle = 0, \tag{6.33h}$$

where h_2 is another homotopy parameter.

Using the solution obtained in the previous step, we can activate one of the system parameters, say α_1, and aim to find a solution with $h_2 = 0$ by continuation in (α_1, h_2) for fixed T. Then we can improve the connection by continuation in (α_1, T), restarting from this latest solution, in the direction of increasing T. Eventually, we fix a sufficiently large value of T and continue the (approximate) connecting orbit in two systems parameters, say (α_1, α_2), using the original BVP without any homotopy parameter as described in Section 6.3.4.

When $\dim W^u_- = 2$, a minor modification of the above homotopy method is required. In this case, we replace (6.24) by the explicit boundary conditions

$$u(0) - \xi - \varepsilon(c_1 v^{(1)} + c_2 v^{(2)}) = 0, \tag{6.34a}$$

$$c_1^2 + c_2^2 = 1, \tag{6.34b}$$

where ε is a small parameter specifying the distance between $u(0)$ and ξ, $v^{(j)}$ are two linear-independent vectors tangent to W^u_- of the saddle ξ, and $c_{1,2}$ are two new scalar homotopy parameters. Note that if $v = (v_1, v_2, v_3)^{\mathrm{T}}$ is a solution to (6.13) with $v_2 \neq 0$, then one can use the normalized vectors

$$v^{(1)} = \begin{pmatrix} v_2 \\ -v_1 \\ 0 \end{pmatrix}, \; v^{(2)} = \begin{pmatrix} 0 \\ v_3 \\ -v_2 \end{pmatrix}. \tag{6.35}$$

Now consider a BVP composed of (6.13), (6.34), and (6.30). The initial data for this BVP are the same as in the case $\dim W^u_- = 1$, except for

$$c_1 = 1, \quad c_2 = 0. \tag{6.36}$$

The initial "connection" in this case is

$$u(\tau) = \xi + \varepsilon \mathrm{e}^{\tau T A} v^{(1)}, \quad \tau \in [0, 1], \tag{6.37}$$

where $A = f_u(\xi, \alpha)$, to be used to compute the initial value of h_1 in (6.30h).

By continuation in (T, h_1) (and, eventually, in (c_1, c_2, h_1)) for fixed values of all other parameters, we aim to locate a solution with $h_1 = 0$, with $u(1)$ near the base point of the cycle O^+, so that T becomes sufficiently large. We then switch to the BVP composed of (6.11), (6.34), and (6.33), and we aim to locate a solution with $h_2 = 0$, by continuation in (c_1, c_2, h_2) for fixed T. When this is achieved, we have a solution to the original BVP (6.13), (6.24), and (6.25) introduced in Section 6.3.4 and containing no homotopy parameters. Using this BVP, we can continue the approximate connecting orbit in one system parameter, say α_1, with T fixed.

Examples of such successive continuations will be given in Section 6.6, where we consider the standard model of a 3-level food chain. In that section also an alternative BVP formulation for (6.34) is given. When one system parameter is varied, limit points (folds) can be found and then continued in two system parameters.

6.5 Implementation in AUTO

Our algorithms have been implemented in AUTO, which solves the boundary value problems using superconvergent *orthogonal collocation* with adaptive meshes. AUTO can compute paths

of solutions to boundary value problems with integral constraints and non-separated boundary conditions:

$$\dot{U}(\tau) - F(U(\tau), \beta) = 0\ , \quad \tau \in [0,1], \tag{6.38a}$$

$$b(U(0), U(1), \beta) = 0\ , \tag{6.38b}$$

$$\int_0^1 q(U(\tau), \beta) d\tau = 0\ , \tag{6.38c}$$

where

$$U(\cdot), F(\cdot,\cdot) \in \mathbb{R}^{n_d},\ b(\cdot,\cdot) \in \mathbb{R}^{n_{bc}},\ q(\cdot,\cdot) \in \mathbb{R}^{n_{ic}}, \tag{6.39}$$

and

$$\beta \in \mathbb{R}^{n_{fp}}. \tag{6.40}$$

Here β represents the n_{fp} *free parameters* that are allowed to vary, where

$$n_{fp} = n_{bc} + n_{ic} - n_d + 1. \tag{6.41}$$

The function q can also depend on $\dot{U}$ and on the derivative of U with respect to pseudo-arclength, as well as on $\hat{U}$, the value of U at the previously computed point on the solution family.

For our primary BVP problem (6.11) or (6.13) with (6.23) or (6.24), respectively, and (6.25), we have

$$n_d = 9, \quad n_{ic} = 0, \tag{6.42}$$

and $n_{bc} = 19$ or 18, respectively, since (6.11) and (6.13) are treated as boundary conditions.

6.6 A food chain model

In this section we illustrate the performance of our algorithm by applying it to one biologically relevant system.

The following three-level food chain model from theoretical biology is based on the Rosenzweig–MacArthur model [111]. The equations are given by

$$\begin{cases} \dot{x}_1 &= x_1(1 - x_1) - f_1(x_1, x_2), \\ \dot{x}_2 &= f_1(x_1, x_2) - f_2(x_2, x_3) - d_1 x_2, \\ \dot{x}_3 &= f_2(x_2, x_3) - d_2 x_3, \end{cases} \tag{6.43}$$

with Holling Type-II functional responses

$$f_i(u, v) = \frac{a_i u v}{1 + b_i u}\ , \quad i = 1, 2. \tag{6.44}$$

The death rates d_1 and d_2 are used as bifurcation parameters, with the other parameters set at $a_1 = 5$, $a_2 = 0.1$, $b_1 = 3$, and $b_2 = 2$.

It is well known that this model displays chaotic behaviour in a given parameter range, see [61, 66, 90, 92, 99].

Previous work in [18, 19] has also shown that the regions of chaos are intersected by homoclinic and heteroclinic global connections. In particular, a heteroclinic point-to-cycle orbit connecting a saddle with a two-dimensional unstable manifold to a saddle cycle with a two-dimensional stable manifold can exist. It was shown that the stable manifold of this limit cycle forms the basin boundary of the interior attractor and that the boundary has a complicated structure, especially near the equilibrium, when the heteroclinic orbit is present. These and other results were obtained numerically using multiple shooting. In this section we reproduce these results for the heteroclinic point-to-cycle connection. Using our homotopy method we obtain an accurate approximation of the heteroclinic orbit. A one-parameter bifurcation diagram then shows limit points, which correspond to tangencies of the above-mentioned two-dimensional manifolds. We then continue the limit points in two parameters.

A starting point can be found, for example, at $d_1 \approx 0.2080452$, $d_2 = 0.0125$, where there is a fold bifurcation in which two limit cycles appear. This also corresponds to the birth of the heteroclinic point-to-cycle connection.

Before using the homotopy method to obtain an approximation of the point-to-cycle connection, we locate a Hopf bifurcation, for instance at $d_1 \approx 0.51227$, $d_2 = 0.0125$. The limit cycle born at this Hopf bifurcation is continued up to a selected value of d_1, say, $d_1 = 0.25$.

We now have an equilibrium

$$\xi = (0.74158162, 0.16666666, 11.997732) \tag{6.45}$$

and a saddle limit cycle with the base point

$$x^+(0) = (0.839705, 0.125349, 10.55289) \tag{6.46}$$

and period $T^+ = 24.282248$. Its nontrivial multipliers are

$$\mu_s^+ = 0.6440615, \mu_u^+ = 6.107464 \cdot 10^2. \tag{6.47}$$

The eigenfunction w is obtained as described in the previous sections. Continuation of the trivial solution of the BVP (6.25a), (6.25b), (6.26), and (6.29) and the subsequent continuation of the bifurcating family until $h = 1$, yields the multiplier

$$\lambda = \ln(\mu_s^+) = -0.439961. \tag{6.48}$$

Note that we use the stable multiplier, because of the projection boundary conditions. The associated nontrivial eigenfunction $w(t)$ with $\|w(0)\| = 1$ has

$$w(0) = (0.09306, -0.87791, -4.69689)^{\mathrm{T}}. \tag{6.49}$$

We now consider a BVP composed of (6.13), (6.34a), and (6.30). Using CONTENT and MATLAB we obtain an approximation of the connection with the boundary condition

$$\Psi[x^+] = x_2^+(0) - 0.125349 \tag{6.50}$$

and period $T = 155.905$. The starting point is calculated by splitting the normalized adjoint stable vector (evaluated at $d_1 = 0.25, d_2 = 0.0125$)

$$v = (0.098440, 0.168771, 0.0049532)^{\mathrm{T}} \tag{6.51}$$

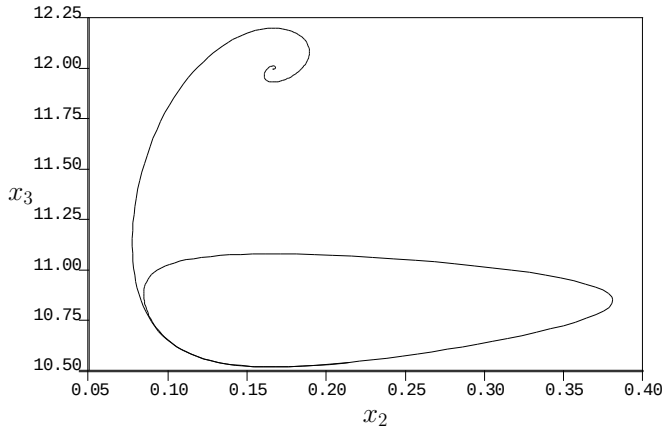

Figure 6.3: An approximation to the point-to-cycle connection projected onto the (x_2, x_3)-plane for the food chain model with $a_1 = 5$, $a_2 = 0.1$, $b_1 = 3$, $b_2 = 2$, $d_1 = 0.25$, and $d_2 = 0.0125$.

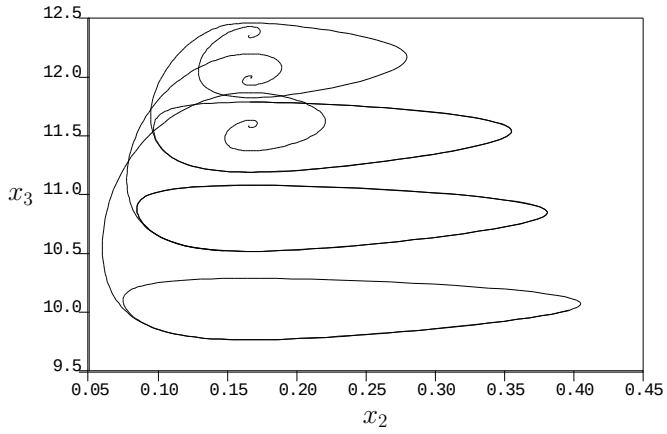

Figure 6.4: Several point-to-cycle connections in the food chain model with different values of d_1.

into $v^{(1)}$ and $v^{(2)}$, as described in Section 6.4.3, and multiplying it by a small ε, say $\varepsilon = 0.001$. In our case the starting point was

$$u(0) = (0.742445, 0.166163, 11.997732). \tag{6.52}$$

The first homotopy step involves continuation in (h_1, T). However, this does not lead to zeroes of h_1. To obtain $h_1 = 0$ we expand the previous set of BVPs with (6.34b). Subsequent continuation in (c_1, c_2, h_1) gives a solution with $h_1 = 0$ that indeed ends near the base point $x^+(0)$ of the limit cycle.

For continuation in the second homotopy step, a switch is made to a BVP composed of (6.13), (6.33) and (6.34). Continuation in (c_1, c_2, h_2) leads to some solutions with $h_2 = 0$.

The obtained approximate connecting point-to-cycle connection now suffices for continuation in system parameters. Before doing a continuation in a system parameter the connection is improved by increasing the connection period. A user-defined point of $T = 300$ suffices. Next, the parameter ε is decreased up to a user-defined point of $\varepsilon = -1 \cdot 10^{-5}$, so that the

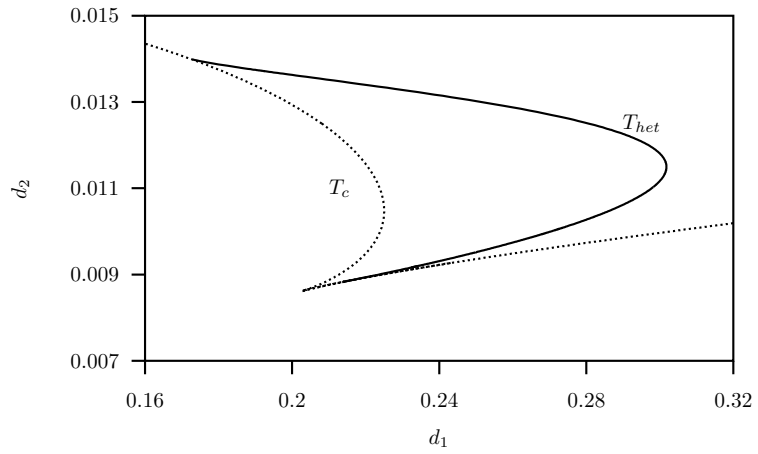

Figure 6.5: A two-parameter bifurcation diagram of the food chain model that shows the region where there exist point-to-cycle connections. The region is bounded on one side by the cycle fold, (T_c), and on the other side by the curve T_{het}, the locus of limit points of the heteroclinic connections.

starting point $u(0)$ is slightly away from the equilibrium ξ. Figure 6.3 displays a projection of the point-to-cycle connection onto the (x_2, x_3)-plane.

Now the connecting orbit can be continued up to a limit point in one system parameter. Figure 6.4 displays three connecting orbits obtained after continuation with respect to $\alpha_1 = d_1$. Continuations in d_1 result in the detection of the points

$$d_1 = 0.280913 \quad \text{and} \quad d_1 = 0.208045 \tag{6.53}$$

where the first one is a limit point and the second one a termination point. This point coincides with a tangent bifurcation for the limit cycle to which the point-to-cycle orbit connects. Continuations in d_2 result in the detection of the points

$$d_2 = 0.0130272 \quad \text{and} \quad d_2 = 9.51660 \cdot 10^{-3} \tag{6.54}$$

which are both limit points. Any of the detected limit points can now be used as a starting point for a two-parameter continuation in $\alpha = d_1$ or d_2. In practice, the connection period may have to be increased or decreased to obtain the full two-parameter continuation curve. In the demo, the last limit point ($d_2 = 9.51660 \cdot 10^{-3}$) is the one selected for the food chain model. The two-parameter continuation curve terminates at both ends in codim 2 points lying on the above-mentioned tangent bifurcation for the limit cycle. These points coincide with the log multiplier $\lambda = 0$. Observe that this corresponds to the point $d_1 = 0.208045$, detected in the one-parameter continuation, where also $\lambda = 0$.

For the continuation in two system parameters, the BC (6.34) proves ineffective, since it leads to the detection of several spurious limit points. This is, because the orbit spiralling out from the equilibrium has an elliptical shape. The circle of a small radius, centered at the equilibrium, intersects the spiral at several points, one of which is the starting point of the connecting orbit. During continuation, with a changing problem parameter, the spiral will change size and the starting point on the circle may collide with another such point where the circle and the spiral intersect. This intersection would correspond to a fold with respect to the problem parameter. As a result, to obtain a full continuation curve of the connecting orbit in two system parameters, some restarts are required.

In order to avoid these spurious folds, we returned to the original BC (6.24) with (6.24b) in the form

$$u_j(0) - \xi_j = 0 \ , \tag{6.55}$$

where j is either 1,2 or 3. By setting $j = 2$ we are in line with the work in [19], who used a Poincaré plane through the equilibrium ξ where $x_2 = \xi_2$.

Figure 6.5 shows the curve of limit points T_{het} that is computed with the method described above, using the standard switching and fold-following facilities of AUTO. This curve can be obtained in one run, given the connection period is chosen conveniently. It agrees with the results previously obtained in [18] by labourious multiple shooting.

6.7 Discussion

Our continuation method for point-to-cycle connections, using homotopies in a boundary value setting is both robust and time-efficient. Detailed AUTO demos carry out the computations described here are freely downloadable [36]. Although the method was presented for 3D-systems, it can be extended directly to point-to-cycle connections in n-dimensional systems, when the unstable invariant manifold of the equilibrium ξ is either one-dimensional or has codimension one, while the stable invariant manifold of the cycle O^+ has codimension one.

In [34] the methodis extended to include detection and continuation of cycle-to-cycle connections.

6.8 Monodromy matrices

In order to approximate the invariant manifolds of a limit cycle we use eigenvalues and eigenfunctions of appropriate variational problems. These eigenvalues in turn are the eigenvalues of the so-called *monodromy matrix*.

To define an eigenfunction of the periodic solution $x(t+T) = x(t)$, where T is the period of the cycle, of an autonomous system of smooth ODE's

$$\dot{u} = f(u), \quad f : \mathbb{R}^n \to \mathbb{R}^n, \tag{6.56}$$

write a solution of this system near the cycle in the form

$$u(t) = x(t) + \xi(t) \ , \tag{6.57}$$

where $\xi(t)$ is a small deviation from the periodic solution. After substitution and truncation of the $O(\|\xi\|^2)$-terms, we obtain the following *variational system*:

$$\dot{\xi} = A(t)\xi \ , \quad \xi \in \mathbb{R}^n \ , \tag{6.58}$$

where $A(t) = f_u(x(t))$ is the Jacobian matrix evaluated along the periodic solution; $A(t+T) = A(t)$.

Now, consider the matrix initial-value problem

$$\dot{Y} = A(t)Y \ , \quad Y(0) = I_n, \tag{6.59}$$

where I_n is the unit $n \times n$ matrix. Its solution $Y(t)$ at $t = T$ is the *monodromy matrix* of the cycle:

$$M = Y(T). \tag{6.60}$$

The monodromy matrix is nonsingular. Any solution $\xi(t)$ to (6.58) satisfies

$$\xi(T) = M\xi(0)\ . \tag{6.61}$$

The eigenvalues of the monodromy matrix M are called the *Floquet multipliers* of the cycle. There is always a multiplier $+1$. Moreover, the product of all multipliers is positive:

$$\mu_1\mu_2\cdots\mu_n = \exp\left(\int_0^T \text{div } f(x(t))\ dt\right). \tag{6.62}$$

Together with (6.58), consider the *adjoint variational system*

$$\dot\zeta = -A^{\mathrm{T}}(t)\zeta\ \ , \quad \zeta \in \mathbb{R}^n \tag{6.63}$$

and the corresponding matrix initial-value problem

$$\dot Z = -A^{\mathrm{T}}(t)Z\ , \qquad Z(0) = I_n, \tag{6.64}$$

which is the adjoint system to (6.59). Note, that the multipliers of the adjoint monodromy matrix

$$N = Z(T) \tag{6.65}$$

are the *inverse* multipliers of the monodromy matrix $M = Y(T)$. The proof of this well-known fact goes as follows. Compute

$$\begin{aligned}\frac{d}{dt}(Z^{\mathrm{T}}Y) &= \frac{dZ^{\mathrm{T}}}{dt}Y + Z^{\mathrm{T}}\frac{dY}{dt}\\ &= (-A^{\mathrm{T}}Z)^{\mathrm{T}}Y + Z^{\mathrm{T}}AY\\ &= Z^{\mathrm{T}}(-A)Y + Z^{\mathrm{T}}AY = 0\ .\end{aligned}$$

Since $Z(0) = Y(0) = I_n$, we get $Z^{\mathrm{T}}(T)Y(T) = I_n$, which implies

$$N = [M^{-1}]^{\mathrm{T}}. \tag{6.66}$$

Due to (6.61), a multiplier μ satisfies $v(T) = \mu v(0)$ with $v(0) \neq 0$ or, equivalently, it is a solution component of the following BVP on the unit interval $[0, 1]$:

$$\left\{\begin{array}{rcl}\dot v + TA(t)v &=& 0\ ,\\ v(1) - \mu v(0) &=& 0\ ,\\ \langle v(0), v(0)\rangle - 1 &=& 0\ .\end{array}\right. \tag{6.67}$$

First assume that $\mu > 0$ and write

$$\mu = \mathrm{e}^{\lambda}, \quad v(t) = \mathrm{e}^{\lambda t}w(t). \tag{6.68}$$

Then w satisfies a periodic BVP, namely:

$$\left\{\begin{array}{rcl} \dot{w} + TA(t)w + \lambda w &=& 0\,, \\ w(1) - w(0) &=& 0\,, \\ \langle w(0), w(0)\rangle - 1 &=& 0\,. \end{array}\right. \tag{6.69}$$

Similarly, when $\mu < 0$, we can introduce

$$\mu = -\mathrm{e}^{\lambda}, \quad v(t) = \mathrm{e}^{\lambda t} w(t) \tag{6.70}$$

and obtain an anti-periodic BVP

$$\left\{\begin{array}{rcl} \dot{w} + TA(t)w + \lambda w &=& 0\,, \\ w(1) + w(0) &=& 0\,, \\ \langle w(0), w(0)\rangle - 1 &=& 0\,. \end{array}\right. \tag{6.71}$$

This technique can easily be adapted to the multipliers of the adjoint variational problem (6.63).

Finally, we note that the eigenvalue problem for a Floquet multiplier

$$Mv - \mu v = 0 \tag{6.72}$$

can be considered as a *continuation problem* with $n+1$ variables $(v, \mu) \in \mathbb{R}^n \times \mathbb{R}$ defined by n equations. This continuation problem has a trivial solution family $(v, \mu) = (0, \mu)$. An eigenvalue μ_1 corresponds to a *branch point*, from which a *secondary solution family* (v, μ_1) with $v \neq 0$ emanates. This nontrivial family can be continued using an extended continuation problem

$$\left\{\begin{array}{rcl} Mv - \mu v &=& 0\,, \\ \langle v, v\rangle - h &=& 0, \end{array}\right. \tag{6.73}$$

which consists of $n+1$ equation with $n+2$ variables (v, μ, h). If $h = 1$ is reached, we get a normalized eigenvector v corresponding to the eigenvalue μ_1, since along this branch $\mu \equiv \mu_1$. Generalization of this procedure to the BVP (6.67) (as well as to (6.69), (6.71), and their adjoint versions) is straightforward.

Chapter 7

Cycle-to-cycle connections in food chain

Continuation of connecting orbits in 3D-odes: (II) Cycle-to-cycle connections
E.J. Doedel, B.W. Kooi, G.A.K. van Voorn and Yu.A. Kuznetsov
International Journal of Bifurcation and Chaos, 19(1):159-169.

In [34] we discussed new methods for the numerical continuation of point-to-cycle connecting orbits in 3-dimensional autonomous ODEs using projection boundary conditions. In this second part we extend the method to the numerical continuation of cycle-to-cycle connecting orbits. In our approach, the projection boundary conditions near the cycles are formulated using eigenfunctions of the associated adjoint variational equations, avoiding costly and numerically unstable computations of the monodromy matrices. The equations for the eigenfunctions are included in the defining boundary-value problem, allowing a straightforward implementation in AUTO, in which only the standard features of the software are employed. Homotopy methods to find the connecting orbits are discussed in general and illustrated with an example from population dynamics. Complete AUTO demos, which can be easily adapted to any autonomous 3-dimensional ODE system, are freely available.

7.1 Introduction

In a diversity of scientific fields bifurcation theory is used for the analysis of systems of ordinary differential equations (ODEs) under parameter variation. Many interesting phenomena in ODE systems are linked to global bifurcations. Examples of such are overharvesting in ecological models with bistability properties [5, 9, 124], and the occurrence and disappearance of chaotic behaviour in such models. For example, it has been shown (see [18, 19, 90]) that chaotic behaviour of the classical food chain models is associated with global bifurcations of point-to-point, point-to-cycle, and cycle-to-cycle connecting orbits.

In [34] we discussed *heteroclinic* connections between equilibria and cycles. Here we look at connections that link a cycle to itself (a *homoclinic* cycle-to-cycle connection, for which the cycle is necessarily saddle), or to another cycle (a *heteroclinic* cycle-to-cycle connection). Orbits homoclinic to the same hyperbolic cycle are classical objects of the Dynamical Systems Theory. It is known thanks to [15, 101, 109, 116, 117] that a transversal intersection of the stable and unstable invariant manifolds of the cycle along such an orbit implies the existence

of infinite number of saddle cycles nearby. Disappearance of the intersection via collision of two homoclinic orbits (*homoclinic tangency*) is an important global bifurcation for which the famous Hénon map turns to be a model Poincaré mapping [44, 45, 88, 106].

Numerical methods for homoclinic orbits to equilibria have been devised by [30] but see [34], who approximated homoclinic orbits by periodic orbits of large but fixed period. In [13] a direct numerical method has been developed for the computation of such connecting orbits and their associated parameter values, based on integral conditions and a truncated boundary value problem (BVP) with projection boundary conditions.

The continuation of homoclinic connections in AUTO [36] improved with the development of HomCont by [20, 22]. However, it is only suited for the continuation of bifurcations of homoclinic point-to-point connections and some heteroclinic point-to-point connections. A modification of this software was introduced in [27], that uses the continuation of invariant subspaces (CIS-algorithm) for the location and continuation of homoclinic point-to-point connections.

In [29]) significant progress has been made by developing methods to continue point-to-cycle and cycle-to-cycle connecting orbits based on another work in [14]. Their method employs a multiple shooting technique and requires the numerical solving for the monodromy matrices associated with the periodic cycles involved in the connection. Recently, Krauskopf and Rieß (2008) used a Lins method approach to finding and continuing similar connections.

Our previous paper [34] we dealt with a method for the detection and continuation of point-to-cycle connections. Here this method is adapted for the continuation of homoclinic and heteroclinic cycle-to-cycle connections. The method is set up such that the homoclinic case is essentially a heteroclinic case where the same periodic orbit (but not the periodic solution) is doubled. In Section 7.2 we give a short overview of a BVP formulation to solve a heteroclinic cycle-to-cycle problem. In Section 7.3 it is shown how boundary conditions are implemented. In Section 7.4 we discuss starting strategies to obtain approximate connecting orbits using homotopy. In Section 6.5 the BVP is made suitable for numerical implementation.

Results are presented of the continuation of a homoclinic cycle-to-cycle connection in the standard three-level food chain model in Section 7.6. Previously numerically in [18] the two-parameter continuation curve of this connecting orbit has been obtained using a shooting method, combined with the Poincaré map technique. In [34] we reproduced the results for the structurally stable heteroclinic point-to-cycle connection of the same food chain model using the homotopy method. In this paper we discuss how the homoclinic cycle-to-cycle connection can be detected, and continued in parameter space using the homotopy method. Also, it is set up such that it can be used as well for a heteroclinic cycle-to-cycle connection.

7.2 Truncated BVPs with projection BCs

Before presenting the BVP that describes a cycle-to-cycle connection, let us first set up some notation. Consider a general system of ODEs

$$\frac{du}{dt} = f(u, \alpha), \tag{7.1}$$

where $f : \mathbb{R}^n \times \mathbb{R}^p \to \mathbb{R}^n$ is sufficiently smooth, given that state variables $u \in \mathbb{R}^n$, and control parameters $\alpha \in \mathbb{R}^p$. Thus, the dimension of the state space is n and the dimension of the parameter space is p. The (local) flow generated by (7.1) is denoted by φ^t. Whenever possible, we will not indicate explicitly the dependence of various objects on parameters.

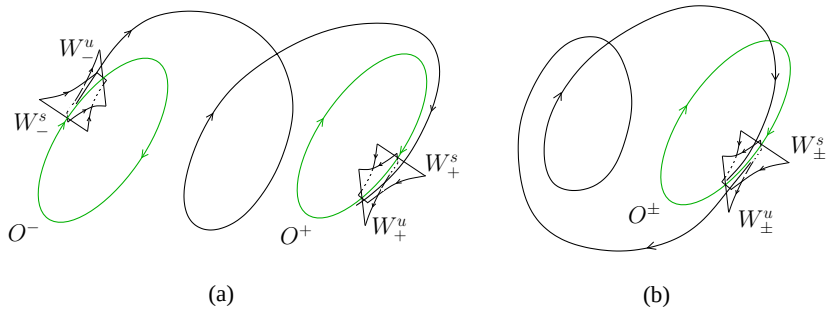

Figure 7.1: Cycle-to-cycle connecting orbits in $\mathbb{R}^3$: (a) heteroclinic orbit, $O^+ \neq O^-$; (b) homoclinic orbit, $O^+ = O^-$.

We assume that both O^- and O^+ are saddle limit cycles of (7.1). A solution $u(t)$ of (7.1) for fixed α defines a *connecting orbit* from O^- to O^+ if

$$\lim_{t\to\pm\infty} \operatorname{dist}(u(t), O^\pm) = 0 \,. \tag{7.2}$$

(Figure 7.1 depicts such a connecting orbit in the 3D-space.) Since $u(t+\tau)$ satisfies (7.1) and (7.2) for any phase shift τ, an additional phase condition

$$\psi[u, \alpha] = 0 \,, \tag{7.3}$$

should be imposed to ensure uniqueness of the connecting solution. This condition will be specified later.

For numerical approximations, the asymptotic conditions (7.2) are substituted by *projection boundary conditions* at the end-points of a large *truncation interval* $[\tau_-, \tau_+]$, following [14]. It is prescribed that the points $u(\tau_-)$ and $u(\tau_+)$ belong to the linear subspaces, which are tangent to the unstable and stable invariant manifolds of O^- and O^+, respectively.

Now, denote by $x^\pm(t)$ a periodic solution (with minimal period $T^\pm$) corresponding to $O^\pm$ and introduce the *monodromy matrix*

$$M^\pm = D_x \varphi^{T^\pm}(x)\Big|_{x=x^\pm(0)} \,,$$

i.e. the linearization matrix of the $T^\pm$-shift along orbits of (7.1) at point $x_0^\pm = x^\pm(0) \in O^\pm$. Its eigenvalues are called *Floquet multipliers*, of which one (trivial) equals 1. Let $m_s^+ = n_s^+ + 1$ be the dimension of the stable invariant manifold W^s_+ of the cycle O^+, where n_s^+ is the number of its multipliers satisfying

$$|\mu| < 1.$$

Along the same line, $m_u^- = n_u^- + 1$ is the dimension of the unstable invariant manifold W^u_- of the cycle O^-, and n_u^- is the number of its multipliers satisfying

$$|\mu| > 1.$$

To have an isolated branch of cycle-to-cycle connecting orbits of (7.1) it is necessary that

$$p = n - m_s^+ - m_u^- + 2 \,, \tag{7.4}$$

Table 7.1: List of notation used in the paper.

sym.	meaning
$x^{\pm}$	Periodic solution
$v^{\pm}$	Eigenfunction
$w^{\pm}$	Scaled adjoint eigenfunction
u	Connection
α	Bifurcation parameters
O^+	Limit cycle where connection ends
O^-	Limit cycle where connection starts
W^s_+	Stable manifold of the cycle O^+
W^u_-	Unstable manifold of the cycle O^-
μ^+_u	Unstable multiplier of the cycle O^+
μ^-_s	Stable multiplier of the cycle O^-
μ^-_u	Unstable multiplier of the cycle O^-
μ^+	Adjoint multiplier $1/\mu^+_u$
μ^-	Adjoint multiplier $1/\mu^-_s$
$\lambda^{\pm}$	$\ln(\mu^{\pm})$
$T^{\pm}$	Period of the cycle $O^{\pm}$
T	Connection time

(see [14]).

The projection boundary conditions in this case become

$$L^{\pm}(u(\tau_{\pm}) - x^{\pm}(0)) = 0 \,, \tag{7.5}$$

where L^- is a $(n - m^-_u) \times n$ matrix whose rows form a basis in the orthogonal complement to the linear subspace that is tangent to W^u_- at $x^-(0)$. Similarly, L^+ is a $(n - m^+_s) \times n$ matrix, such that its rows form a basis in the orthogonal complement to the linear subspace that is tangent to W^s_+ at $x^+(0)$.

The above construction also applies in the case when O^+ and O^- coincide, *i.e.* we deal with a *homoclinic orbit* to a saddle limit cycle $O^+ = O^-$. Note that, in general, the base points $x^{\pm}(0) \in O^{\pm}$ remain different (and so do the periodic solutions $x^{\pm}(t)$).

It can be proved that, generically, the truncated BVP composed of (7.1), a truncation of (7.3), and (7.5), has a unique solution branch $(\hat{u}(t, \hat{\alpha}), \hat{\alpha})$, provided that (7.1) has a connecting solution branch satisfying (7.3) and (7.4).

The truncation to the finite interval $[\tau_-, \tau_+]$ causes an error. If u is a generic connecting solution to (7.1) at parameter α, then the following estimate holds in both cases:

$$\|(u|_{[\tau_-,\tau_+]}, \alpha) - (\hat{u}, \hat{\alpha})\| \leq C\mathrm{e}^{-2\min(\mu_-|\tau_-|, \mu_+|\tau_+|)}, \tag{7.6}$$

where $\|\cdot\|$ is an appropriate norm in the space $C^1([\tau_-, \tau_+], \mathbb{R}^n) \times \mathbb{R}^p$, $u|_{[\tau_-,\tau_+]}$ is the restriction of u to the truncation interval, and $\mu_{\pm}$ are determined by the eigenvalues of the monodromy matrices. For exact formulations, proofs, and references to earlier contributions, see [28, 29, 107], including the Erratum.

7.3 New defining systems in $\mathbb{R}^3$

In this section we show how to implement the boundary conditions (7.5). We consider the case $n = 3$ where O^- and O^+ are saddle cycles and therefore always $m_s^- = m_u^- = 2$ and $m_s^+ = m_u^+ = 2$. Substitution in (7.4) gives the number of free parameters for the continuation $p = 1$.

Note that the complete BVP will consist of 15 equations (2 saddle cycles, 2 eigendata for these cycles, and the connecting orbit) and 19 boundary conditions.

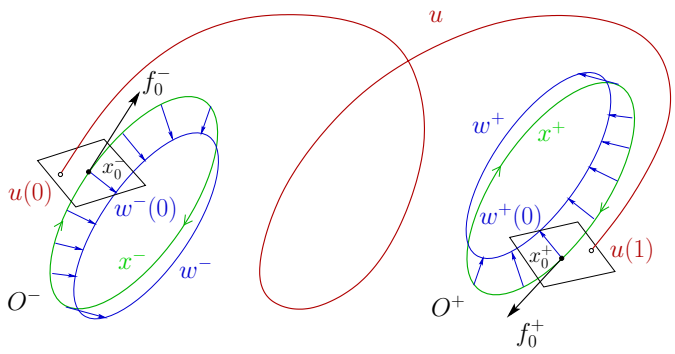

Figure 7.2: Ingredients of a BVP to approximate a heteroclinic connecting orbit. The homoclinic cycle-to-cycle connection is also approached as the heteroclinic case, where two saddle cycles coincide.

7.3.1 The cycle and eigenfunctions

To compute the saddle limit cycles O^- and O^+ involved in the heteroclinic connection (see Figure 7.2) we need a BVP. The standard periodic BVP can be used

$$\begin{cases} \dot{x}^\pm - f(x^\pm, \alpha) &= 0\,, \\ x^\pm(0) - x^\pm(T^\pm) &= 0\,, \end{cases} \tag{7.7}$$

A unique solution of this BVP is determined by using an appropriate phase condition, which is actually a boundary condition for the truncated connecting solution, and which will be introduced below.

To set up the projection boundary condition for the truncated connecting solution u near $O^\pm$, we also need a vector, say $w^+(0)$, that is orthogonal at $x^+(0)$ to the stable manifold W^s_+ of the saddle limit cycle O^+, as well another vector, say $w^-(0)$, that is orthogonal at $x^-(0)$ to the unstable manifold W^u_- of the saddle limit cycle O^- (see Figure 7.2). Each vector $w^\pm(0)$ can be obtained from an *eigenfunction* $w^\pm(t)$ of the *adjoint variational problem* associated with (7.7), corresponding to eigenvalue $\mu^\pm$. These eigenvalues satisfy

$$\mu^+ = \frac{1}{\mu_u^+}\,,\ \mu^- = \frac{1}{\mu_s^-}\,,$$

where μ_u^+ and μ_s^- are the multipliers of the monodromy matrix $M^\pm$ with

$$|\mu_u^+| > 1\,,\ |\mu_s^-| < 1\,.$$

The corresponding BVP is

$$\left\{\begin{array}{rcl} \dot{w}^{\pm} + f_u^{\mathrm{T}}(x^{\pm},\alpha)w^{\pm} &=& 0\,, \\ w^{\pm}(T^{\pm}) - \mu^{\pm}w^{\pm}(0) &=& 0\,, \\ \langle w^{\pm}(0), w^{\pm}(0)\rangle - 1 &=& 0\,, \end{array}\right. \tag{7.8}$$

where $x^{\pm}$ is the solution of (7.7). In our implementation the above BVP is replaced by an equivalent BVP

$$\left\{\begin{array}{rcl} \dot{w}^{\pm} + f_u^{\mathrm{T}}(x^{\pm},\alpha)w^{\pm} + \lambda^{\pm}w^{\pm} &=& 0\,, \\ w^{\pm}(T^{\pm}) - s^{\pm}w^{\pm}(0) &=& 0\,, \\ \langle w^{\pm}(0), w^{\pm}(0)\rangle - 1 &=& 0\,, \end{array}\right. \tag{7.9}$$

where $s^{\pm} = \operatorname{sign}\mu^{\pm}$ and

$$\lambda^{\pm} = \ln|\mu^{\pm}|\,. \tag{7.10}$$

(See [34, Appendix]).

In (7.9), the boundary conditions become periodic or anti-periodic, depending on the sign of the multiplier $\mu^{\pm}$, while the logarithm of its absolute value appears in the variational equation. This ensures high numerical robustness.

Given $w^{\pm}$ satisfies (7.9), the projection boundary conditions (7.5) become

$$\langle w^{\pm}(0), u(\tau_{\pm}) - x^{\pm}(0)\rangle = 0. \tag{7.11}$$

7.3.2 The connection

We use the following BVP for the connecting solution:

$$\left\{\begin{array}{rcl} \dot{u} - f(u,\alpha) &=& 0\,, \\ \langle f(x^{\pm}(0),\alpha), u(\tau_{\pm}) - x^{\pm}(0)\rangle &=& 0\,. \end{array}\right. \tag{7.12}$$

For each cycle, a phase condition is needed to select a unique periodic solution among those which satisfy (7.7), *i.e.* to fix a *base point* $x_0^{\pm} = x^{\pm}(0)$ on the cycle $O^{\pm}$ (see Figure 7.2). For this we require the end-point of the connection to belong to a plane orthogonal to the vector $f(x^{+}(0),\alpha)$, and the starting point of the connection to belong to a plane orthogonal to the vector $f(x^{-}(0),\alpha)$. This allows the base points $x^{\pm}(0)$ to move freely and independently upon each other along the corresponding cycles $O^{\pm}$.

7.3.3 The complete BVP

The complete truncated BVP to be solved numerically consists of

$$\dot{x}^{\pm} - T^{\pm} f(x^{\pm}, \alpha) = 0, \tag{7.13a}$$
$$x^{\pm}(0) - x^{\pm}(1) = 0\ , \tag{7.13b}$$
$$\dot{w}^{\pm} + T^{\pm} f_u^{\mathrm{T}}(x^{\pm}, \alpha) w^{\pm} + \lambda^{\pm} w^{\pm} = 0\ , \tag{7.13c}$$
$$w^{\pm}(1) - s^{\pm} w^{\pm}(0) = 0, \tag{7.13d}$$
$$\langle w^{\pm}(0), w^{\pm}(0) \rangle - 1 = 0\ , \tag{7.13e}$$
$$\dot{u} - T f(u, \alpha) = 0\ , \tag{7.13f}$$
$$\langle f(x^{+}(0), \alpha), u(1) - x^{+}(0) \rangle = 0\ , \tag{7.13g}$$
$$\langle f(x^{-}(0), \alpha), u(0) - x^{-}(0) \rangle = 0\ , \tag{7.13h}$$
$$\langle w^{+}(0), u(1) - x^{+}(0) \rangle = 0\ , \tag{7.13i}$$
$$\langle w^{-}(0), u(0) - x^{-}(0) \rangle = 0\ , \tag{7.13j}$$
$$\| u(0) - x^{-}(0) \|^2 - \varepsilon^2 = 0\ , \tag{7.13k}$$

where the last equation places the starting point $u(0)$ of the connection at a small fixed distance $\varepsilon > 0$ from the base point $x^{-}(0)$. The time variable is scaled to the unit interval $[0, 1]$, so that both the cycle periods $T^{\pm}$ and the connection time T become parameters. Hence, besides a component of α, there are five more parameters available for continuation: the connection time T, the cycle periods $T^{\pm}$, and the multipliers $\lambda^{\pm}$.

7.4 Starting strategies

The BVP described in the previous section are only usable when good initial starting data are available. Usually, such data are not present. Here we demonstrate how initial data can be generated through a series of successive continuations in AUTO, a method referred to as *homotopy method*, first introduced in [33] for point-to-point problems and extended to point-to-cycle problems in [34].

7.4.1 Saddle cycles

The easiest way to obtain the limit saddle cycles $O^{\pm}$, first calculate a stable equilibrium using software like MAPLE, MATLAB or MATHEMATICA. Then, using AUTO, continue this equilibrium up to an Andronov-Hopf bifurcation, where a stable limit cycle is generated. A continuation of this cycle can result in the detection of a fold bifurcation for the limit cycle. This will yield a saddle limit cycle.

7.4.2 Eigenfunctions

In order to obtain an initial starting point for the connecting orbit we require knowledge about the unstable manifold of the saddle limit cycle O^{-}. Also, we need the linearized adjoint "manifolds" to understand how the connecting orbit leaves O^{-} and approaches O^{+} (or the same cycle in the homoclinic case). For this, we look at the *eigendata*.

First consider the periodic BVP for O^-,

$$\begin{cases} \dot{x}^- - T^- f(x^-, \alpha) &= 0\,, \\ x^-(0) - x^-(1) &= 0\,, \end{cases} \tag{7.14}$$

to which we add the standard integral phase condition

$$\int_0^1 \langle \dot{x}^-_{old}(\tau), x^-(\tau) \rangle = 0\,, \tag{7.15}$$

as well as a BVP similar to (7.8), namely

$$\begin{cases} \dot{v} - T^- f_u(x^-, \alpha) v &= 0\,, \\ v(1) - \mu v(0) &= 0\,, \\ \langle v(0), v(0) \rangle - h &= 0\,. \end{cases} \tag{7.16}$$

In (7.15), x^-_{old} is a reference periodic solution, *e.g.* from the preceding continuation step. The parameter h in (7.16) is a *homotopy parameter*, that is set to zero initially. Then, (7.16) has a trivial solution

$$v(t) \equiv 0, \qquad h = 0,$$

for any real μ. This family of the trivial solutions parameterized by μ can be continued in AUTO using a BVP consisting of (7.14), (7.15), and (7.16) with free parameters (μ, h) and fixed α. The unstable Floquet multiplier of O^- then corresponds to a branch point at $\mu = \mu^-_u$ along this trivial solution family. AUTO can accurately locate such a point and switch to the nontrivial branch that emanates from it. This secondary family is continued in (μ, h) until the value $h = 1$ is reached, which gives a normalized *eigenfunction* v^- corresponding to the multiplier μ^-_u. Note that in this continuation the value of μ remains constant, $\mu \equiv \mu^-_u$, up to numerical accuracy. For the initial starting point of the connection we use $v^-(0)$.

The same method is applicable to obtain the nontrivial *scaled adjoint eigenfunctions* $w^\pm$ of the saddle cycles. For this, the BVP

$$\begin{cases} \dot{w}^\pm + T^\pm f_u^{\mathrm{T}}(x^\pm, \alpha) w^\pm + \lambda^\pm w^\pm &= 0\,, \\ w^\pm(1) - s^\pm w^\pm(0) &= 0\,, \\ \langle w^\pm(0), w^\pm(0) \rangle - h^\pm &= 0\,, \end{cases} \tag{7.17}$$

where $s^\pm = \mathrm{sign}(\mu^\pm)$, replaces (7.16). A branch point at $\lambda^\pm_1$ then corresponds to the adjoint multiplier $s^\pm \mathrm{e}^{\lambda^\pm_1}$. After branch switching the desired eigendata can be obtained.

7.4.3 The connection

Time-integration of (7.1), in MATLAB for instance, can yield an initial connecting orbit, however, this only applies for non-stiff systems. Nevertheless, mostly when starting sufficiently close to the exact connecting orbit *in parameter space* the method of *successive continuation* [33] can be used to obtain an initial connecting orbit.

Let us introduce a BVP that is a modified version of (7.13)

$$\dot{x}^{\pm} - T^{\pm} f(x^{\pm}, \alpha) = 0 \,, \tag{7.18a}$$
$$x^{\pm}(0) - x^{\pm}(1) = 0 \,, \tag{7.18b}$$
$$\Phi^{\pm}[x^{\pm}] = 0 \,, \tag{7.18c}$$
$$\dot{w}^{\pm} + T^{\pm} f_u^{\mathrm{T}}(x^{\pm}, \alpha) w^{\pm} + \lambda^{\pm} w^{\pm} = 0 \,, \tag{7.18d}$$
$$w^{\pm}(1) - s^{\pm} w^{\pm}(0) = 0 \,, \tag{7.18e}$$
$$\langle w^{\pm}(0), w^{\pm}(0) \rangle - 1 = 0 \,, \tag{7.18f}$$
$$\dot{u} - T f(u, \alpha) = 0, \tag{7.18g}$$
$$\langle f(x^{+}(0), \alpha), u(1) - x^{+}(0) \rangle - h_{11} = 0 \,, \tag{7.18h}$$
$$\langle f(x^{-}(0), \alpha), u(0) - x^{-}(0) \rangle - h_{12} = 0 \,, \tag{7.18i}$$
$$\langle w^{+}(0), u(1) - x^{+}(0) \rangle - h_{21} = 0 \,, \tag{7.18j}$$
$$\langle w^{-}(0), u(0) - x^{-}(0) \rangle - h_{22} = 0 \,, \tag{7.18k}$$

where each $\Phi^{\pm}$ in (7.18c) defines any phase condition fixing the base point $x^{\pm}(0)$ on the cycle $O^{\pm}$. An example of such a phase condition is

$$\Phi^{+}[x] = x_j(0) - a_j \,,$$

where a_j is the jth-coordinate of the base point of O^{+} at some given parameter values. Furthermore, h_{jk}, $j, k = 1, 2$, in (7.18h)–(7.18k) are *homotopy parameters*.

For the approximate connecting orbit a small step ε is made in the direction of the unstable eigenfunction v^{-} of the cycle O^{-}:

$$u(\tau) = x^{-}(0) + \varepsilon v^{-}(0) \mathrm{e}^{\mu_u^{-} T^{-} \tau}, \quad \tau \in [0, 1] \,, \tag{7.19}$$

which provides an approximation to a solution of $\dot{u} = T^{-} f(u, \alpha)$ in the unstable manifold W_{-}^{u} near O^{-}. After collection of the cycle-related data, eigendata and the time-integrated approximated orbit, a solution to the above BVP can be continued in (T, h_{11}) and (T, h_{12}) for fixed value of α in order to make $h_{11} = h_{12} = 0$, while $u(1)$ is near the cycle O^{+}, so that T becomes sufficiently large. In the next step, we then try to make $h_{21} = h_{22} = 0$, after which a good approximate initial connecting orbit is obtained.

This solution is now used to activate one of the system parameters, say α_1, and to continue a solution to the primary BVP (7.13). Then, if necessary after having improved the connection first by a continuation in T, continuation in (α_1, T) can be done to detect limit points, using the standard fold-detection facilities of AUTO. Subsequently a fold curve can be continued in two parameters, say (α_1, α_2), for fixed T using the standard fold-following facilities in AUTO.

7.5 Implementation in AUTO

Our algorithms have been implemented in AUTO, which solves the boundary value problems using superconvergent *orthogonal collocation* with adaptive meshes. AUTO can compute paths of solutions to boundary value problems with integral constraints and non-separated boundary

conditions:

$$\dot{U}(\tau) - F(U(\tau), \beta) = 0\ , \quad \tau \in [0,1], \tag{7.20a}$$

$$b(U(0), U(1), \beta) = 0\ , \tag{7.20b}$$

$$\int_0^1 q(U(\tau), \beta) d\tau = 0\ , \tag{7.20c}$$

where

$$U(\cdot), F(\cdot,\cdot) \in \mathbb{R}^{n_d},\ b(\cdot,\cdot) \in \mathbb{R}^{n_{bc}},\ q(\cdot,\cdot) \in \mathbb{R}^{n_{ic}},$$

and

$$\beta \in \mathbb{R}^{n_{fp}},$$

as n_{fp} *free* parameters β are allowed to vary, where

$$n_{fp} = n_{bc} + n_{ic} - n_d + 1\ . \tag{7.21}$$

The function q can also depend on F, the derivative of U with respect to pseudo-arclength, and on $\hat{U}$, the value of U at the previously computed point on the solution family.

For our primary BVP problem (7.13) in three dimensions we have

$$n_d = 15, \quad n_{ic} = 0,$$

and $n_{bc} = 19$, so that any 5 free parameters are allowed to vary.

7.6 Example: food chain model

In this section we describe the performance of the BVP-method for the detection and continuation of a cycle-to-cycle connecting orbit in the standard food chain model, also used in [34].

7.6.1 The model

The three-level food chain model from theoretical biology, based on the Rosenzweig-MacArthur [111] prey-predator model, is given by the following equations

$$\begin{cases} \dot{x_1} &= x_1(1-x_1) - f_1(x_1, x_2)\ , \\ \dot{x_2} &= f_1(x_1, x_2) - d_1 x_2 - f_2(x_2, x_3)\ , \\ \dot{x_3} &= f_2(x_2, x_3) - d_2 x_3\ , \end{cases} \tag{7.22}$$

with Holling Type-II functional responses

$$f_1(x_1, x_2) = \frac{a_1 x_1 x_2}{1 + b_1 x_1}$$

and

$$f_2(x_2, x_3) = \frac{a_2 x_2 x_3}{1 + b_2 x_2}\ .$$

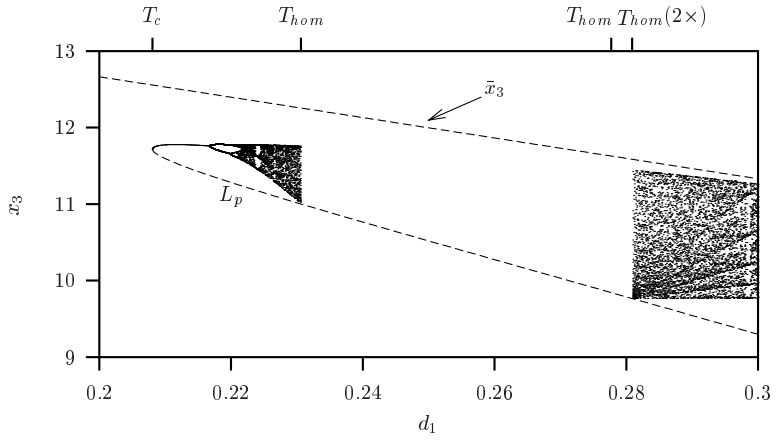

Figure 7.3: One-parameter bifurcation diagram for $d_2 = 0.0125$. The equilibrium is indicated as $\bar{x}_3$. The dashed line L_p is the x_3-value of the local minimum of an unstable (saddle) limit cycle. At the point T_c this limit cycle coincides with a stable limit cycle, of which the local minimum of x_3 is also shown. The stable limit cycle undergoes period doublings until chaos (the dense regions) is reached. The two dense regions are separated by a region where homoclinic cycle-to-cycle connections to the limit cycle L_p exist. Both chaotic regions are bounded by a limit point of the homoclinic connection, indicated by T_{hom}. Observe that near the right chaotic region, between two limit points exist secondary connecting orbits to the cycle. One of these limit points coincides with the limit point of the primary connecting orbit that forms the boundary of the region of chaos (hence T_{hom} twice); after Boer et al., 1999).

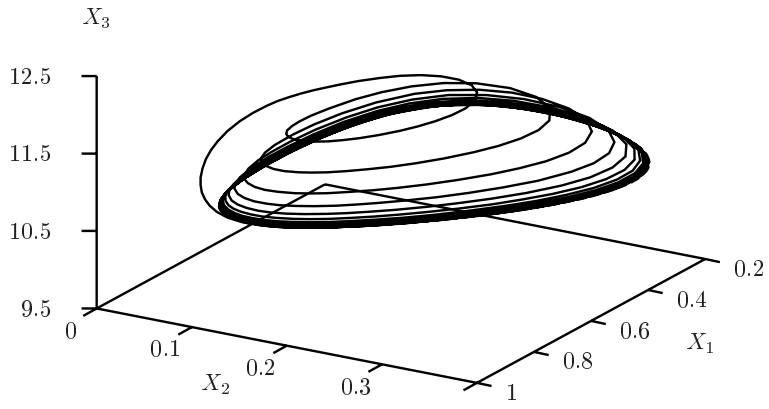

Figure 7.4: Phase plot of the homoclinic cycle-to-cycle connection.

This standard model has been studied by several authors, see *e.g.* [90, 92]) and references there.

The death rates d_1 and d_2 are often used as bifurcation parameters α_1 and α_2, respectively, with the other parameters set at $a_1 = 5$, $a_2 = 0.1$, $b_1 = 3$, and $b_2 = 2$. For these parameter values the model displays chaotic behaviour in a given parameter range of d_1 and d_2 ([60, 66, 99]). The region of chaos can be found starting from a fold bifurcation at for instance $d_1 \approx 0.2080452$, $d_2 = 0.0125$, where two limit cycles appear. The stable branch then undergoes a cascade of period-doublings (see Figure 7.3) until a region of chaos is reached.

Previous work by Boer et al. (1999, 2001) has shown that the parameter region where chaos occurs is intersected by homoclinic and heteroclinic global connections, and that this region is partly bounded by a homoclinic cycle-to-cycle connection, as shown in Figure 7.3. These results were obtained numerically using multiple shooting.

7.6.2 Homotopy

Using the technique discussed in this paper we first find the saddle limit cycle for $d_1 = 0.25$, $d_2 = 0.0125$. Since the cycle O is both O^+ and O^-, we use the same initial base point

$$x^{\pm}(0) = (0.839783, 0.125284, 10.55288)$$

and the period $T^{\pm} = 24.28225$. The logarithms of the nontrivial adjoint multipliers are

$$\lambda^+ = -0.4399607 \ , \ \lambda^- = 6.414681 \ .$$

The starting point of the initial "connecting" orbit is calculated by taking the base point $x^-(0)$ and multiplying the eigenfunction $v^-(0)$ by $\varepsilon = -0.001$

$$u(0) = x^-(0) + \varepsilon v^-(0) \ ,$$

where

$$v^-(0) = (-1.5855 \cdot 10^{-2}, 2.6935 \cdot 10^{-2}, -0.99951) \ ,$$

and the resulting

$$u(0) = (0.839789, 0.125274, 10.55324) \ .$$

The connection time $T = 503.168$.

To obtain a good initial connection we consider a BVP like (7.18), with 6 free parameters: $\mu^{\pm}$, $T^{\pm}$, T, and, in turn, one of the four homotopy parameters $h_{11}, h_{12}, h_{21}, h_{22}$. The selected boundary conditions (7.18c) are

$$\Phi^+[x] = x_2^-(0) - 0.125274 \ ,$$

and

$$\Phi^-[x] = x_1^+(0) - 0.839789 \ ,$$

so, the first condition uses the x_2-coordinate of the initial base point selected on the cycle, while the second condition uses the x_1-coordinate of the initial base point. Observe, that this selection is somewhat arbitrary and that one can select other base point coordinates.

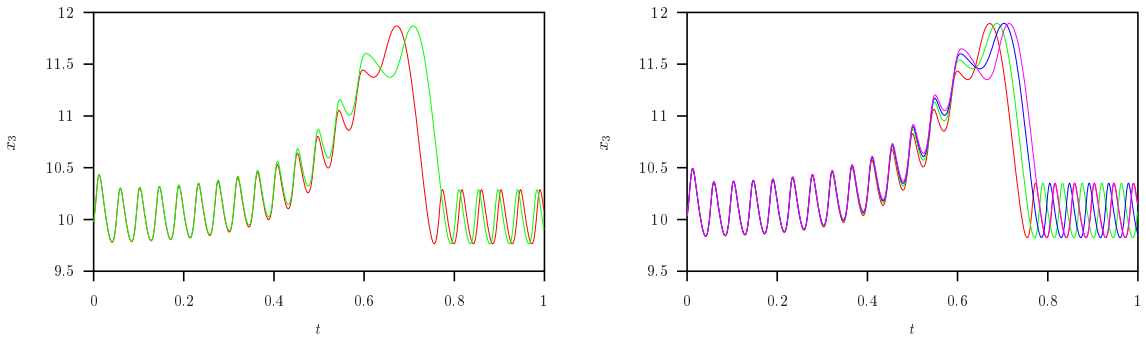

Figure 7.5: Profiles of the homoclinic cycle-to-cycle connections for $d_2 = 0.0125$. The left panel compares the two profiles of the connections for $d_1 = 0.2809078$, the right panel compares the four profiles for $d_1 = 0.27850$, which is between the limit points for the primary and secondary branches. The connection time T is scaled to one.

In the continuation we want $h_{11} = h_{12} = h_{21} = h_{22} = 0$. However, there are several solutions, that correspond to connecting orbits with different numbers of excursions near the limit cycle, both at the starting and the end-part of the orbit. Observe that the success of the future continuation in (d_1, d_2) seems to depend highly on the number of excursions near the cycle at the end-point of the connecting orbit. In the food chain model a decrease in d_2 is accompanied by a decrease in the numbers of excursions near the cycle at the end-point of the connection, like a wire around a reel. If this number is too low, a one-parameter continuation in $d_{1,2}$ will yield incorrect limit points. Also, two-parameter continuations in (d_1, d_2) will most likely terminate at some point. Hence a starting orbit is selected with a sufficient number of excursions near the cycle at the end-point, with $T = 454.04705$ and $\varepsilon^2 = 0.069414$ (see Figure 7.4).

7.6.3 Continuation

The continuation of the connecting orbit can be done in $d_{1,2}$ using the primary BVP (7.13). Equation (6.23) ensures that the base points $x^{\pm}(0) \in O^{\pm}$ become different (and so do the periodic solutions $x^{\pm}(t)$).

First, however, using this BVP, the connection can be improved by increasing the connection time, for the same reason as mentioned above with regard to the number of excursions near the cycle at the end-point. The increase in T results in an increase of the number of excursions near the cycle at the end-point of the connecting orbit. Then, the continuation in d_1, T for fixed $d_2 = 0.0125$ results in the detection of four limit points, of which two are identical. Observe that in this way – in accordance with Figure 7.3 – not only the primary ($d_1 = 0.2809078$, twice, and $d_1 = 0.2305987$), but also the secondary ($d_1 = 0.2776909$) branch is detected. Figure 7.5 shows the profiles of the connecting orbits for $d_2 = 0.0125$. Observe that for the region of $0.2776909 < d_1 < 0.2809078$ there are four different connecting orbits with the same connection time T (see right panel).

Using the standard fold-following facilities for BVPs in AUTO, both critical homoclinic orbits can be continued in two parameters (d_1, d_2). Along these orbits the stable and unstable invariant manifold of the cycle are tangent. Starting from $d_1 = 0.2809078$ we continue the primary branch. The secondary branch is continued from $d_1 = 0.2776909$. Both curves are

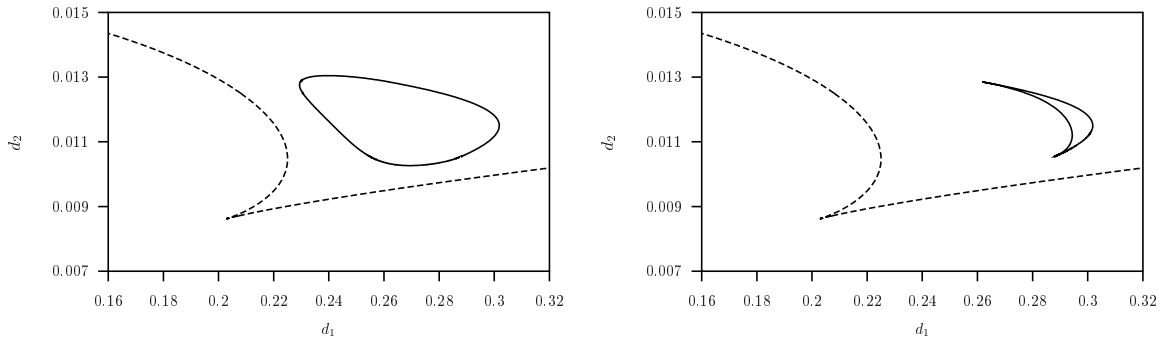

Figure 7.6: Two-parameter curves of the primary (left) and secondary (right) homoclinic tangencies in the food chain model. Depicted is also the fold bifurcation curve of a limit cycle (dashed).

depicted in Figure 7.6.

7.7 Discussion

Our continuation method for cycle-to-cycle connections, using homotopies in a boundary value setting, is a modified method proposed in our previous paper for the continuation of point-to-cycle connections [34]. The results discussed here seem to be both robust and time-efficient.Detailed AUTO demos carry out the computations described here are freely downloadable [36]. Provided that the cycle has one simple unstable multiplier, the proposed method can be extended directly to homoclinic cycle-to-cycle connections in n-dimensional systems.

Chapter 8

Ecological consequences of global bifurcations

Ecological consequences of global bifurcations in some food chain models.
G.A.K. van Voorn, B.W. Kooi and M.P. Boer, Submitted

Food chain models of ordinary differential equations (ODE's) are examples of models that are used in ecology to gain insight in the dynamics of populations of species, and the interactions of these species with each other and their environment. To investigate the validity of these models they have to be analysed. One powerful analysis technique is local bifurcation analysis, focusing on the changes in long-term (asymptotic) behaviour under parameter variation, and for which there exists standardised software. Here we revisit the analyses of four previously published ecological ODE food chain models. One model is a two-dimensional stoichiometric model. Due to Liebig minimum growth rate the resulting model is piecewise continuous. The model will be compared with a smooth version of the model, and this allows for an interpretation of some "pseudo-bifurcations", associated with piecewise continuous systems. Two other models are three-dimensional food chain models. We particularly focus on *global* bifurcations. Techniques, previously developed for this type of analysis, are applied here to locate and continue globally connecting orbits and, if applicable, their tangencies occurring in these models. We will show how global bifurcations in these models are related to each other and to local bifurcations. Furthermore, we consider the ecological implications of the global bifurcations. For example, the Shil'nikov homoclinic bifurcation functions as the organising centre of chaos in three-dimensional food chain models. Other global bifurcations "cut" the chaotic attractors and, combined with bistability, can even cause hysteresis is some models.

8.1 Introduction

Ecological modelling is the field were the time dynamics of populations of species are studied, and how these populations interact with each other and with their abiotic environment. It is useful to investigate diverse subjects, like extinction thresholds, the effects of sublethal toxicants or global warming on ecosystem functioning and structure, to name a few examples. A large portion of the ecological modelling consists of food chain studies, where sets of ordinary differential equations (ODE's) are used to describe population sizes in time.

To test the ecological validity of these models, extensive analysis is required. Food chain

models can be analysed using *bifurcation theory* [38, 54, 88, 125, 126], where the asymptotic behaviour of the system (equilibria, periodic cycles, chaos) is evaluated under parameter variation for qualitative changes. A qualitative change in the asymptotic behaviour is then referred to as a bifurcation point.

For examples of an ecological application see [7, 9, 55, 70]. Four types of bifurcation points are often encountered in food chain models: the transcritical bifurcation (an equilibrium that did not exist in the positive plane shifts to the positive plane, which in an ecological context gives an existence or extinction boundary), the tangent bifurcation (two equilibria, with usually different stability properties, coincide and disappear, ecologically often associated with the disappearance of a system separatrix), the Hopf bifurcation (a stable equilibrium that changes stability, while a limit cycle is born, which marks the transition to periodic behaviour), and the flip bifurcation (a limit cycle undergoes periodic doubling, and usually a series of these bifurcations marks the onset of chaotic behaviour). Of these four so-called *local* bifurcation points, only two types have been shown to have potentially radical effects, that is, small changes in a parameter lead to large changes, and also changes that cannot be easily reverted by restoring the parameter to its old value. The subcritical Hopf bifurcation is one type, but in general the subcritical Hopf bifurcation has not received much attention in the literature. The tangent bifurcation is the other type, and it has been discussed that the occurrence of a tangent bifurcation in a food chain model that at least basicly represent a real-life ecosystem might explain why species suddenly go extinct under only small (parameter) changes [113].

Not all extinction events, however, can be explained by the occurrence of any of the above-mentioned *local* bifurcations. For example, the bifurcation analyses of some two-dimensional food chain models with Allee-effect [3] revealed that extinction events named overexploitation, where the whole system collapses, were coupled to so-called *global* bifurcations [124]. A similar type of collapse is observed in food chain chemostat models after the introduction of sub-lethal toxicants [75]. And there are also other examples where global bifurcations are essential for understanding the dynamics of a food chain model. For instance, in the three-dimensional prey-predator-top-predator Rosenzweig-MacArthur model it has been shown that the parameter region of chaotic behaviour is bounded by a global bifurcation [17], [18], [35].

These results suggest it is interesting to take a closer look at global bifurcation analysis. However, previously it proved to be notoriously difficult to detect and continue global bifurcations, where either a saddle equilibrium or saddle limit cycle is connected to itself (homoclinic), or where two saddle equilibria and/or saddle limit cycles are connected via their manifolds (heteroclinic). Local information, that suffices to track local bifurcations, reveals nothing about the existence of globally connecting orbits other than whether or not one of more saddles exist. Limit cycles can grow to asymptotically large period under parameter variation, and this can be an indication that a homoclinic point-to-point connection exists. The existence of a bifurcation point of higher codimension (like Bogdanov–Takens or Gavrilov–Guckenheimer) can indicates there must be a point-to-point connection.

Recently there has been a significant jump in the development and successful testing of techniques to both find and continue global bifurcations. Now it is possible to find homoclinic connections in 2D models (HomCont, [20], [22], [23], as part of auto, [36]), 2D heteroclinic connections [124], and point-to-cycle and cycle-to-cycle connections in 3D systems [29], [28], [34], [35], [84], [36]. This shows that previously unexplained phenomena can be explained by the occurrence of global bifurcations. We discuss here four previously published food chain models, two two- and two three-dimensional, and apply our previously developed techniques

Table 8.1: List of parameters used in the model by [94], and the additional parameters of the smooth version of the model.

symbol	value	meaning
P	0.025	Total phosphorous
$\hat{e}$	0.8	Maximal production efficiency
b	1.2	Maximal growth rate of producer
d	0.25	Grazer loss rate, including respiration
θ	0.03	Grazer constant $\frac{P}{C}$
q	0.0038	Producer minimal $\frac{P}{C}$
c	0.81	Maximum ingestion rate of grazer
a	0.25	Half-saturation of functional response
K	-	Producer carrying capacity
C	-	Total carbon
B_C	0.002	Assimilation preference for C
B_P	2.	Assimilation preference for P
K_{PC}	1.	Saturation constant
j	-	Maximum predator ingestion rate

to detect and continue occurring global bifurcations.

In Section 8.2 we discuss the two-dimensional stoichiometric food chain model by [94], and a smooth version of the model by [119]. In this model a homoclinic point-to-point connection exists that is associated with the destruction of a system's attractor. We revisit the analyses of the 3D food chain models by Rosenzweig and MacArthur [111], [17], [19], [90]. In these models there are homoclinic point-to-point connections that form the "skeleton" in the generation of chaos (Shil'nikov bifurcation), while there are homoclinic cycle-to-cycle connections that are associated with the disappearance of the chaotic behaviour. Finally, in Section 4.4 there is a discussion of the known global bifurcations in ecological food chain models, and the ecological consequences of their occurrence.

8.2 2D stoichiometric model

The first, two-dimensional model we discuss is given as

$$\frac{dX_1}{dt} = b\left(1 - \frac{X_1}{\min(K, (P - \theta X_2)/q)}\right)X_1 - cf(X_1)X_2 \ , \tag{8.1a}$$

$$\frac{dX_2}{dt} = \hat{e}\ \min\left(1, \frac{(P - \theta X_2)/X_1}{\theta}\right)cf(X_1)X_2 - dX_2 \ , \tag{8.1b}$$

and was first given as Eqn. (6a,b) by [94], where $f(X_1)$ is the Holling type II functional response [62]. The parameter values are given in Table 8.1.

The individuals of both the producer and grazer populations are composed of two nutrients, carbon (an energy source) and phosphorous. X_1 and X_2 denote the carbon content of the two populations. The phosphorus in the system is divided over the grazer and producer populations. The ratio in phosphorus and carbon ($P : C$) can vary in the producer popula-

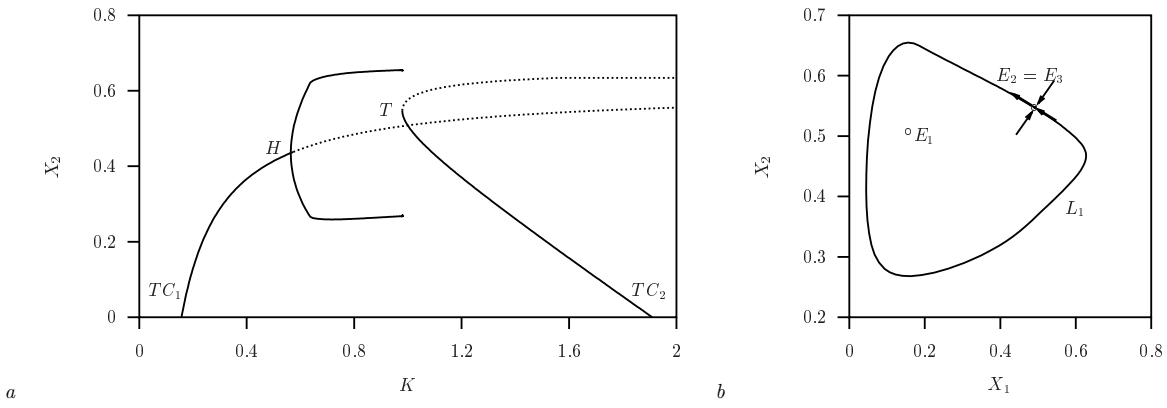

Figure 8.1: Diagrams of the model by [94], where $d = 0.25$. From left to right a: One-parameter bifurcation diagram, identical to Figure 4 in [94], where K is the bifurcation parameter. The limit cycle attractor is born at the Hopf bifurcation. At $K \approx 0.979435$ the tangent bifurcation where the equilibria E_2 and E_3 are born occurs simultaneously with the global bifurcation. b: State space picture at $K \approx 0.979435$. The limit cycle L_1 collides with the equilibrium $E_2 = E_3$ and forms a saddle-node homoclinic connection.

tion, but by introduction of the parameter q it is assumed that there is a minimum in this ratio.

The populations can be limited either by carbon or by phosphorus, as is given by the Liebig minimum function. The use of this switch-function results in a piecewise continuous model, that satisfies the Lipschitz condition with respect to both variables X_1 and X_2. The initial value problem is therefore mathematically well-posed and there is generally continuous dependence on initial conditions and parameters in the system. The derivative of the system, the Jacobian matrix, is however undetermined at the switching point.

In [94] the two types of displayed qualitative behaviour were discussed. In Fig. 8.1a (a replica of [94, Fig. 4]) it is shown that for the situation where $0.17 \lesssim K \lesssim 0.979435$ the producer population is limited by energy (carbon). There are only two equilibria, the trivial unstable equilibrium $E_0 = (0, 0)$ and the stable internal equilibrium E_1. Under an increase of parameter K the system displays the classical "paradox of enrichment" (POE) [110], [46]: a stable limit cycle L_1 is born at a Hopf bifurcation, while the equilibrium E_1 becomes unstable. For $0.979435 \lesssim K \lesssim 1.9$ the producer population is limited by phosphorous. The limit cycle and POE are not present, but instead there are four equilibria: the unstable equilibria E_0 and E_1, the stable equilibrium E_2 and a saddle equilibrium E_3.

The switch at $K \approx 0.979$ in Fig. 8.1a was described in [94] as an "infinite period bifurcation", and coincides with a tangent bifurcation where the two equilibria E_2 and E_3 collide. At this bifurcation the limit cycle L_1 disappears and the principle system's attractor becomes E_2, which explains why the POE no longer occurs. This bifurcation is in fact a (global) homoclinic bifurcation, that coincides with a (local) tangent bifurcation. Exactly at the tangent bifurcation there is one equilibrium, $E_2 = E_3$, that is a saddle-node point. The limit cycle touches this equilibrium and thus forms a saddle-node homoclinic connection, as can be seen in Fig. 8.1b. This connection can be obtained either by tracking the limit cycle L_1 up to a period that approximates infinity, or by using homotopy as described in [124, Appendix].

An interesting point is now whether or not the limit cycle L_1 disappears through the

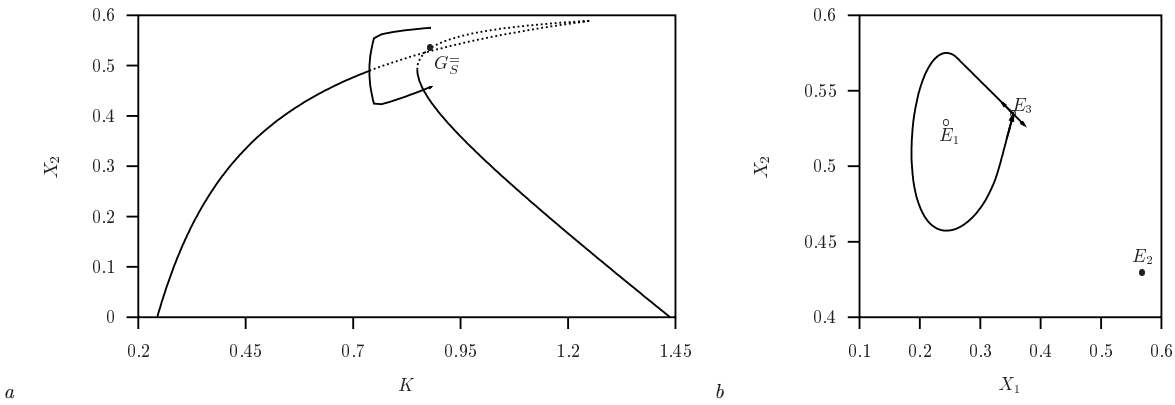

Figure 8.2: Diagrams of the model by [94], where $d = 0.32$. From left to right a: One-parameter bifurcation diagram where K is the bifurcation parameter. The termination of the limit cycle and the birth of the attracting equilibrium do not coincide in this case. b: State space picture at $K \approx 0.879726$, $d = 0.32$. The limit cycle forms a saddle connection orbit to the equilibrium E_3. The eigenvectors are indicated using arrows. orbits starting within the limit cycle converge to the limit cycle, while orbits outside converge to E_2. This is known as *bistability*. The grazer biomass density of the point attractor lies below the minimum of the limit cycle. When at the saddle homoclinic curve $G_S^=$ the stable limit cycle is destroyed, all initial densities converge to the lower grazer density of the remaining stable equilibrium.

tangent bifurcation, making it a local bifurcation event, or through the connecting orbit, making it a global bifurcation event. By varying a second parameter (d) we find that it is possible that the point-to-point connection exists as a saddle connection from E_3 to itself, while there is also the stable equilibrium E_2. This situation is depicted in Fig. 8.2 where $d = 0.32$ and $K \approx 0.879726$. In Fig. 8.2a the one-parameter bifurcation diagram of the system is shown, and it can be seen that besides the two types of behaviour described above (POE and stable equilibrium E_2) there is also a third type of behaviour in the region $0.849 \lesssim K \lesssim 0.879726$, namely bistability. In this region there are two attractors, the limit cycle L_1 and the equilibrium E_3, separated by the stable manifold to the saddle equilibrium E_2, as can be seen in Fig. 8.2b.

Fig. 8.3a shows the two-parameter bifurcation diagram of the model, where the bifurcation parameters are K and d. Observe that because of the discontinuous Jacobian we do not only have regular bifurcation curves and bifurcation points of higher codimension, but also discontinuity curves, where one of the minimum functions for the producer and grazer species switch, so the curve A_x is determined by $P = Kq+\theta X_2$, and A_y by $P = \theta(X_1+X_2)$. These curves can be continued using sets of boundary conditions, as shown in the Appendix 8.5. Furthermore there are "pseudo bifurcation" points Z_i, where $i = 1, 2, \cdots$, in which bifurcations curves join with either A_x or A_y. The point-to-point connection can be found and then continued in two-parameter space by using the homotopy techniques discussed in [124], [34], [35].

There are two transcritical bifurcations TC_1 and TC_2 that connect to each other in point Z_1. The tangent bifurcation T_e where $E_2 = E_3$ connects to the curve A_y in point Z_2, which in a sense replaces a Cusp bifurcation. The Hopf bifurcation curve H^- terminates at the curve A_y at Z_3. The two-parameter global bifurcation curve $G_S^=$ indicates the saddle homoclinic connection and terminates at one end at the curve A_y in point Z_4, where the point-to-

point connection has shrunk to a point. At the other end it terminates at the tangent bifurcation curve in a point of higher codimension N, where it is transformed into a saddle-node connection. The saddle-node homoclinic orbit is indicated by $G^{=}_{SN}$ and terminates at A_x in point Z_5.

We can now distinguish the following parameter regions with different dynamical behaviour. A limit cycle attractor occurs in the region right of the H^-, left of the global bifurcation curves $G^{=}_{S}$ and $G^{=}_{SN}$, below A_y. In the rest of the region below TC_1 and TC_2 there are equilibrium attractors. Bistability occurs in the approximately triangular-shaped parameter region bounded between Z_2, Z_4 and N. Hence this region partly overlaps with the region where limit cycles exist, and there is one limit cycle attractor and one point attractor. In the rest of the bistability region there are two point attractors.

8.2.1 Smooth stoichiometric model

Because of problems generated by the non-smoothness of the model, a smooth version of the above-discussed stoichiometric model was developed in [119], where all variables and parameters are kept equal to their counterparts in the original stoichiometric formulation, and all parameter values remain the same. In this model the SU-formulation [104], [79] is used to describe the assimilation in the producer species where both the phosphorus and the carbon are essential nutrients, *i.e.*, the growth depends on both nutrients. The producer species consists of two components, structure and an internal phosphorus reserve pool.

It is assumed that the structure has a fixed stoichiometry, so the phosphorus density of the structure P/C is fixed. The total phosphorus density in the producer is denoted by η. We furthermore assume a closed system, so the mass conservation principle can be applied (which is not applied in the original model in [94]. The growth depends on the carbon influx from the environment and equals $C - X_1 - X_2$, where C is the total carbon in the system, and the internal phosphorus $P - \theta X_2 - qX_1$. Since all phosphorus is in the biota, the pool $\eta - q$ and the total phosphorus density in the producer η are time-dependent. The whole formulation is given as

$$\frac{dX_1}{dt} = b\frac{j}{g(X_1, X_2)}X_1 - cf(X_1)X_2 \ , \tag{8.2a}$$

$$\frac{dX_2}{dt} = \hat{e}\frac{1.2}{1 + \frac{\theta}{\eta} - 1/(1 + \frac{\eta}{\theta})}cf(X_1)X_2 - dX_2 \ , \tag{8.2b}$$

where the functional response is Holling type II again

$$f(X_1) = \frac{X_1}{a + X_1} \ ,$$

the producer intake flux is written as

$$j = 1 + \frac{K_{PC}}{C\ B_C} + \frac{K_{PC}}{P\ B_P} - \frac{K_{PC}}{C\ B_C + P\ B_P} \ ,$$

and

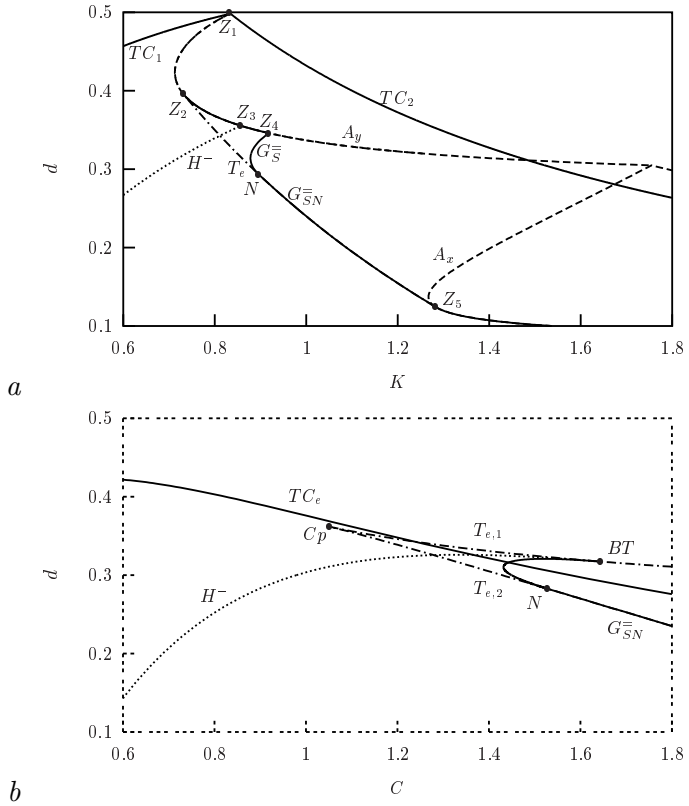

Figure 8.3: Two-parameter bifurcation diagrams. From top to bottom *a*: The model by [94], where K and d are the bifurcation parameters. The saddle-node homoclinic curve $G^{=}_{SN}$ corresponds with the dashed tangent bifurcation curve T_e, as could be expected. In the point D the saddle-node homoclinic connection turns into a saddle homoclinic connection. The saddle homoclinic curve $G^{=}_{S}$ stops in point Z_4, where the connection has shrunk to a point (not shown). *b*: The smooth analogue model by [119]. The Hopf bifurcation H^- and the global bifurcation $G^{=}_{SN}$ terminate on a tangent curve in a Bogdanov-Takens point

$$g(X_1, X_2) = 1 + \frac{K_{PC}}{(C - X_1)B_C} + \frac{K_{PC}}{(P - \theta X_2 - qX_1)B_P} - \frac{K_{PC}}{(C - X_1)B_C + (P - \theta X_2 - qX_1)B_P},$$

where the extra parameters are also given in Table 8.1. In Eq. 8.2b it is assumed that after ingestion the carbon and phosphorus are independently available again for growth. The factor 1.2 is a scaling factor in order to better match the original model by [94].

The dynamics of this smooth version of the stoichiometric model are summarised in Fig. 8.3b. Apart from quantitative there are also qualitative differences between the two models. In the smooth model version neither the points Z_i nor the discontinuity curves A_x and A_y exist. The two transcritical bifurcation curves TC_1 and TC_2 are here the same curve TC_e. There are now two tangent bifurcation curves $T_{e,1}$ and $T_{e,2}$ that collide in a cusp bifurcation Cp, a point of higher codimension. The Hopf bifurcation H^- terminates in a Bogdanov-Takens point BT, also a point of higher codimension that is on one of the tangent

bifurcation curves. The BT is also the origin for the global bifurcation curve $G_S^=$, depicted in solid line type. The global bifurcation curve continues as a saddle-node connection $G_{SN}^=$ after it has collided with the lower tangent bifurcation curve in point N.

There are the following regions of dynamical behaviour. In the region left of H^- and below TC_e there is a point attractor. This turns into a limit cycle attractor in the region right of H^- and left of the global bifurcations curves $G_S^=$ and $G_{SN}^=$. There is a point attractor right of the global bifurcation curves, below TC_e. There is also a point attractor in the small region between H^-, $T_{e,1}$ and TC_e. Bistability occurs in the four-cornered region bounded by $G_S^=$, $T_{e,2}$, $T_{e,1}$ and TC_e. Left of H^- there are two point attractors, right of H^- there is a point attractor and stable limit cycle.

8.2.2 Comparison of the two model versions

The original stoichiometric model in [94] displays not only bifurcation curves and bifurcation points of higher codimension, but also discontinuity curves, and bifurcation-like points. At these points bifurcation curves coincide with switches of the Liebig minimum associated with the model formulation of the trophic interaction. These points seem to be the analogue of real codim-2 points that occur in the smooth version of the stoichiometric model by [119]. The tangent curve in the original model terminates in a pseudo-bifurcation point, while in the smooth model there is also a second tangent curve that terminates together with the first tangent curve in a Cusp bifurcation. Also, in the original model the Hopf and saddle homoclinic bifurcation curves terminate separately in pseudo-bifurcation points, while in the smooth model it terminates at the same point of higher codimension on a tangent curve, as corresponding with theory on the Bogdanov-Takens point [88].

With regard to the global bifurcation occurring in the stoichiometric model we have two possible scenario's. In the first scenario there is only one system attractor, the limit cycle. With increased K the saddle-node connection occurs occurs at the exact point where a tangent bifurcation takes place. In this case, a global bifurcation coincides with a local bifurcation. Upon the immediate destruction of the system attractor a new attractor is created. There is no extinction of species, and there is no disappearance or creation of bistability properties. However, the time dynamics of the system changes from periodic to steady state.

In the second scenario the occurrence of the (saddle) homoclinic orbit is not connected to any local bifurcation. In this scenario there is a parameter region where there are two attractors, namely a stable limit cycle and a stable equilibrium, separated by the stable manifold to the saddle equilibrium E_3. With the occurrence of the connecting orbit to this saddle equilibrium, both the limit cycle and the separatrix are destroyed. As such, with this global bifurcation, a system attractor *and* the bistability properties of the model disappear.

This second scenario resembles the phenomenon of "overexploitation" in Allee models [124]. In contrast to the previously studied Allee-models, where after the destruction of the limit cycle attractor a zero-equilibrium becomes the new global attractor, the equilibrium that remains after the global bifurcation in the stoichiometric model is positive, although it does have a lower grazer density than the minimum of the destroyed limit cycle attractor (see Figure 8.1, right panel). Therefore, although no overexploitation occurs, a small, stochastic shift in K can result in a sudden drop in biomass densities. Also, the new lower grazer density cannot be reverted back to its old state without a larger step back in K, since the system is in its new attractor. As such we have some kind of "catastrophic shift" [113], but now occurring because of a global bifurcation instead of a local bifurcation (tangent).

8.3 3D food chain models with chaos

In this section we review the analysis of the three-dimensional Rosenzweig-MacArthur food chain model.

8.3.1 Rosenzweig-MacArthur food chain model

The Rosenzweig-MacArthur food chain model is given as

$$\frac{dX_1}{dt} = rX_1\left(1 - \frac{X_1}{K}\right) - \frac{A_{1,2}X_1X_2}{\kappa_{1,2} + X_1}\,, \tag{8.4a}$$

$$\frac{dX_2}{dt} = X_2\left(y_{1,2}\frac{A_{1,2}X_1}{\kappa_{1,2} + X_1} - \gamma_1 - \frac{A_{2,3}X_3}{\kappa_{2,3} + X_2}\right)\,, \tag{8.4b}$$

$$\frac{dX_3}{dt} = X_3\left(y_{2,3}\frac{A_{2,3}X_2}{\kappa_{2,3} + X_2} - \gamma_2\right)\,. \tag{8.4c}$$

In these equations X_1 is the prey, X_2 the predator and X_3 the top-predator. The parameters $A_{1,2}$ and $A_{2,3}$ are the ingestion rates, $y_{1,2}$ and $y_{2,3}$ are the yields over ingested biomass from the previous trophic level, and γ_1 and γ_2 are the linear predator death rates. The RM model is effectively a combination of the logistic growth curve with Holling type II functional responses. The model can be rewritten after rescaling as

$$\dot{x_1} = x_1(1 - x_1) - f_1(x_1)x_2\,, \tag{8.5a}$$

$$\dot{x_2} = f_1(x_1)x_2 - d_1x_2 - f_2(x_2)x_3\,, \tag{8.5b}$$

$$\dot{x_3} = f_2(x_2)x_3 - d_2x_3\,, \tag{8.5c}$$

which is dimensionless. The variables and parameters are given in Table 8.2. The carrying capacity has disappeared in the rescaling process, therefore it can no longer be used as bifurcation parameter. The two death rate parameters d_i are the most obvious selection to perform a two-dimensional bifurcation analysis of the model, since the other remaining parameters are associated to physiological properties and can therefore be assumed to remain fixed.

Table 8.2: List of rescaled variables and parameters of the three-dimensional RM model.

$x_1 = \frac{X_1}{K}$	$a_1 = \frac{KA_{1,2}y_{1,2}}{r\kappa_{1,2}} = 5.$	$d_1 = \frac{\gamma_1}{r}$
$x_2 = \frac{X_2}{Ky_{1,2}}$	$a_2 = \frac{KA_{2,3}y_{1,2}y_{2,3}}{r\kappa_{2,3}} = 0.1$	$d_2 = \frac{\gamma_2}{r}$
$x_3 = \frac{X_3}{Ky_{1,2}y_{2,3}}$	$b_1 = \frac{K}{\kappa_{1,2}} = 3.$	$f_1(x_1) = \frac{a_1x_1}{1+b_1x_1}$
$t = rT$	$b_2 = \frac{Ky_{1,2}}{\kappa_{2,3}} = 2.$	$f_2(x_2) = \frac{a_2x_2}{1+b_2x_2}$

The equilibria of System (8.5) are

$$E_0 = (0, 0, 0) \ , \tag{8.6a}$$

$$E_1 = (1, 0, 0) \ , \tag{8.6b}$$

$$E_2 = \big(\frac{d_1}{a_1 - b_1 d_1} \ , \frac{a_1 - d_1(b_1 + 1)}{(a_1 - b_1 d_1)^2} \ , 0\big) \ , \tag{8.6c}$$

$$E_3 = (x_1^*, x_2^*, x_3^*) \ , \tag{8.6d}$$

where

$$x_1^* = \frac{b_1 - 1 + \sqrt{(b_1 + 1)^2 - \frac{4 a_1 b_1 d_2}{a_2 - b_2 d_2}}}{2 b_1} \ , \tag{8.7a}$$

$$x_2^* = \frac{d_2}{a_2 - b_2 d_2} \ , \tag{8.7b}$$

$$x_3^* = \frac{f_1(x_1^*) - d_1}{a_2 - b_2 d_2} \ . \tag{8.7c}$$

for $0.16 \leq d_1 \leq 0.32$, $0.0075 \leq d_2 \leq 0.015$ (see also [67]).

The stability of the equilibria, and the local bifurcation analysis of the RM model, are described in detail in [92]. We will give a short overview here of the system, that is rich in bifurcations, both for equilibria and limit cycles.

Fig. 8.4a shows a one-parameter local bifurcation diagram, with $d_1 = 0.25$ and d_2 as free parameter. The value of x_3 is displayed as a function of d_2. In the case that it is a limit cycle, the minimal and maximal values of x_3 are also displayed. The system has a stable equilibrium E_3 where all three species exist only between the two Hopf bifurcations H^- and H^+. Increasing the value of d_2, at the subcritical H^+ the stable equilibrium becomes a saddle point, while an unstable limit cycle is born. The unstable limit cycle can be continued up to a cycle tangent bifurcation T_c, where also a stable limit cycle emerges. This stable limit cycle disappears from the positive plane at a transcritical bifurcation TC_c. The saddle point collides with an unstable equilibrium, born from a transcritical bifurcation TC_e, in the tangent bifurcation T_e.

On the other side, when decreasing the value of d_2, at the supercritical H^-, the stable equilibrium E_3 is replaced by a stable limit cycle as the system's attractor. The equilibrium becomes a saddle point. When decreasing the value of d_2 further the stable limit cycle goes through a series of flip bifurcations, until a chaotic attractor appears, as is depicted in Fig. 8.4b.

In Fig. 8.5a a two-parameter diagram is shown, where $d_2 = 0.1$, and d_1 and the cycle period T_0 are varied. The cycle period goes to infinity at $d_1 \approx 0.3166$, after an infinite number of tangent and flip bifurcations. This figure indicates there is a Shil'nikov global bifurcation, of which the connection has one spiralling end. The "skeleton" of the route to chaos is this Shil'nikov bifurcation, a point-to-point connection to itself of the equilibrium E_3 that has become a saddle point after the Hopf bifurcation H^-.

The point-to-point connection can be detected, and continued, using the techniques discussed by [34] in adapted form. There are actually two connections very close to each other in parameter space, that are depicted in Fig. 8.5b. One connecting orbit connects from the saddle equilibrium to itself after one rotation (dashed-dotted). The other orbit makes two full rotations before connecting (dotted).

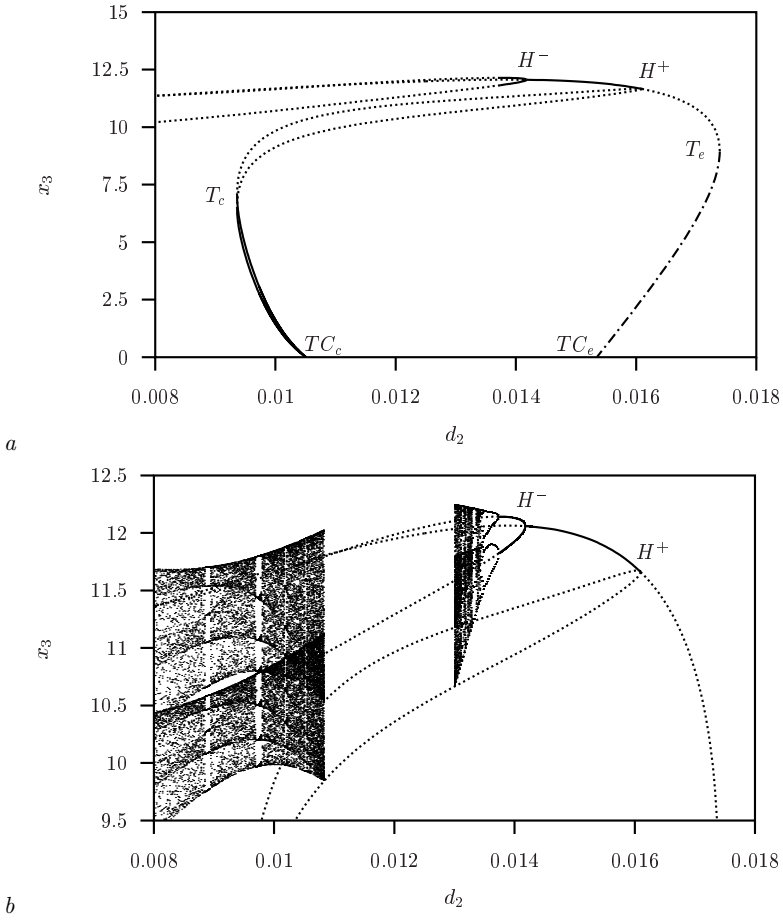

Figure 8.4: From top to bottom *a*: One-parameter bifurcation diagram of the 3D RM model, Eqn. (8.5), with d_2 as free parameter ($d_1 = 0.25$). Depicted are the equilibrium densities and the extremum values of x_3. Solid indicates stable, dotted indicated saddle or unstable. *b*: Detail of Figure *a*, now with the regions indicated where chaos occurs. The labels are explained in the main text.

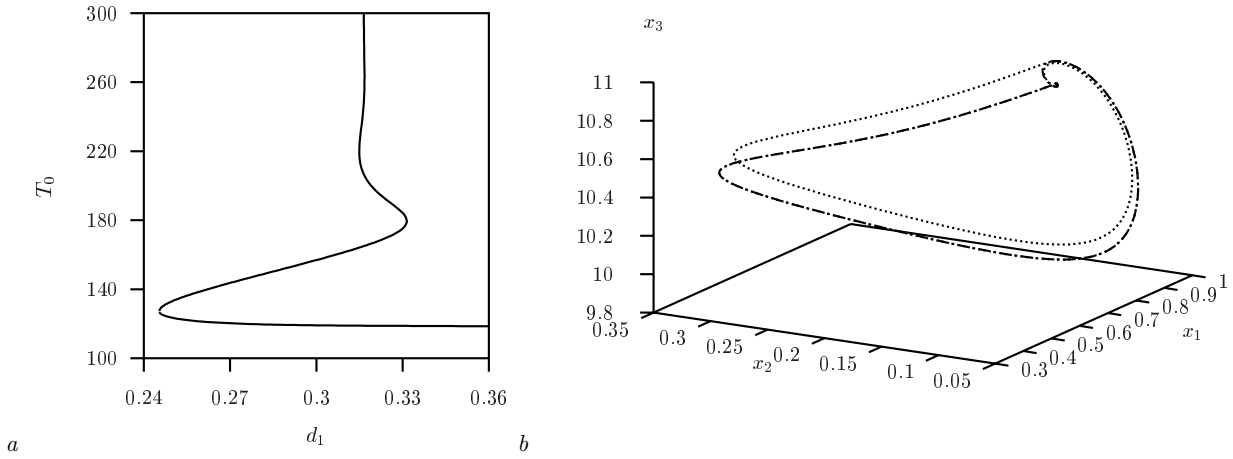

Figure 8.5: From left to right *a*: Diagram of the 3D RM model Eqn. (6.43), where T_0 is plotted as a function of d_1, with $d_2 = 0.01$. The cycle period goes to infinity after an infinite series of tangent and flip bifurcations. Each turning point is a tangent bifurcation. Flip bifurcations are not indicated. This leads to a Shil'nikov global bifurcation, the organising centre of chaos in this model. *b*: Three-dimensional state space where $d_2 = 0.01$. There are two point-to-point connections: one single-period (dashed-dotted) at $d_1 \approx 0.3166$, and one double-period (dotted) connection very close by at a different value of d_1.

From Fig. 8.4b it can be concluded that the chaos suddenly disappears. The parameter values where this happens are the values where the minimal value of the chaotic attractor collides with the minimal value of the unstable limit cycle. At the left-hand side, at a lower parameter value, a similar thing happens. At those parameter values a global bifurcation occurs, that destroys the chaotic attractor [18], [19].

In Fig. 8.6a a two-parameter diagram is shown with d_1 and d_2 as bifurcation parameters.

Two extra local bifurcations are visible now. The first is the transcritical bifurcation TC_e, where the stable three-dimensional equilibrium appears. The second is the planar Hopf bifurcation H_p. For values of d_1 lower than where H_p occurs, a two-dimensional stable limit cycle exists, that functions as the system attractor when the top predator does not exist. Most local bifurcations (T_e, both TC_e, H_p, TC_c, and H^+) originate from the same organising centre, a point M of higher codimension. This point has been analysed in detail in [92]. The two Hopf bifurcations H^+ and H^- collide in a second codim-2 point, a Bautin point B, which is also the end point for the curve T_c.

In Fig. 8.6b a detail of the two-parameter bifurcation diagram is shown. The first and second order flip bifurcations $F^{1,2}$ of the stable limit cycle are displayed, and indicate where approximately the region of chaos is located. They originate from the Shil'nikov bifurcation curve, labeled as $G_e^=$. Also originating from the Shil'nikov are cycle tangent bifurcations T_c, of which one is depicted. The full unfolding around a Shil'nikov bifurcation has been discussed in detail in [90]. The region of chaos is bounded internally by the global bifurcation curve $G_c^=$, that indicates a homoclinic cycle-to-cycle connection that creates the "hole" in the region of chaos. Observe also, that the two global bifurcation curves $G_e^=$ and $G_c^=$ do not intersect.

Finally there is also a curve $G^{\neq}$, that indicates a heteroclinic point-to-cycle connecting

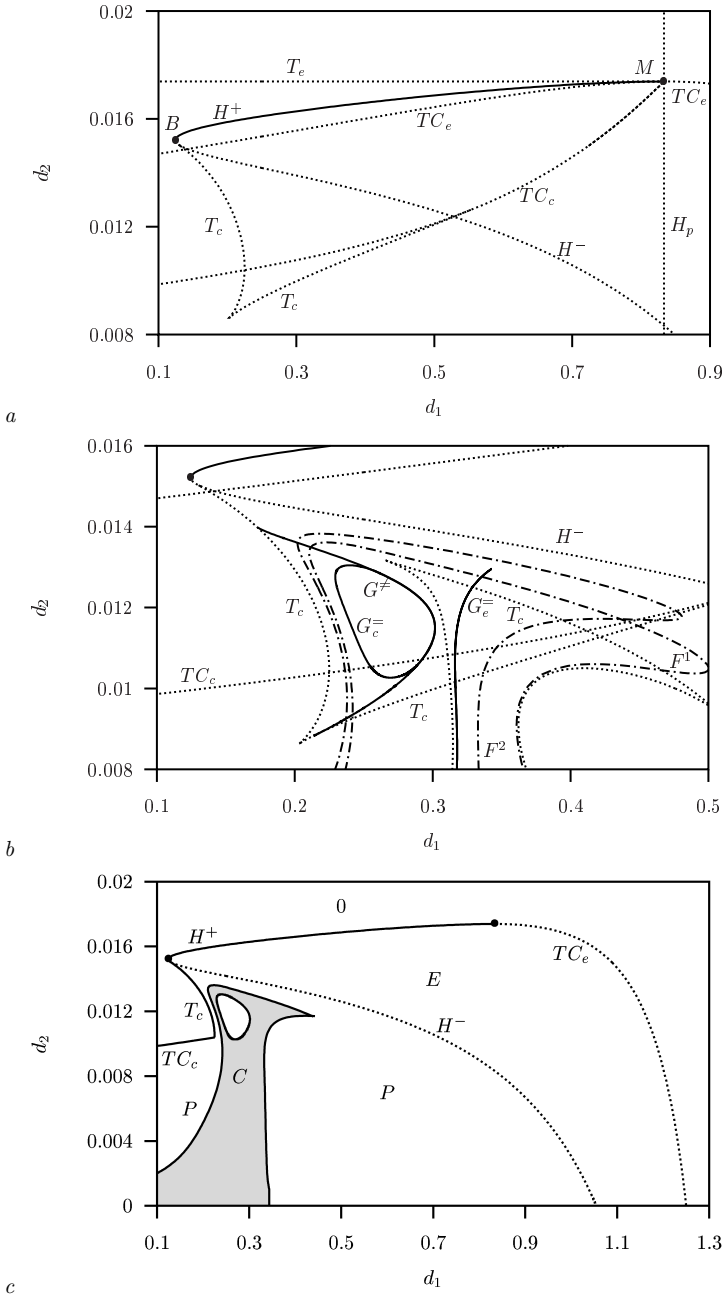

Figure 8.6: From top to bottom *a*: Two-parameter bifurcation diagram of the 3D RM model, Eqn. (8.5), with d_1 and d_2 as free parameters. *b*: Detail of the upper panel, where also flip and global bifurcations are depicted. See text for explanation. The curves $G_e^{=}$, $G^{\neq}$, and $G_c^{=}$ have been obtained using the techniques discussed by [34], [35]. *c*: Biologically separated regions. 0 = no species, E = equilibrium with all three species, P = periodic solutions, C = chaos.

orbit. This connection forms the boundary of the region, where there is a separatrix, that divides two basins of attraction. Orbits starting in one basin evolve to the limit cycle or chaotic attractor, orbits in the other basin converge to a solution where the top-predator is extinct [17].

In Fig. 8.6c the bifurcation diagram has been simplified to indicate the biological different regions in parameter space. The region above the subcritical Hopf bifurcation curve H^+ is indicated by 0, meaning there is no positive system attractor there. In the region labeled E there exists a stable three-dimensional equilibrium. It is bounded by the subcritical Hopf bifurcation curve H^+, the supercritical Hopf bifurcation curve H^- and the transcritical bifurcation TC_e. The region below H^-, bounded right of T_c, and then below TC_c, contains a non-equilibrium attractor. In the regions indicated by P it is a limit cycle, in the region marked C it is a chaotic attractor. In the "eye" bounded by the global bifurcation $G_c^=$ the top-predator does not exists.

8.3.2 Overview of food chain models

In two resembling three-dimensional food chain models, the 3D Rosenzweig-MacArthur (RM) model and the model by [93], the Shilni'kov homoclinic point-to-point connection is the organising centre of chaos in the system. Around the Shilni'kov there is an unfolding of tangent and flip bifurcations, that generates chaotic behaviour in these models. The Shilni'kov bifurcation, although a global bifurcation, is however not the origin for the cycle-to-cycle connections in these models.

In the 3D RM model there exists one chaotic attractor in a region of parameter space. Depending on the initial condition the system evolves to this three-dimensional attractor or to a planar limit cycle, where the top predator is extinct. The chaotic attractor disappears through the tangency of a homoclinic cycle-to-cycle connection. This tangency is coupled to the existence of a saddle limit cycle, born at a subcritical Hopf bifurcation. After this event, also referred to as a "boundary crisis", there remains only the saddle limit cycle and no coexistence of the three species is possible [19]. The global bifurcation curve that indicates this boundary crisis forms an "eye" in two-parameter space.

8.4 General discussion

Four food chain models, two consisting of two, and two of three ODE's, have been analysed in this paper with specific focus on global bifurcations. We define a global bifurcation as either a structurally unstable connecting orbit, that disappears when one parameter is varied, or the tangency of a structurally stable connecting orbit. Although there is no way to know for certain we have detected or identified all existing global bifurcations in these models, we can give the following list of connections that can occur in ODE-models

- Homoclinic point-to-point, for example in stoichiometric models by [94], [81], in a chemostat model with added sub-lethal toxicants [75], and the Shil'nikov bifurcation in the three-dimensional food chain models [93]

- Heteroclinic point-to-point, for example in two-dimensional food chain models with Allee-effect [124]

- Point-to-cycle, for example in the three-dimensional Rosenzweig-MacArthur food chain model [34]
- Homoclinic cycle-to-cycle, for example in the same RM model [35] and the model by [93]
- Heteroclinic cycle-to-cycle, of which there exists no example in theoretical ecology thus far, but see for instance [29].

Most of the examples of global bifurcations in food chain models studied here result in events that resemble the "catastrophic shift" normally associated with a tangent bifurcation [113], where after a small parameter change there is a loss of bistability. This is automatically coupled to *hysteresis*, meaning that a larger decrease of the parameter is required to restore the system to its old state. Because the bistability region is re-entered after a small decrease, the system remains in the "new" state that only disappears after the bistability is left again at the other side. Second, there is a sudden change is average biomass. For example, in the stoichiometric model by [94] after the occurrence of the saddle homoclinic connection the remaining stable equilibrium has a lower biomass than the minimum value of the stable limit cycle that has disappeared.

In many previously studied systems the system even goes extinct after a global bifurcation. In predator-prey models with Allee-effect the bistability is lost after a global bifurcation that destroys the stable positive limit cycle, leaving only a stable zero-equilibrium. This event was named "overharvesting" because it occurs under a decrease of the predator mortality parameter [124]. In [75] it was shown that chemostat models display bistability after the addition of sub-lethal toxicants. The system goes extinct after a global bifurcation that destroys a stable limit cycle.

This last phenomenon is also interesting in terms of the "paradox of enrichment" [110], [46]. The paradox describes that the limit cycle grows in amplitude under an increase of the enrichment parameter, until extinction because of demographic stochasticity becomes more and more likely. The occurrence of a global bifurcation in this context seems more appropriate. The destruction of the limit cycle through a global bifurcation, and the following extinction of the system because only the zero-equilibrium is left, is a more "clean" way of how the paradox of enrichment could occur.

A third effect, next to loss of bistability and a sudden change in average biomass densities, is not found in a catastrophic shift caused by a tangent. That is that there is a "simplification" of the dynamics. For example, in the model by [93] the chaotic attractor disappears after a global bifurcation, leaving a limit cycle of low frequency as sole attractor. The simplification of dynamics is not necessarily coupled to the existence of bistability in the model. After a saddle-node homoclinic bifurcation the dynamics in the model by [94] simplify from periodic to steady state, but the system is immediately restored to the periodic behaviour after a small parameter decrease.

An interesting note is that the simplification in combination with bistability can be perceived as "stabilising". For example, in the model by [94] after a saddle homoclinic bifurcation the steady state remains and only disappears after a significant decrease in the parameter K, where the system reverts to the periodic behaviour again. In a similar fashion, in the model by [93] the chaotic behaviour is only restored after a significant decrease in a_1. As such, the system could become more stable after a "parameter-shift trick", a small increase followed by a small decrease in the parameter.

Thus far, all discussed homoclinic and heteroclinic connections indicate a boundary where bistability or chaos disappears. A different type of boundary is formed by the point-to-cycle connection. An example is provided by the three-dimensional RM model. In some regions in parameter space there is bistability, and orbits can converge either to a chaotic or a planar attractor where the top-predator goes extinct. The basins of attraction have a very complicated structure, and it is not obvious to which attractor an initial condition will converge. The tangency of the point-to-cycle connection is the boundary of the region in parameter space where these complicated basins of attraction exist, and after this global bifurcation has occurred the basin of attraction for the chaotic attractor is "closed" and non-complicated [19]. Biologically these complicated basins of attraction could lead to very dramatic changes in biomass densities under stochastic changes.

Some global bifurcations have a different function. The Shil'nikov bifurcation is the organising centre for chaos in the three-dimensional models so far. In the RM model there is one chaotic attractor [90] born through a series of flip bifurcations that sprout from the Shil'nikov. In the model by [93] there can be two chaotic attractors at the same parameter set, that seem to be unrelated: one chaotic attractor traces back to a stable equilibrium like in the RM model, and the other to a stable limit cycle born in a cycle tangent bifurcation. However, the tangent bifurcation stems from the Shil'nikov, just like the flip bifurcations.

What is striking is that the Shil'nikov bifurcation is a homoclinic saddle point-to-point connection, just like the global bifurcation involved in the destruction of the limit cycle in the model by [94], for instance. The difference between the two homoclinic connections is that the Shil'nikov orbit connects a focus-saddle point to itself in a system of more than two variables, while the boundary orbit connects a simple saddle point to itself. An example of a three-dimensional homoclinic simple saddle point-to-point connection that forms a boundary occurs in a producer-consumer model where the consumer population is split into searchers and handlers [81].

An important aspect in global bifurcation analysis is the preferred use of continuation software over simulations. A simulator is a useful tool to obtain chaos diagrams, but a poor tool to obtain a good bifurcation diagram. Especially near the bifurcation points the integration time required to get an approximation of the stable asymptotic state increases, and detection of the exact bifurcation point is almost impossible. Furthermore, saddle points and saddle cycles cannot be found by doing simulations, since any orbit that approaches a saddle in the stable direction will be diverted again when close to the saddle. Because saddles are the start and end points of global connections, knowledge of their location is of vital importance. A good example of this point is the dynamics of the model by [93], where it is crucial to know the location of the saddle cycle that is involved in both the boundary and interior crises. The use of continuation software like AUTO can result in the detection of the saddle cycle by continuing the stable limit cycle through a tangent bifurcation. The saddle cycle data can then be used in the application of the homotopy techniques to find global bifurcations as developed by [34], [35].

The results seen and discussed here suggests that global bifurcation analysis is vital for a good understanding of the dynamics of many food chain models. It remains to be seen what other possible global bifurcations might exist, especially in food chain models of more than three variables, and what the ramifications of their occurrence are, but the global bifurcations studied so far can have potentially significant effects that cannot be understood without knowledge of their occurrence. We argue that in future model analyses of food chain models more attention is paid to the possible occurrence of global bifurcations.

8.5 Discontinuity curves

The set of boundary conditions used to calculate the discontinuity curve A_x in Figure 8.3, upper panel, is given as the three equations

$$\left\{ \begin{array}{rcl} \phi(\xi, \alpha) & = & 0\,, \\ P - \theta X_2 - qK & = & 0\,, \end{array} \right. \tag{8.8}$$

where α is the parameter set and $\phi(\xi, \alpha)$ is the equilibrium setting of Eq. (8.1), so the solution of $dX_1/dt = dX_2/dt = 0$.

The second boundary condition is the minimum function for the producer species. For the discontinuity curve A_y a similar set can be given

$$\left\{ \begin{array}{rcl} \phi(\xi, p) & = & 0\,, \\ P - \theta(X_2 + X_1) & = & 0\,, \end{array} \right. \tag{8.9}$$

where the second condition is the minimum function for the grazer species.

In a two-dimensional system, like the stoichiometric model, these are three equations with four free parameters. We select as parameters the two equilibrium values $\xi = X_1^*, X_2^*$, and the two bifurcation parameters K and d.

Chapter 9

Exercises

9.1 Exercise 1

The nutrient–prey model reads

$$\frac{dN}{dt} = (N_r - N)D - I_{NR}\frac{N}{k_{NR}+N}\,R\,, \tag{9.1a}$$

$$\frac{dR}{dt} = \left(\mu_{NR}(c_R)\frac{N}{k_{NR}+N} - (D + m_R(c_R))\right) R\,, \tag{9.1b}$$

$$\frac{dc_T}{dt} = (c_r - c_T)D\,, \qquad \text{where} \quad c_T = c_W + c_R R = c_W\,(1 + \text{BCF}_{WR} R)\,. \tag{9.1c}$$

The parameter values are given in Table 9.1:

Table 9.1: Parameter set for bacterium-ciliate model: m mass of toxicant, t time, v is dimension of the volume of the reactor and V biovolume or biomass of organism.

Nutrient–Prey			
μ_{NR}	Max. growth rate	t^{-1}	0.5 h^{-1}
I_{NR}	Max. ingestion rate	t^{-1}	1.25 h^{-1}
k_{NR}	Saturation constant	$\text{V}\,\text{v}^{-1}$	8.0 mg dm^{-3}
m_{R0}	Maintenance rate coefficient	t^{-1}	0.025 h^{-1}
c_{RM0}	NoEffect Concentration (NEC)	$\text{m}\,\text{V}^{-1}$	0.1 μg mg^{-1}
c_{RM}	Tolerance concentration	$\text{m}\,\text{V}^{-1}$	0.5 μg mg^{-1}
BCF_{WR}	BioConcentration Factor	$\text{v}\,\text{V}^{-1}$	1.0 dm^3 mg^{-1}

- Analyse the nutrient–prey model described in this document using AUTO or another computer package. Use the parameter values in Table 9.1. Generate a two-parameter bifurcation diagram with nutrient inflow N_r and dilution rate c_r as free parameters for the nutrient–prey system (9.1) with toxicity stress in the chemostat where the dilution rate equals $D = 0.02$.
- Calculate the discontinuity curve in the (N_r, c_r)-diagram where $c_W = c_{RM0}$. At this point the elements of the Jacobian matrix evaluated at the equilibrium point can be discontinuous functions of the state variables. This makes this problem piece-wise smooth. Describe the region in the diagram with no toxic effects.

9.2 Exercise 2

The three-level food chain the Rosenzweig–MacArthur model is given by

$$\begin{cases} \dot{x}_1 &= x_1(1-x_1) - f_1(x_1,x_2), \\ \dot{x}_2 &= f_1(x_1,x_2) - f_2(x_2,x_3) - d_1 x_2, \\ \dot{x}_3 &= f_2(x_2,x_3) - d_2 x_3, \end{cases} \tag{9.2}$$

with Holling Type-II functional responses

$$f_i(u,v) = \frac{a_i u v}{1+b_i u}\ , \quad i=1,2. \tag{9.3}$$

The death rates d_1 and d_2 are used as bifurcation parameters, with the other parameters set at $a_1 = 5$, $a_2 = 0.1$, $b_1 = 3$, and $b_2 = 2$.

- Analyse the bi-trophic Rosenzweig–MacArthur model. Derive for this two-dimensional system expressions for the equilibria. Derive the critial values for the carrying capacity at the transcritical and Hopf bifurcation. Show that at the Hopf bifurcation the two nullclines intersect at the top of the parabola.
- Analyse with AUTO the Rosenzweig–MacArthur tri-trophic food chain model. First calculate the local bifurcation curves.
- Run the demos in Auto the continu the heteroclinic point–to–cycle connection and the homoclinic cycle-to-cycle connection.

9.3 Exercise 3

A Forest-Pest model reads

$$\frac{dx}{dt} = \rho y - (y-l)^2 x - sx - xz\ , \tag{9.4a}$$

$$\frac{dy}{dt} = x - hy\ , \tag{9.4b}$$

$$\frac{dz}{dt} = \epsilon z + Bxz\ , \tag{9.4c}$$

The parameter values are given in Table 9.2:

- Analyse this model where ρ and h are compound parameters which serve as bifurcation parameters. Use the dimensioneless parameter values given in Table 9.2. Use AUTO or another computer package to continue the local bifurcations.
- Use the Homcont facilities of AUTO to continue the heteroclinic point–to–point connection.

Table 9.2: Parameter values after [5, Table 1] and the used dimensionless values with the calculation of the bifurcation diagrams.

Parameter	Units	Values	dimensionless Values
a	$\text{ha}^2(103\text{ trees})^{-2}\text{yr}^{-1}$	0.00606	—
b	10^3 trees ha^{-1}	0.247	—
c	yr^{-1}	0.01	—
ρ	yr^{-1}	0.134	variable
f	yr^{-1}	0.017	—
h	yr^{-1}	0.04	variable
A	yr^{-1}	0.004	—
ϵ	yr^{-1}	1.5	2
B	yr^{-1}	0.8	1
s	yr^{-1}	—	1

Bibliography

[1] P. A. Abrams. Dynamics and interactions in food webs with adaptive foragers. In G. A. Polis and K. O. Winemiller, editors, *Food webs*, pages 113–121, New York, 1996. Chapman & Hall.

[2] V. S. Afraimovich, V. V. Bykov, and L. P. Shil'nikov. The origin and structure of the Lorenz attractor. *Dokl. Akad. Nauk SSSR*, 234:336–339, 1977.

[3] W.C. Allee. *Animal aggregations, a study in general sociology*. The University of Chicago Press, Chicago, Ill, 1931.

[4] E. L. Allgower and K. Georg. *Numerical Continuation Methods. An introduction*, volume 13 of *Springer series in computational mathematics*. Springer-Verlag, 1990.

[5] M. Ya. Antonovsky, R. A. Fleming, Yu. A. Kuznetsov, and W. C. Clark. Forest–pest interaction dynamics: The simplest mathematical models. *Theoretical Population Biology*, 37:343–367, 1990.

[6] M. A. Aziz-Alaoui. Study of a Leslie-Gower-type tritrophic population model. *Chaos, Solitons and Fractals*, 14:1275–1293, 2002.

[7] F. S. Bacelar, S. Dueri, E. (Hernandez-Garcia), and J. M. Zaldivar. Joint effects of nutrients and contaminants on the dynamics of a food chain in marine ecosystems. *Mathematical Biosciences*, 218(1):24–32, 2009.

[8] A. Back, J. Guckenheimer, M. R. Myers, F. J. Wicklin, and P. A. Worfolk. DsTool:computer assisted exploration of dynamical systems. *Notices Amer. Math. Soc.*, 39(4):303–309, 1992.

[9] A. D. Bazykin. *Nonlinear dynamics of interacting populations*. World Scientific, Singapore, 1998.

[10] A. D. Bazykin, Yu. A. Kuznetsov, and A. I. Khibnik. *Bifurcation diagrams of planar dynamical systems*. Series Mathematics and Cybernetics. Research Computing Centre, USSR Academy of Sciences, Pushchino, Moscow Region, 1985. in Russian.

[11] M. Begon, J. L. Harper, and C. R. Townsend. *Ecology*. Blackwell Science, Oxford, 1996.

[12] W.-J. Beyn. Global bifurcations and their numerical computation. In D. Roose, A. Spence, and B. De Dier, editors, *Continuation and Bifurcation: Numerical Techniques and Applications*, pages 169–181. Kluwer, Dordrecht, Amsterdam, The Netherlands, 1990.

[13] W.-J. Beyn. The numerical computation of connecting orbits in dynamical systems. *IMA J. Num. Anal.*, 9:379–405, 1990.

[14] W.-J. Beyn. On well-posed problems for connecting orbits in dynamical systems. In *Chaotic Numerics (Geelong, 1993)*, volume 172 of *Contemp. Math.*, pages 131–168. Amer. Math. Soc., Providence, RI, 1994.

[15] G. Birkhoff. Nouvelles recherches sur les systèmes dynamiques. *Memoriae Pont. Acad. Sci. Novi. Lincaei, Ser. 3*, 1:85–216, 1935.

[16] M. P. Boer, B. W. Kooi, and S. A. L. M. Kooijman. Food chain dynamics in the chemostat. *Mathematical Biosciences*, 150(1):43–62, 1998.

[17] M. P. Boer, B. W. Kooi, and S. A. L. M. Kooijman. Homoclinic and heteroclinic orbits in a tri-trophic food chain. *Journal of Mathematical Biology*, 39:19–38, 1999.

[18] M. P. Boer, B. W. Kooi, and S. A. L. M. Kooijman. Multiple attractors and boundary crises in a tri-trophic food chain. *Mathematical Biosciences*, 169(2):109–128, 2001.

[19] M. P. Boer, B. W. Kooi, and S. A. L. M. Kooijman. Multiple attractors and boundary crises in a tri-trophic food chain. *Mathematical Biosciences*, 169(2):109–128, 2001.

[20] A. R. Champneys and Yu. A. Kuznetsov. Numerical detection and continuation of codimension-two homoclinic bifurcations. *Int. Journal of Bifurcation and Chaos*, 4:795–822, 1994.

[21] A. R. Champneys, Yu. A. Kuznetsov, and B. Sandstede. A numerical toolbox for homoclinic bifurcation analysis. *Int. Journal of Bifurcation and Chaos*, 6(5):867–887, 1996.

[22] A. R. Champneys, Yu. A. Kuznetsov, and B. Sandstede. A numerical toolbox for homoclinic bifurcation analysis. *Int. Journal of Bifurcation and Chaos*, 6(5):867–887, 1996.

[23] A. R. Champneys and G. J. Lord. Computation of homoclinic solutions to periodic orbits in a reduced water-wave problem. *Physica D*, 102:101–124, 1997.

[24] A. Cunningham and R. M. Nisbet. Transients and oscillations in continuous culture. In M. J. Bazin, editor, *Mathematics in Microbiology*, pages 77–103, London, 1983. Academic Press.

[25] A. M. De Roos and L. Persson. Size-dependent life-history traits promote catastrophic collapses of top predators. *Proc. Nat. Acad. Sci. U. S. A.*, 99:12907–12912, 2002.

[26] A. M. de Roos, L. Persson, and H. R. Thieme. Emergent Allee effects in top predators feeding on structured prey populations. *Proc. Roy. Soc. London (B)*, 270:611–618, 2003.

[27] J. W. Demmel, L. Diece, and M. J. Friedman. Computing connecting orbits via an improved algorithm for continuing invariant subspaces. *SIAM J. Sci. Comput.*, 22(1):81–94, 2000.

[28] L. Dieci and R. Rebaza. Point-to-periodic and periodic-to-periodic connections. *BIT Num. Math.*, 44:617–618, 2004.

[29] L. Dieci and R. Rebaza. Point-to-periodic and periodic-to-periodic connections. *BIT Num. Math.*, 44:41–62, 2004.

[30] E. Doedel and J. Kernévez. Auto: Software for continuation problems in ordinary differential equations with applications. Technical report, California Institute of Technology, Applied Mathematics, 1986.

[31] E. J. Doedel, A. R. Champneys, T. F. Fairgrieve, Y. A. Kuznetsov, B. Sandstede, and X. Wang. Auto 97: Continuation and bifurcation software for ordinary differential equations. Technical report, Concordia University, Montreal, Canada, 1997.

[32] E. J. Doedel and M. J. Friedman. Numerical computation of heteroclinic orbits. *J. Comput. Appl. Math.*, 26:155–170, 1989.

[33] E. J. Doedel, M. J. Friedman, and A. C. Monteiro. On locating connecting orbits. *Applied Mathematics and Computation*, 65:231–239, 1994.

[34] E. J. Doedel, B. W. Kooi, G. A. K. van Voorn, and YU. A. Kuznetsov. Continuation of connecting orbits in 3d-odes (I): Point-to-cycle connections. *International Journal of Bifurcation and Chaos*, 18(7):1889–1903, 2008.

[35] E. J. Doedel, B. W. Kooi, G. A. K. van Voorn, and YU. A. Kuznetsov. Continuation of connecting orbits in 3d-odes (II): Cycle-to-cycle connections. *International Journal of Bifurcation and Chaos*, 19(1):159–169, 2009.

[36] E. J. Doedel and B. Oldeman. Auto 07p: Continuation and bifurcation software for ordinary differential equations. Technical report, Concordia University, Montreal, Canada, 2009.

[37] F. Dumortier, R. Roussarie, J. Sotomayor, and H. Żoladek. *Bifurcations of planar vector fields. Nilpotent singularities and Abelian Integrals.* Springer-Verlag, Berlin, 1991.

[38] L. Edelstein-Keshet. *Mathematical Models in Biology.* Random House, 1988.

[39] C. Elton. *Animal ecology.* Macmillan, New York, 1927.

[40] B. Ermentrout. *Simulating, Analyzing, and Animating Dynamical Systems: A Guide to Xppaut for Researchers and Students.* Society for Industrial and Applied Mathematics, Philadelphia, 2002.

[41] M. J. Friedman and E. J. Doedel. Numerical computation and continuation of invariant manifolds connecting fixed points. *SIAM Journal on Numerical Analysis*, 28:789–808, 1991.

[42] G. F. Fussmann, S. P. Ellner, K. W. Shertzer, and N. G. Hairston Jr. Crossing the Hopf bifurcation in a live predator-prey system. *Science*, 290:1358–1360, 2000.

[43] E. Gamero, E. Freire, and E. Ponce. On the normal forms for planar systems with nilpotent linear parts. In R. Seydel, F. W. Schneider, T. Küpper, and H. Troger, editors, *Bifurcation and Chaos: Analysis, Algorithms, Applications*, pages 123–127. Birkhäuser, 1991.

[44] N.K. Gavrilov and L.P. Shilnikov. On three-dimensional systems close to systems with a structurally unstable homoclinic curve: I. *Math. USSR-Sb.*, 17:467–485, 1972.

[45] N. K. Gavrilov and L. P. Shilnikov. On three-dimensional systems close to systems with a structurally unstable homoclinic curve: II. *Math. USSR-Sb.*, 19:139–156, 1973.

[46] M. E. Gilpin. Enriched predator-prey systems: theoretical stability. *Science*, 177:902–904, 1972.

[47] F. A. P. C. Gobas. A model for predicting the bioaccumulation of hydrophobic organic chemicals in aquatic food-webs: application to Lake Ontario. *Ecological Modelling*, 69:1–17, 1992.

[48] W. Govaerts, Yu. A. Kuznetsov, and B. Sijnave. Numerical methods for the generalized Hopf bifurcation. *SIAM Journal on Numerical Analysis*, 38:329–346, 2000.

[49] A. Gragnani, O. De Feo, and S. Rinaldi. Food chains in the chemostat: relationships between mean yield and complex dynamics. *Bulletin of Mathematical Biology*, 60:703–719, 1998.

[50] C. Grebogi, E. Ott, and J. A. Yorke. Basin boundary metamorphoses: Changes in accessible boundary orbits. *Physica D*, 24:243–262, 1987.

[51] C. Grebogi, E. Ott, and J. A. Yorke. Chaos, strange attractors, and fractal basin boundaries in nonlinear dynamical systems. *Science*, 238:632–638, 1987.

[52] V. Grimm and C. Wissel. Babel, or the ecological stability discussion: an inventory and analysis of terminology and a guide for avoiding confusion. *Oecologia*, 109:323–334, 1997.

[53] J. P. Grover. *Resource Competition*. Population and Community Biology series. Chapman & Hall, London, 1997.

[54] J. Guckenheimer and P. Holmes. *Nonlinear Oscillations, Dynamical Systems and Bifurcations of Vector Fields*, volume 42 of *Applied Mathematical Sciences*. Springer-Verlag, New York, 2 edition, 1985.

[55] C. R. Gwaltney, W. Luo, and M. A. Stadtherr. Computation of equilibrium states and bifurcations using interval analysis: Application to food chain models. *Ecological Modelling*, 203:495–510, 2007.

[56] M. Gyllenberg, I. Hanski, and T. Lindström. Continuous versus discrete single species population models with adjustable reproductive strategies. *Bulletin of Mathematical Biology*, 59:679–705, 1997.

[57] N. G. Hairston, F. E. Smith, and L. B. Slobodkin. Community structure, population control, and competition. *The American Naturalist*, 94:421–425, 1960.

[58] T. G. Hallam, G. A. Canziani, and R. R. Lassiter. Sublethal narcosis and population persistence: A modelling study on growth effects. *Environmental Toxicology and Chemistry*, 12:947–954, 1993.

[59] A. Hastings. What equilibrium behaviour of Lotka-Volterra models does not tell us about food webs. In G. A. Polis and K. O. Winemiller, editors, *Food webs*, pages 211–217, New York, 1996. Chapman & Hall.

[60] A. Hastings and T. Powell. Chaos in a three-species food chain. *Ecology*, 72(3):896–903, 1991.

[61] P. Hogeweg and B. Hesper. Interactive instruction population interactions. *Computational Biology and Medicine*, 8:319–327, 1978.

[62] C. S. Holling. Some characteristics of simple types of predation and parasitism. *Canadian Entomologist*, 91:385–398, 1959.

[63] J. Huisman and F. J. Weissing. Oscillations and chaos generated by competition for interactively essential resources. *Ecological Research*, 17:175–181, 2002.

[64] A. Kent, C. P. Doncaster, and T. Sluckin. Consequences for predators of rescue and allee effects on prey. *Ecological Modelling*, 162:233–245, 2003.

[65] A. I. Khibnik, Yu. A. Kuznetsov, V. V. Levitin, and E. V. Nikolaev. Continuation techniques and interactive software for bifurcation analysis of ODEs and iterated maps. *Physica D*, 62:360–371, 1993.

[66] A. Klebanoff and A. Hastings. Chaos in three-species food chain. *Journal of Mathematical Biology*, 32:427–451, 1994.

[67] Aaron Klebanoff and Alan Hastings. Chaos in three-species food chains. *J. Math. Biol.*, 32:427–451, 1994.

[68] E. Knobloch. Normal forms for bifurcations at a double zero eigenvalue. *Physics Letters A*, 115(5):199–201, 1986.

[69] M. Kondoh. Foraging adaption and the relationship between food-web complexity and stability. *Science*, 299:1388–1391, 2003.

[70] B. W. Kooi. Numerical bifurcation analysis of ecosystems in a spatially homogeneous environment. *Acta Biotheoretica*, 51(3):189–222, 2003.

[71] B. W. Kooi and M. P. Boer. Bifurcations in ecosystem models and their biological interpretation. *Applicable Analysis*, 77(1-2):29–59, 2001.

[72] B. W. Kooi and M. P. Boer. Chaotic behaviour of a predator-prey system. *Dynamics of Continuous, Discrete and Impulsive Systems, Series B: Applications and Algorithms*, 10(2):259–272, 2003.

[73] B. W. Kooi, M. P. Boer, and S. A. L. M. Kooijman. On the use of the logistic equation in food chains. *Bulletin of Mathematical Biology*, 60(2):231–246, 1998.

[74] B. W. Kooi, M. P. Boer, and S. A. L. M. Kooijman. Resistance of a food chain to invasion by a top predator. *Mathematical Biosciences*, 157:217–236, 1999.

[75] B. W. Kooi, D. Bontje, G. A. K. van Voorn, and S. A. L. M. Kooijman. Sublethal toxic effects in a simple aquatic food chain. *Ecological Modelling*, 212(3/4):304–318, 2008.

[76] B. W. Kooi and S. A. L. M. Kooijman. Invading species can stabilize simple trophic systems. *Ecological Modelling*, 133(1-2):57–72, 2000.

[77] B. W. Kooi, L. D. J. Kuijper, M. P. Boer, and S. A. L. M. Kooijman. Numerical bifurcation analysis of a tri-trophic food web with omnivory. *Mathematical Biosciences*, 177:201–228, 2002.

[78] S. A. L. M. Kooijman. *Dynamic Energy and Mass Budgets in Biological Systems*. Cambridge University Press, Cambridge, 2000.

[79] S. A. L. M. Kooijman. *Dynamic Energy Budget theory for metabolic organisation*. Cambridge University Press, Cambridge, 2010.

[80] S. A. L. M. Kooijman and J. J. M. Bedaux. *The analysis of aquatic toxicity data*. VU University Press, Amsterdam, 1996.

[81] S. A. L. M. Kooijman, J. Grasman, and B. W. Kooi. A new class of non-linear stochastic population models with mass conservation. *Mathematical Biosciences*, 210:378–394, 2007.

[82] T. Kostova, J. Li, and M. Friedman. Two models for competition between age classes. *Mathematical Biosciences*, 157:65–89, 1999.

[83] M. Kot. *Elements of Mathematical Ecology*. Cambridge University Press, Cambridge, 2001.

[84] B. Krauskopf and T. Rieß. Lin's method approach to finding and continuing heteroclinic connections involving periodic orbits. *Nonlinearity*, 21:1655–1690, 2008.

[85] L. D. J. Kuijper, B. W. Kooi, C. Zonneveld, and S. A. L. M. Kooijman. Omnivory and food web dynamics. *Ecological Modelling*, 163:19–32, 2003.

[86] Yu. A. Kuznetsov. *Elements of Applied Bifurcation Theory*, volume 112 of *Applied Mathematical Sciences*. Springer-Verlag, New York, 2 edition, 1998.

[87] Yu. A. Kuznetsov. Numerical normalization techniques fro all codim 2 difurcations of equilibria in ODE's. *SIAM Journal on Numerical Analysis*, 36:1104–1124, 1999.

[88] Yu. A. Kuznetsov. *Elements of Applied Bifurcation Theory*, volume 112 of *Applied Mathematical Sciences*. Springer-Verlag, New York, 3 edition, 2004.

[89] Yu. A. Kuznetsov. Practical computation of normal forms on center manifolds at codim 3 Bogdanov-Takens bifurcations. *International Journal of Bifurcation and Chaos*, 15(11):3535–3546, 2005.

[90] Yu. A. Kuznetsov, O. De Feo, and S. Rinaldi. Belyakov homoclinic bifurcations in a tritrophic food chain model. *SIAM Journal on Applied Mathematics*, 62(2):462–487, 2001.

[91] Yu. A. Kuznetsov and V. V. Levitin. *CONTENT: Integrated environment for the analysis of dynamical systems*. Centrum voor Wiskunde en Informatica (CWI), Kruislaan 413, 1098 SJ Amsterdam, The Netherlands, 1.5 edition, 1997.

[92] Yu. A. Kuznetsov and S. Rinaldi. Remarks on food chain dynamics. *Mathematical Biosciences*, 124(1):1–33, 1996.

[93] C. Letellier and M. A. Aziz-Alaoui. Analysis of the dynamics of a realistic ecological model. *Chaos, Solitons and Fractals*, 13:95–107, 2002.

[94] I. Loladze, Y. Kuang, and J. J. Elser. Stoichiometry in producer-grazer systems:Linking energy flow with element cycling. *Bulletin of Mathematical Biology*, 62:1137–1162, 2000.

[95] V. I. Lukyanov. Bifurcations of dynamical systems with a saddle-point separatrix loop. *Differential Equations*, 18:1049–1059, 1982.

[96] R. M. May. *Stability and Complexity in Model Ecosystems*. Princeton University Press, New Haven, 1973.

[97] R. M. May. Simple mathematical models with very complicated dynamics. *Nature*, 261:459–467, 1976.

[98] K. McCann and P. Yodzis. Biological conditions for chaos in a tree-species food chain. *Ecology*, 75(2):561–564, 1994.

[99] K. McCann and P. Yodzis. Bifurcation structure of a tree-species food chain model. *Theoretical Population Biology*, 48:93–125, 1995.

[100] P. J. Morin. *Community Ecology*. Blackwell Science, Malden, Massachusetts, 1999.

[101] Ju. I. Neimark. Motions close to doubly-asymptotic motion. *Soviet Math. Dokl.*, 8:228–231, 1967.

[102] R. M. Nisbet. Delay-differential equations for structured populations. In S. Tuljapurkar and H. Caswell, editors, *Structured-Population models in marine, terrestrial, and freshwater systems*, pages 89–118, New York, 1997. Chapman & Hall.

[103] V. P. Nozdracheva. Bifurcation of structurally unstable separatrix loop. *Differentsial'nyye Uravneniya*, 18:1551–1558, 1982.

[104] R.V. O'Neill, D.L. DeAngelis, J.J. Pastor, B.J. Jackson, and W.M. Post. Multiple nutrient limitations in ecological models. *Ecological Modelling*, 46:495–510, 1989.

[105] E. Ott. *Chaos in Dynamical Systems*. Cambridge University Press, Cambridge, 1993.

[106] J. Palis and F. Takens. *Hyperbolicity and Sensitive Chaotic Dynamics at Homoclinic Bifurcations: Fractal Dimensions and Infinitely Many Attractors*, volume 35 of *Cambridge Studies in Advanced Mathematics*. Cambridge University Press, Cambridge, 1993.

[107] T. Pampel. Numerical approximation of connecting orbits with asymptotic rate. *Numer. Math.*, 90:309–348, 2001.

[108] T. S. Parker and L. O. Chua. *Practical Numerical Algorithms for Chaotic Systems*. Springer-Verlag, 1989.

[109] H. Poincaré. *Sur les propriétés des fonctions définies par les équations aux différences partielles. Thèse*. Gauthier-Villars, Paris, 1879.

[110] M. L. Rosenzweig. Paradox of enrichment: destabilization of exploitation ecosystems in ecological time. *Science*, 171:385–387, 1971.

[111] M. L. Rosenzweig and R. H. MacArthur. Graphical representation and stability conditions of predator-prey interactions. *The American Naturalist*, 97:209–223, 1963.

[112] S. Ruan and W. Wang. Dynamical behavior of an epidemic model with a nonlinear incidence rate. *J. Diff. Eqns.*, 188:135–163, 2003.

[113] M. Scheffer, S. Carpenter, J. A. Foley, C. Folke, and B. Walker. Catastrophic shifts in ecosystems. *Nature*, 413:591–596, 2001.

[114] M. Scheffer, S. Rinaldi, and Y. A. Kuznetsov. Effects of fish on plankton dynamics: a theoretical analysis. *Canadian Journal of Fisheries and Aquatic Sciences*, 57:1208–1219, 2000.

[115] K. W. Shertzer, S. P. Ellner, G. F. Fussmann, and N. G. Hairston Jr. Predator-prey cycles in an aquatic microcosm: testing hypotheses of mechanism. *Journal of Animal Ecology*, 71:802–815, 2002.

[116] L. P. Shil'nikov. On a Poincaré–Birkhoff problem. *Math. USSR-Sb.*, 3:353–371, 1967.

[117] S. Smale. Diffeomorphisms with many periodic points. In S.S. Carins, editor, *Differential and Combinatorial Topology*, pages 63–80. Princeton University Press, Princeton, NJ, 1963.

[118] H. L. Smith and P. Waltman. *The Theory of the Chemostat.* Cambridge University Press, Cambridge, 1994.

[119] D. Stiefs, G. A. K. van Voorn, B. W. Kooi, T. Gross, and U. Feudel. Food quality in producer-grazer models – a generalized approach. *American Naturalist*, ?:?–?, 2010.

[120] H. R. Thieme. *Mathematics in Population Biology.* Princeton University Press, Princeton, NJ, 2003.

[121] D. Tilman. *Resource competition and community structure.* Princeton University Press, Princeton, 1982.

[122] R. K. Upadhyay. Multiple attractors and crisis route to chaos in a model food-chain. *Chaos, Solitons and Fractals*, 16:737–747, 2003.

[123] H. A. van den Berg. Propagation of permanent perturbations in food chains and food webs. *Ecological Modelling*, 107:225–235, 1998.

[124] G. A. K. van Voorn, L. Hemerik, M. P. Boer, and B. W. Kooi. Heteroclinic orbits indicate overexploitation in predator–prey systems with a strong Allee effect. *Mathematical Biosciences*, 209(2):451–469, 2007.

[125] S. Wiggins. *Global Bifurcations and Chaos: Analytical methods.* Springer-verlag: New York, Heidelberg, Berlin, 1988.

[126] S. Wiggins. *Introduction to Applied Nonlinear Dynamical Systems and Chaos*, volume 2 of *Texts in Applied Mathematics.* Springer-Verlag, New York, 1990.

[127] D. Xiao and S. Ruan. Bogdanov-takens bifurcations in predator-prey systems with constant harvesting. *Fields Inst. Comm.*, 21:493–506, 1999.

[128] D. Xiao and S. Ruan. Codimension two bifurcations in a predator-prey system with group defense. *International Journal of Bifurcation and Chaos*, 11:2123–2131, 2001.